Studies of Initial-State Nuclear Modifications with the ATLAS Experiment

Ben Gilbert
Lawrence Livermore National Laboratory

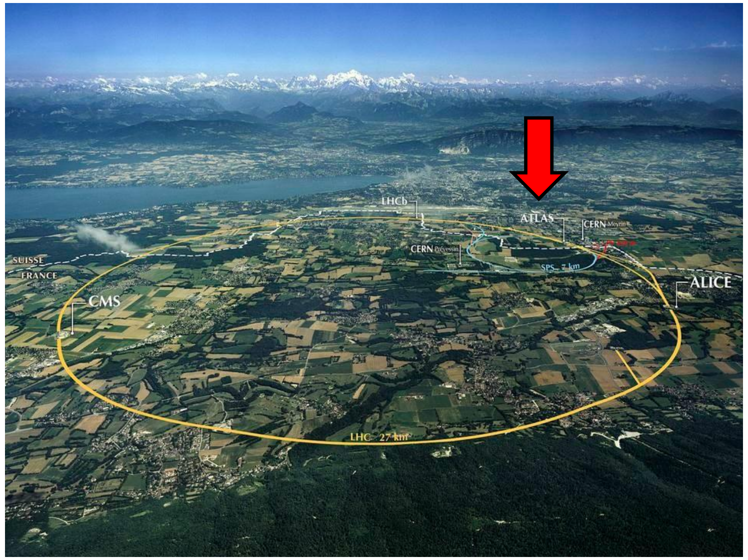

Introduction: Nuclear PDFs

- The kinematic coverage of world data constraining nuclear Parton Distribution Functions (nPDFs) has expanded massively with contributions from the LHC.

- Gaps still remain in the data determining nPDFs, leaving large stretches of phase space un-constrained.
  - We must currently rely on interpolation and miss the finer details of their evolution.

- The EIC will provide more coverage, but it is years away.
  - It still will not extend as high in Q^2 as measurements from the LHC.

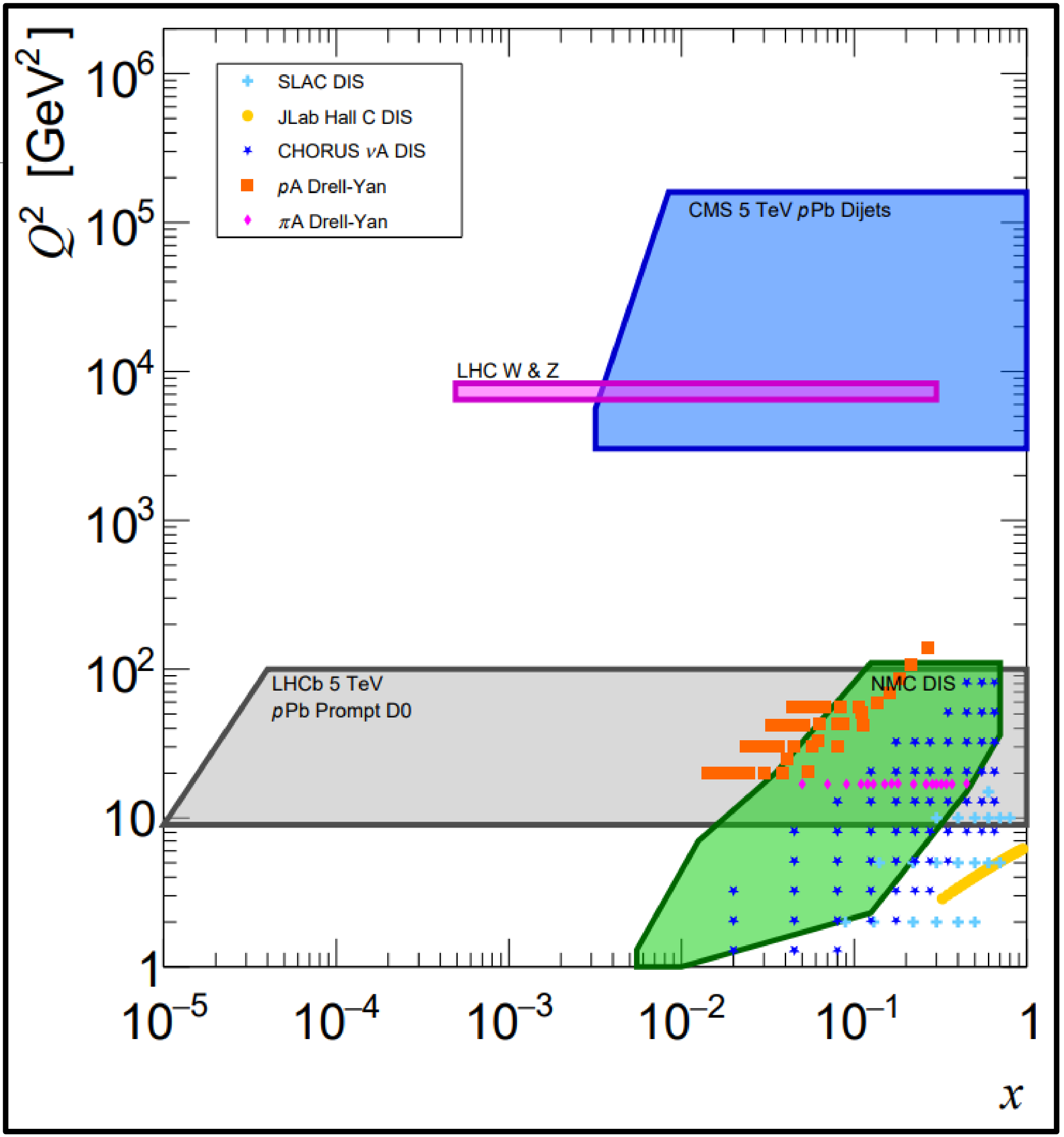

Figure inspired by arXiv:2112.12462

Introduction: Nuclear PDFs

- The kinematic coverage of world data constraining nuclear Parton Distribution Functions (nPDFs) has expanded massively with contributions from the LHC.

- Gaps still remain in the data determining nPDFs, leaving large stretches of phase space un-constrained.
    - We must currently rely on interpolation and miss the finer details of their evolution.

- The EIC will provide more coverage, but it is years away.
    - It still will not extend as high in Q^2 as measurements from the LHC.

- Two recent ATLAS measurements will help to constrain a large region of this phase-space:
    - 5.02 TeV UPC dijets
    - 8.16 TeV p+Pb dijets

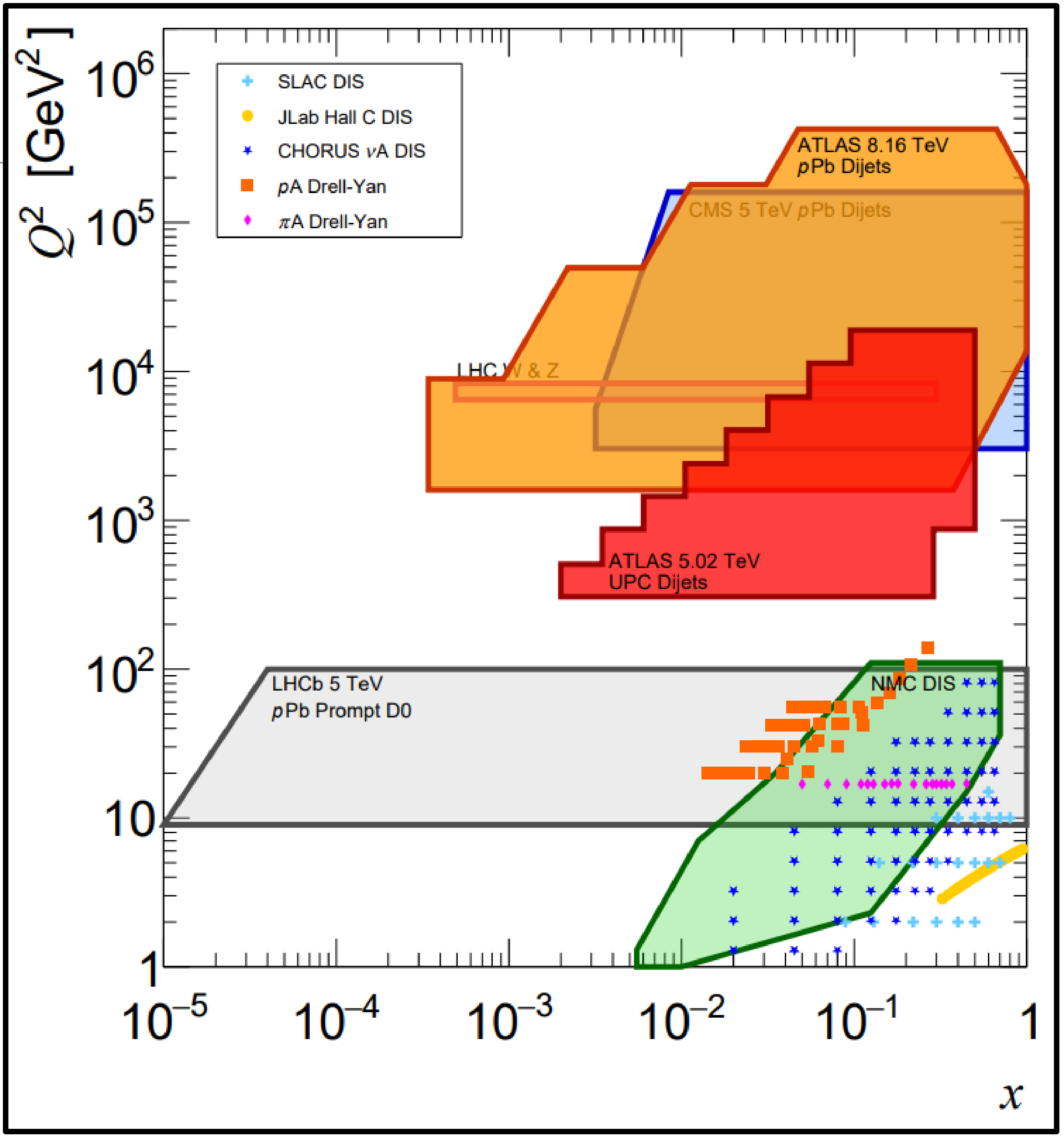

Figure inspired by arXiv:2112.12462

Introduction: Nuclear PDFs

- The kinematic coverage of world data constraining nuclear Parton Distribution Functions (nPDFs) has expanded massively with contributions from the LHC.
- Gaps still remain in the data determining nPDFs, leaving large stretches of phase space un-constrained.
  - We must currently rely on interpolation and finer details of their evolution.
- The EIC will provide more coverage, but it is year
  - It still will not extend as high in Q^2 as measureme from the LHC.
- Two recent ATLAS measureme will help to constrai large region of this phase ace:
  - 5.02 TeV UPC dijets
  - 8.16 TeV p+Pb dijets

Constraining nPDF effects with a clean, electromagnetic probe

Directly measuring initial-state effects from the hadronic probe

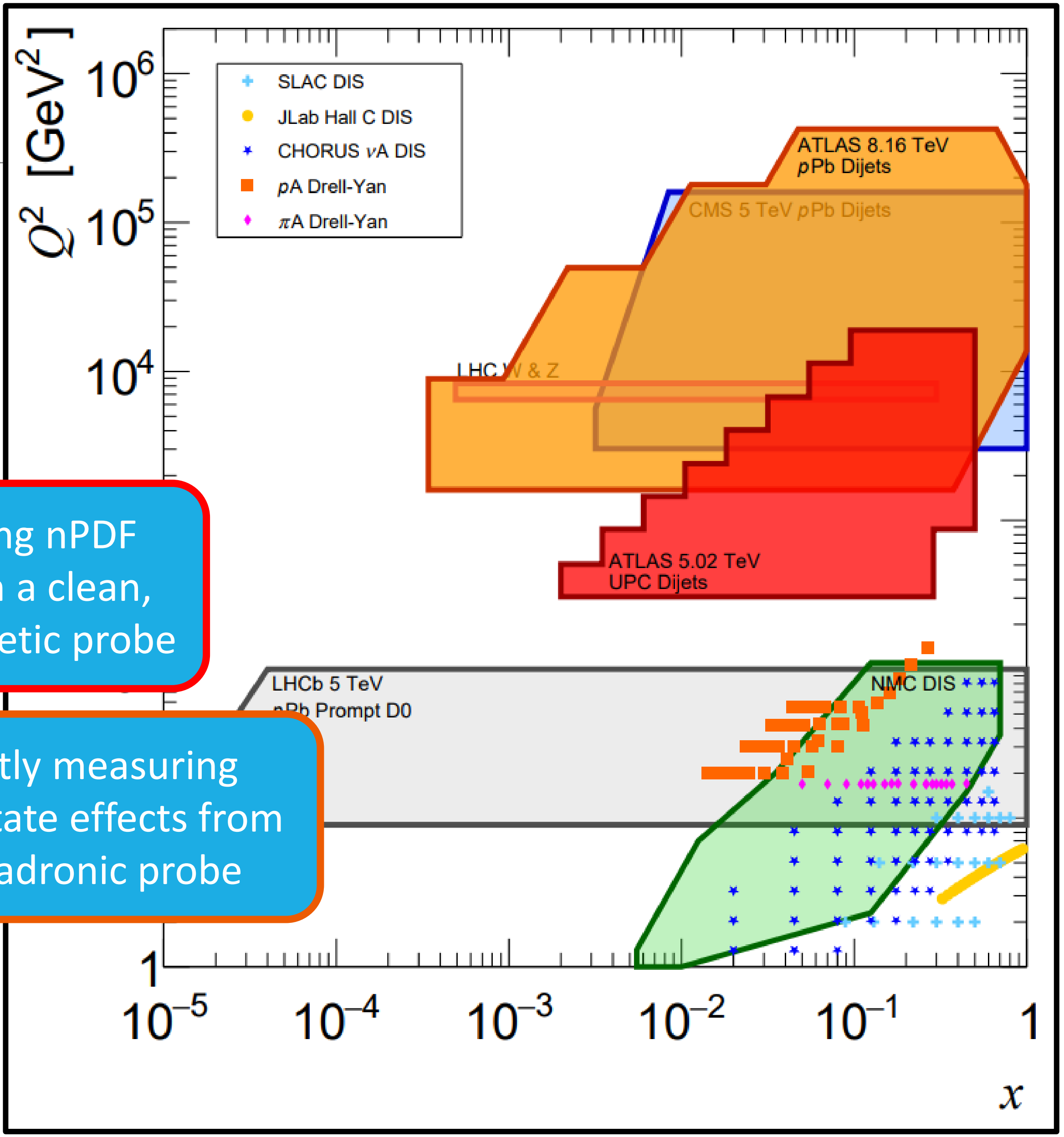

Figure inspired by arXiv:2112.12462

Dijet Measurements in Two Collision Systems

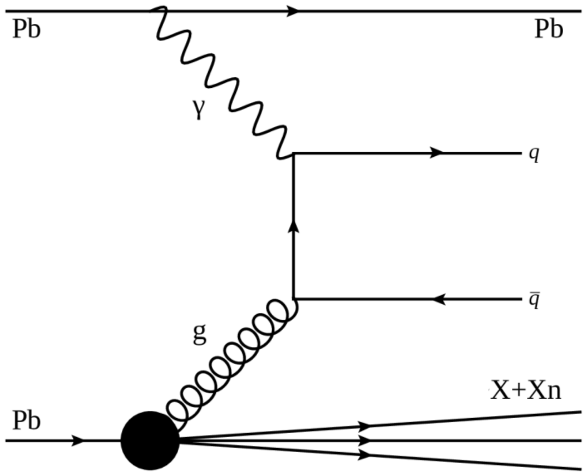

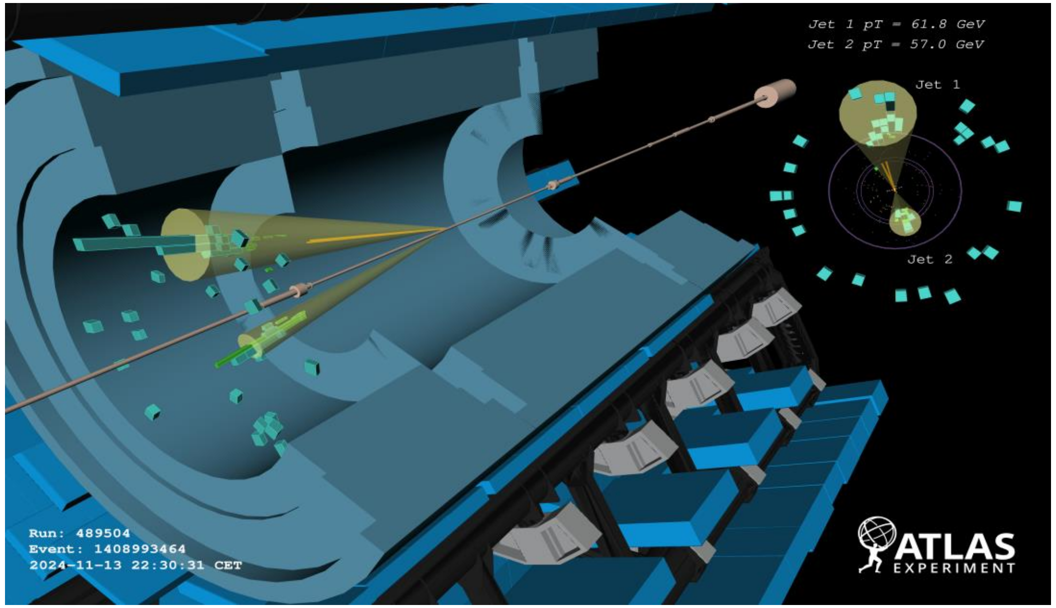

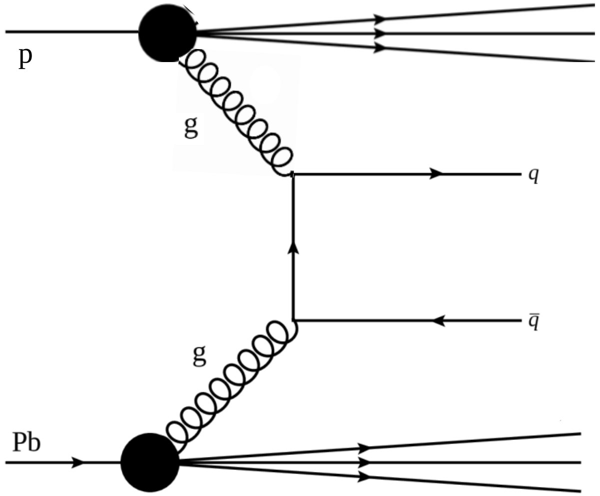

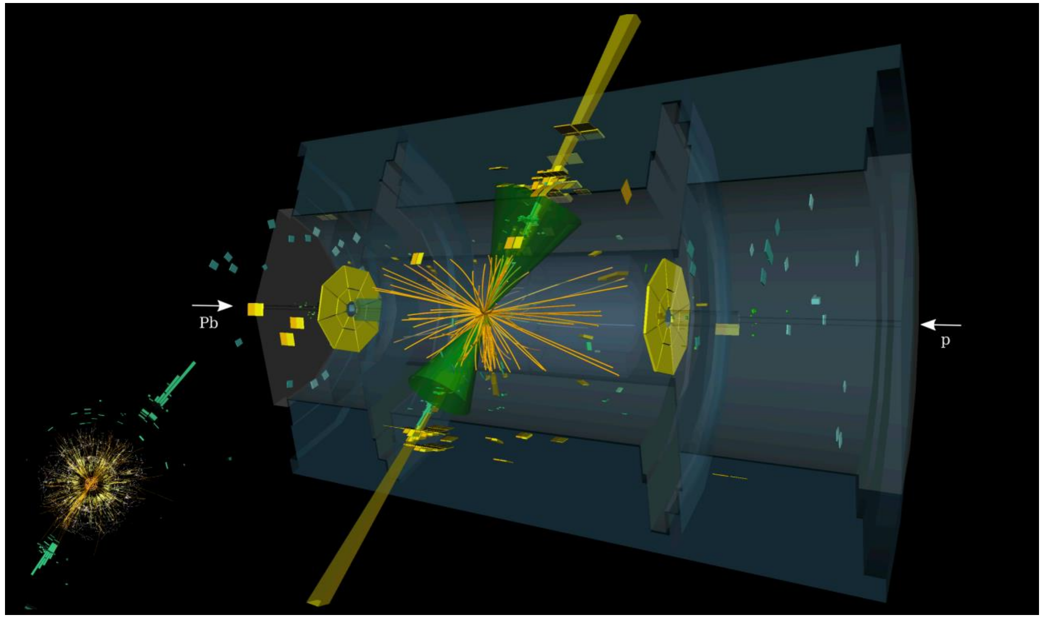

Dijet Measurements in Two Collision Systems

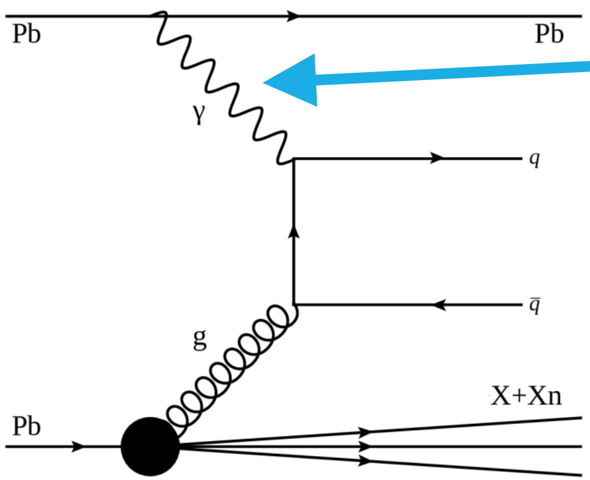

In ultra-relativistic heavy ion collisions, the intense electromagnetic fields provide a flux of quasi-real photons.

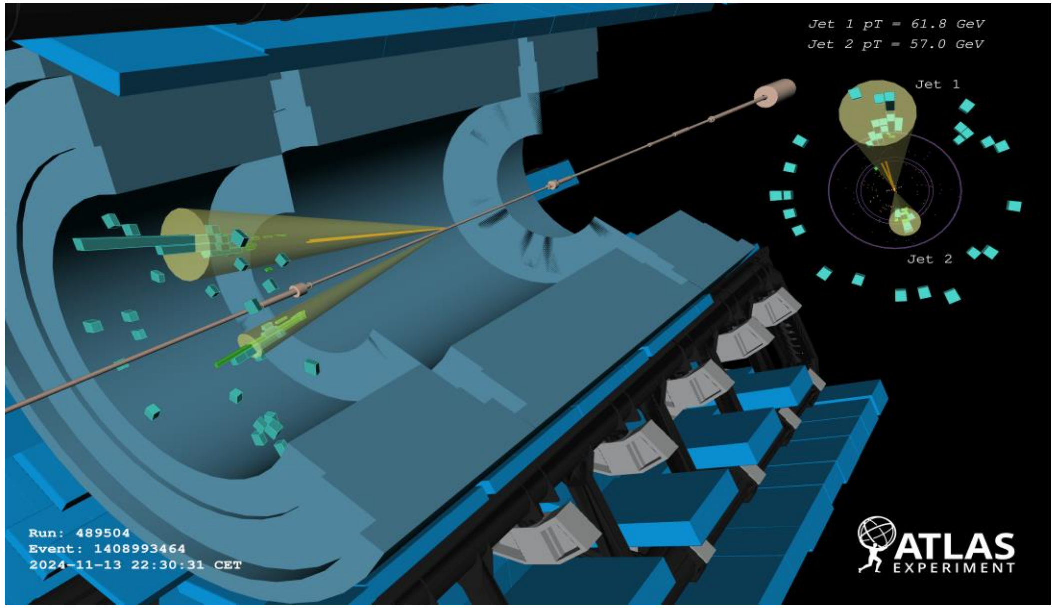

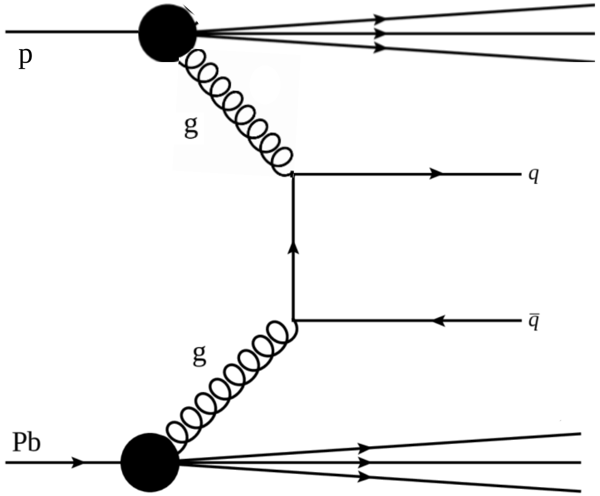

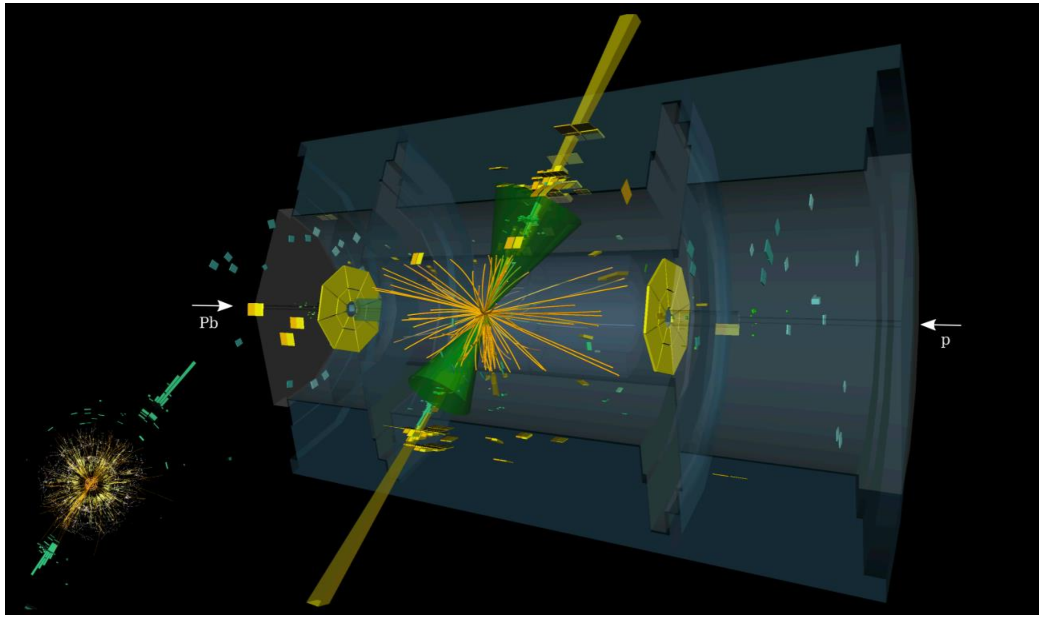

Dijet Measurements in Two Collision Systems

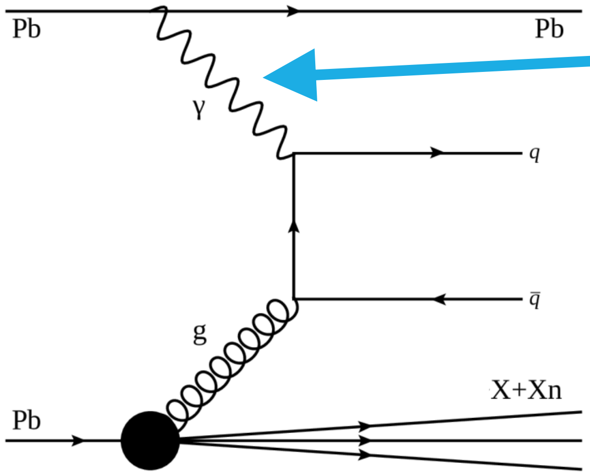

In ultra-relativistic heavy ion collisions, the intense electromagnetic fields provide a flux of quasi-real photons.

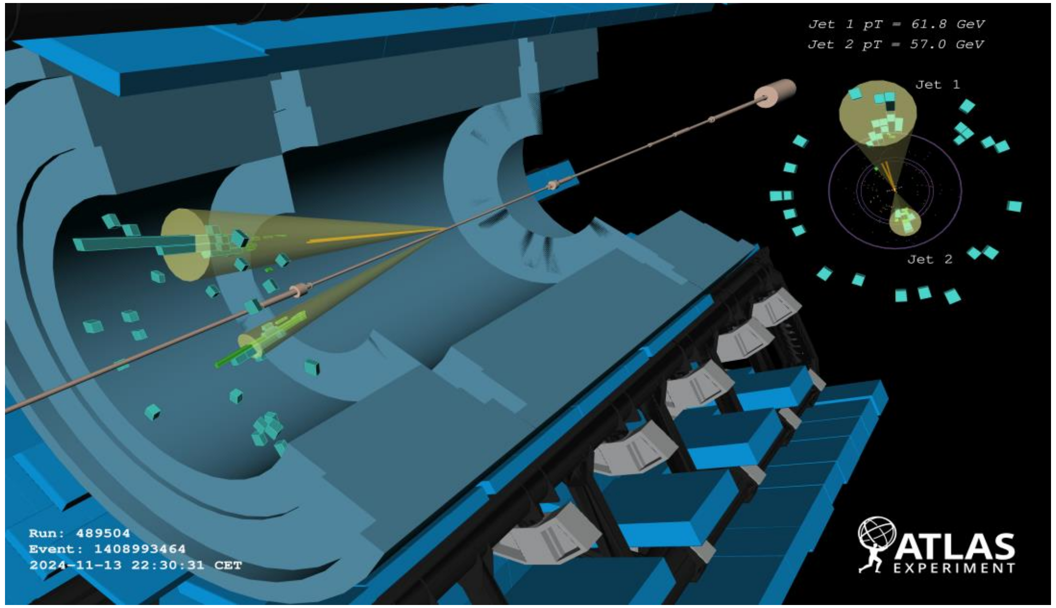

In p+Pb collisions, a partonic constituent from the proton strikes the Pb nucleus.

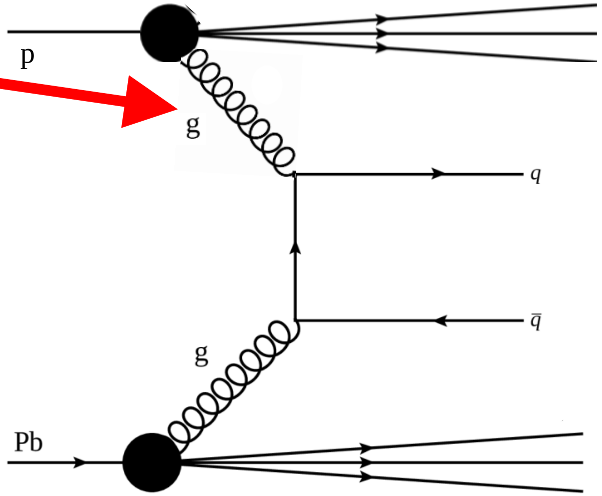

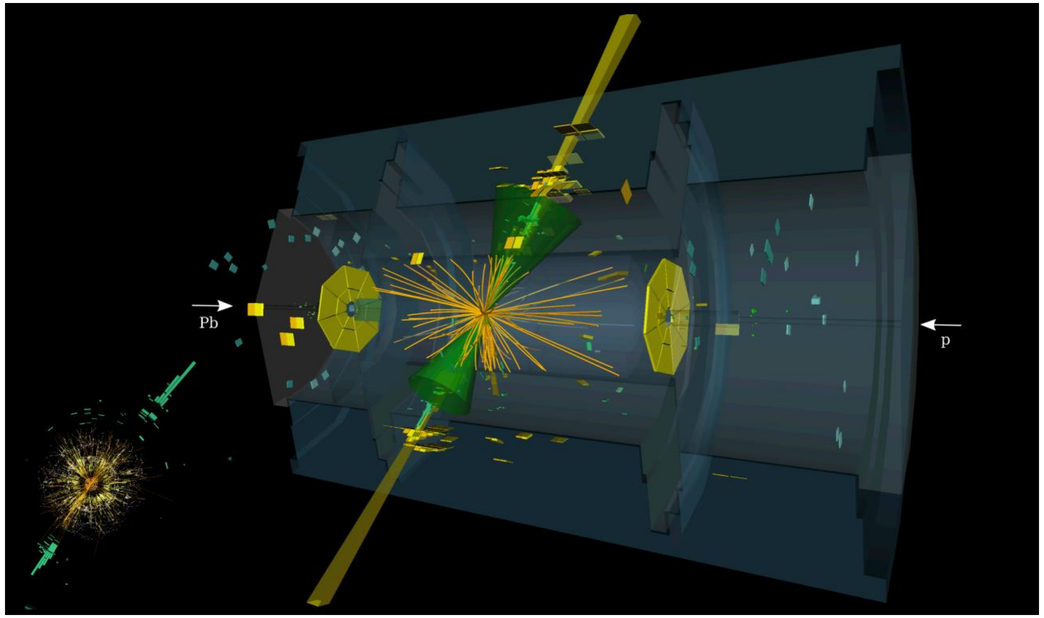

Dijet Measurements in Two Collision Systems

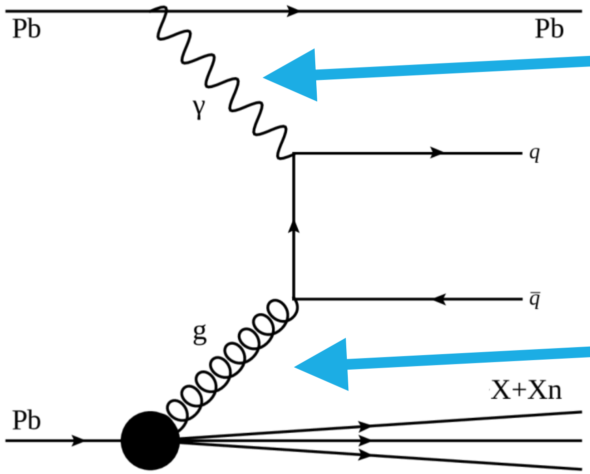

In ultra-relativistic heavy ion collisions, the intense electromagnetic fields provide a flux of quasi-real photons.

In p+Pb collisions, a partonic constituent from the proton strikes the Pb nucleus.

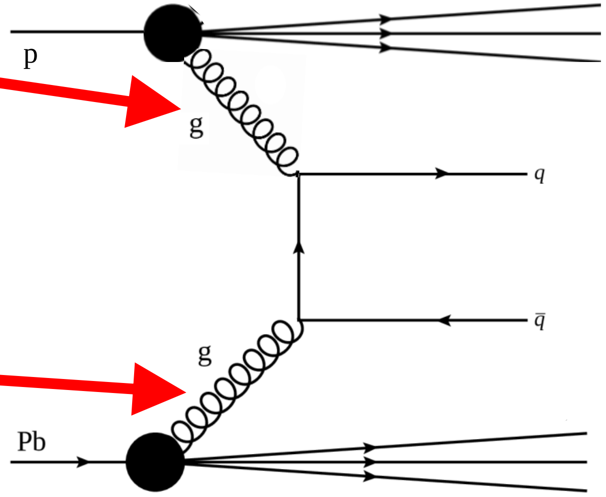

In both cases, they scatter from a parton in the Pb target, probing its nPDF.

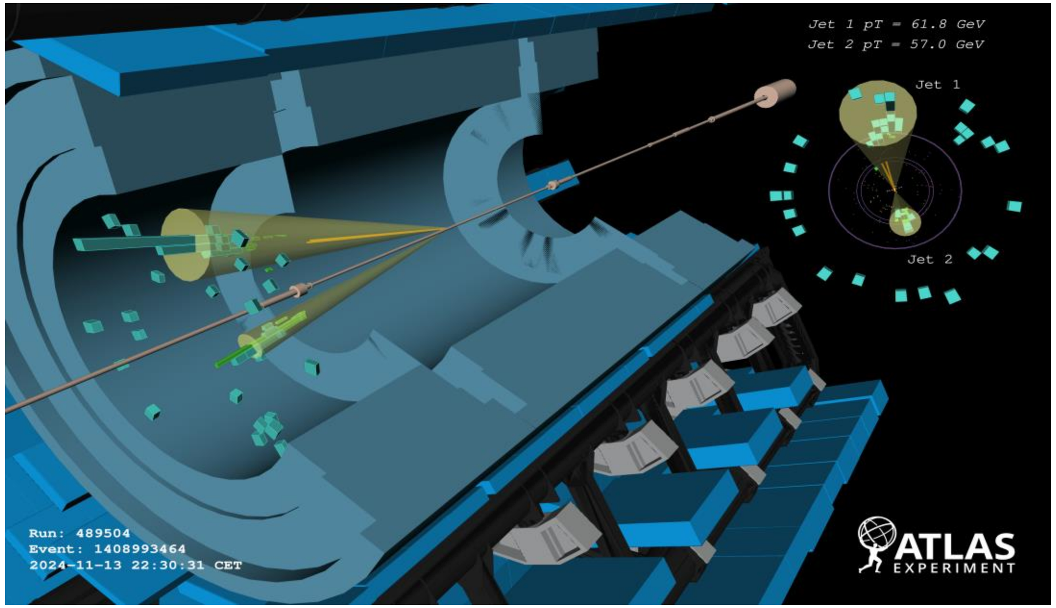

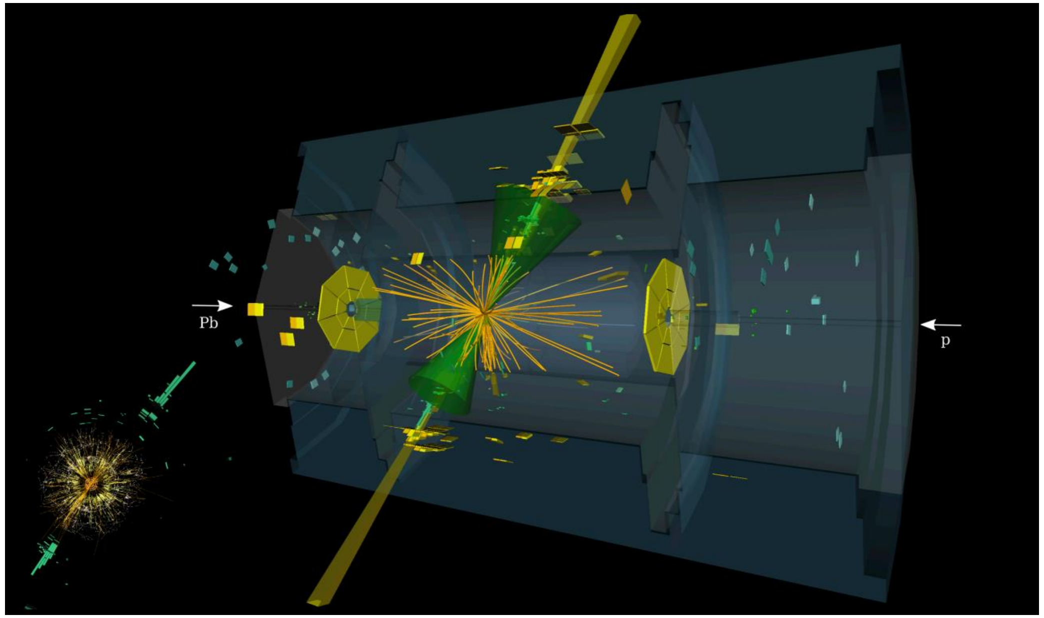

Dijet Measurements in Two Collision Systems

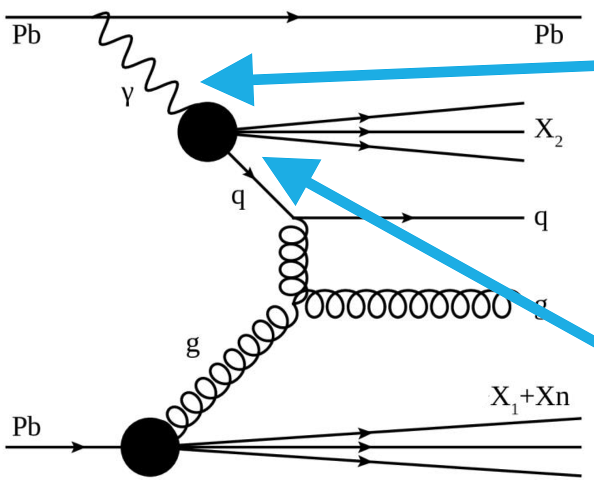

In ultra-relativistic heavy ion collisions, the intense electromagnetic fields provide a flux of quasi-real photons.

In resolved processes, the photon can fluctuate to some hadronic state.

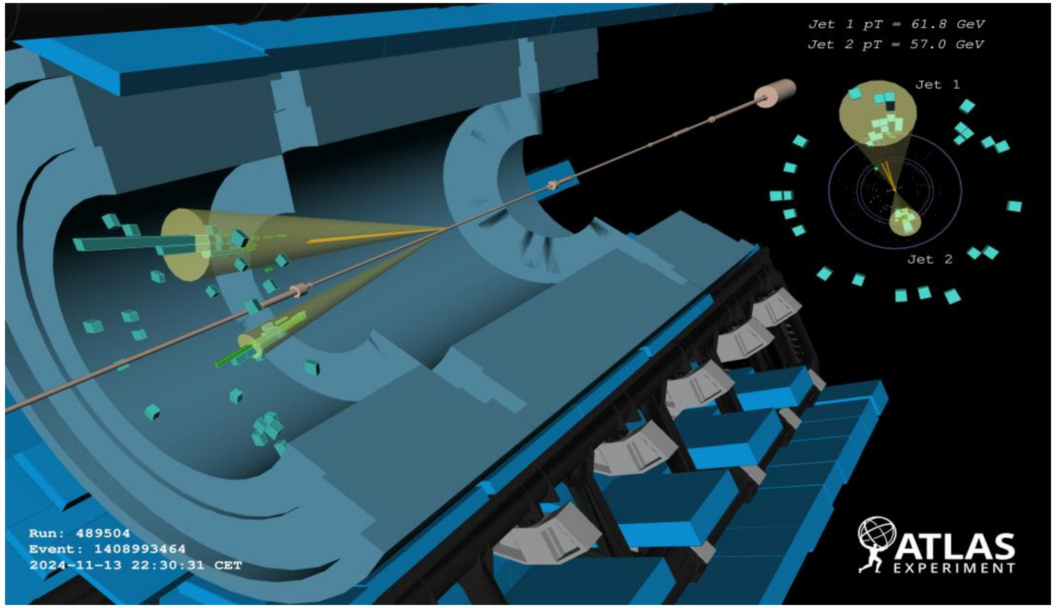

In p+Pb collisions, a partonic constituent from the proton strikes the Pb nucleus.

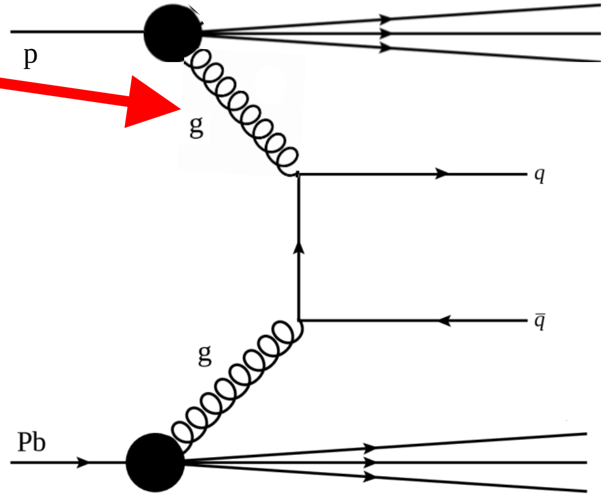

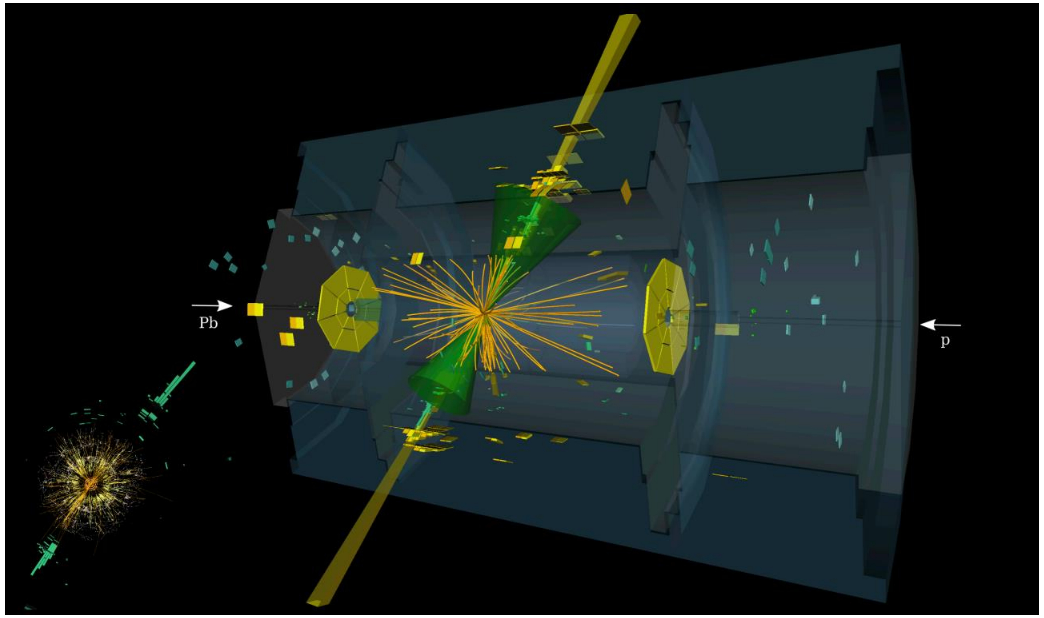

Dijet Measurements in Two Collision Systems

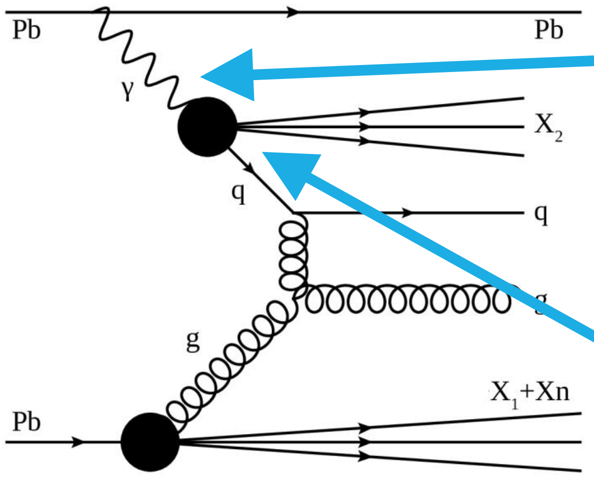

In ultra-relativistic heavy ion collisions, the intense electromagnetic fields provide a flux of quasi-real photons.

In resolved processes, the photon can fluctuate to some hadronic state.

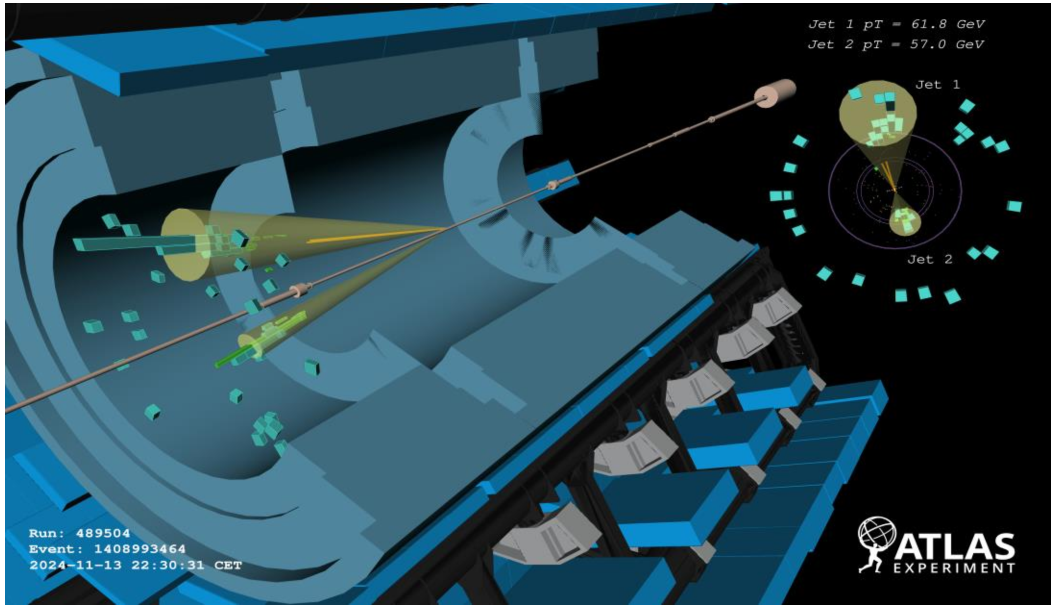

In p+Pb collisions, a partonic constituent from the proton strikes the Pb nucleus.

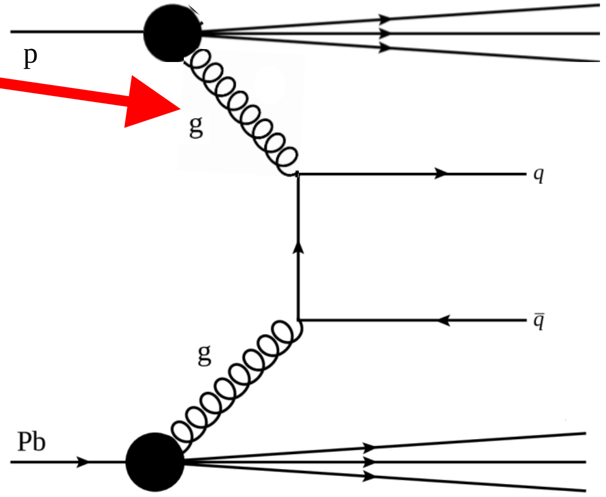

The probe in p+Pb collisions always has a more complex hadronic structure.

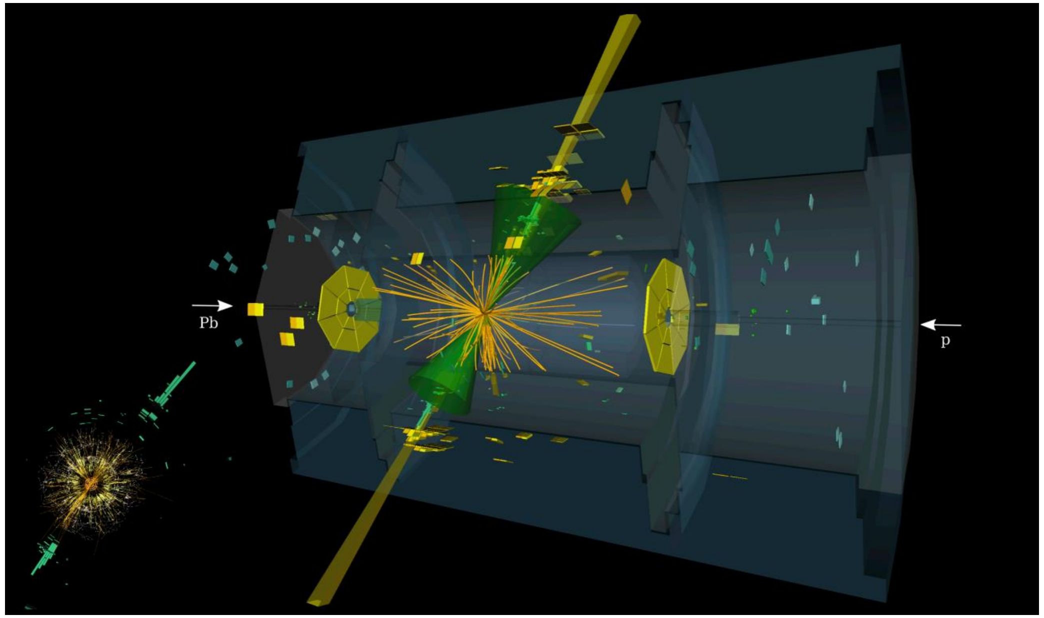

Dijet Measurements in Two Collision Systems

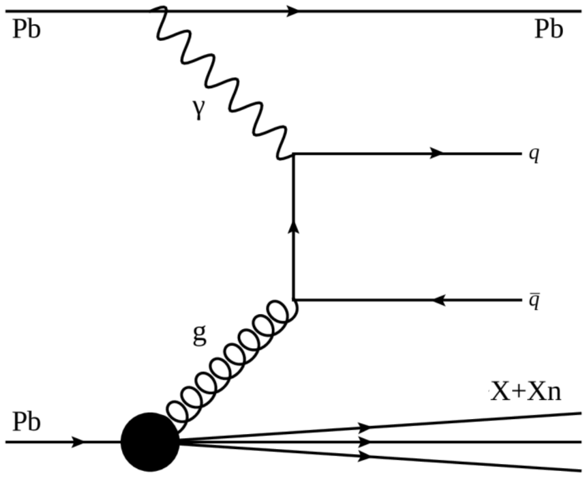

$$H_T = \sum_i p_T^i$$

$$z_\gamma = \frac{M_{jets} e^{+y_{jets}}}{\sqrt{s_{NN}}}$$

$$x_A = \frac{M_{jets} e^{-y_{jets}}}{\sqrt{s_{NN}}}$$

$$p_T^{avg} = \frac{p_T^1 + p_T^2}{2}$$

$$x_p = \frac{2 p_T^{avg} \cosh(y^*) e^{+y_b}}{\sqrt{s}}$$

$$x_{Pb} = \frac{2 p_T^{avg} \cosh(y^*) e^{-y_b}}{\sqrt{s}}$$

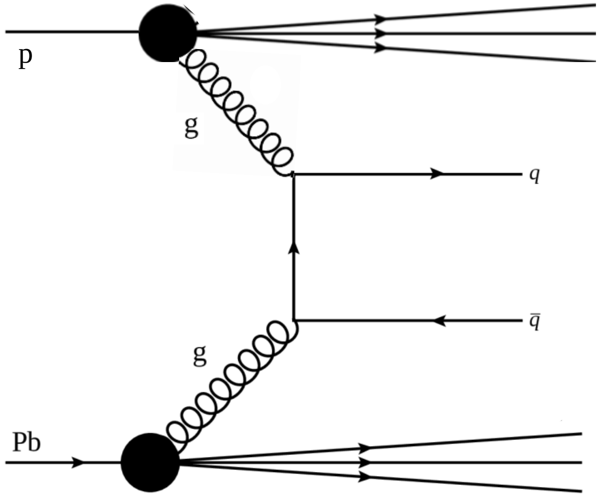

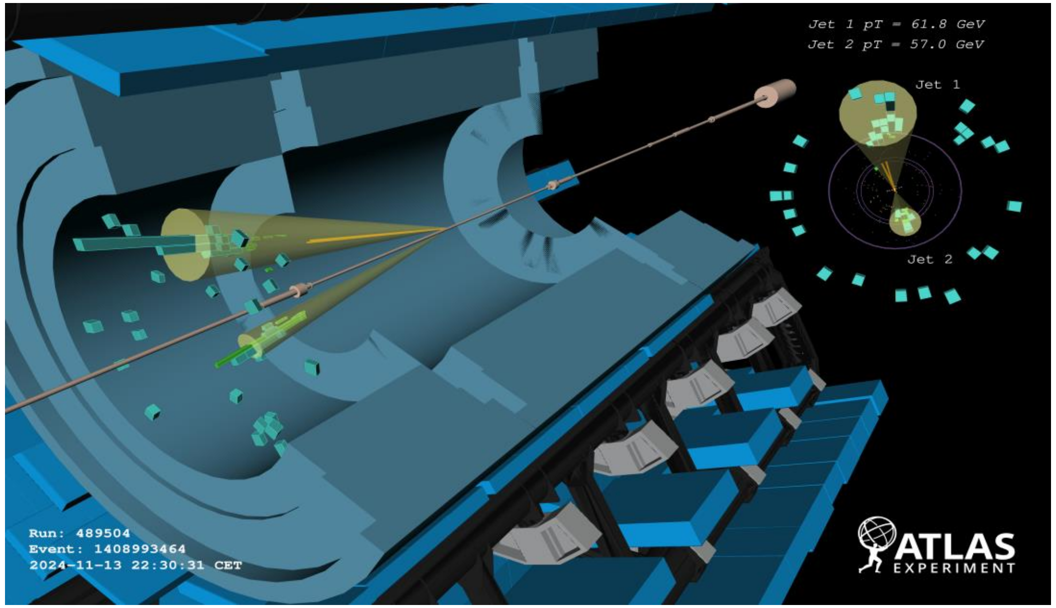

$$y_b = \frac{y_1 + y_2}{2}$$

$$y^* = \frac{|y_1 - y_2|}{2}$$

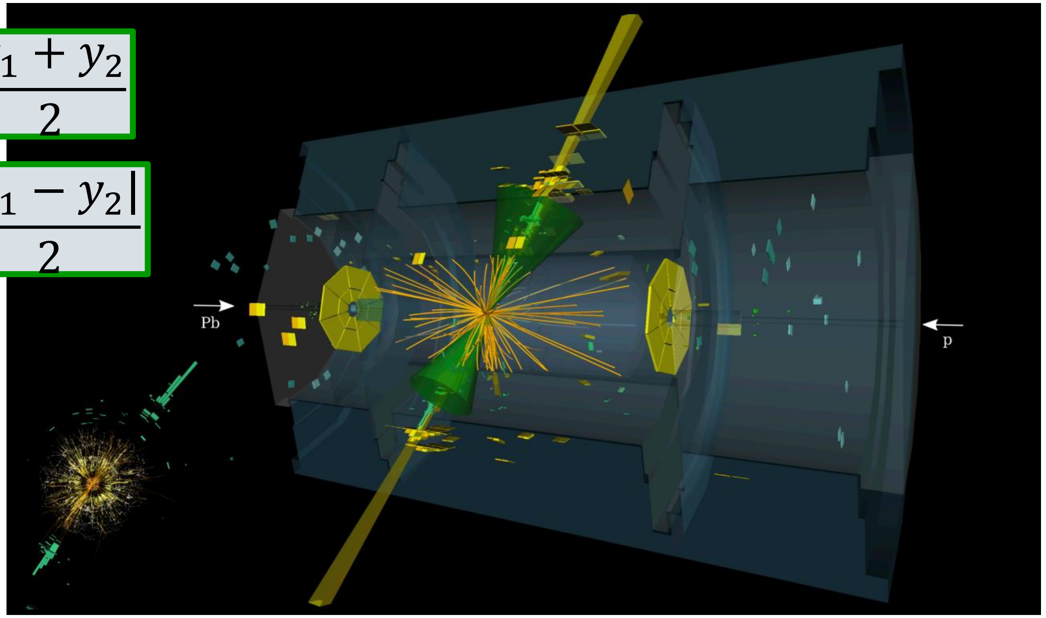

Dijet Measurements in Two Collision Systems

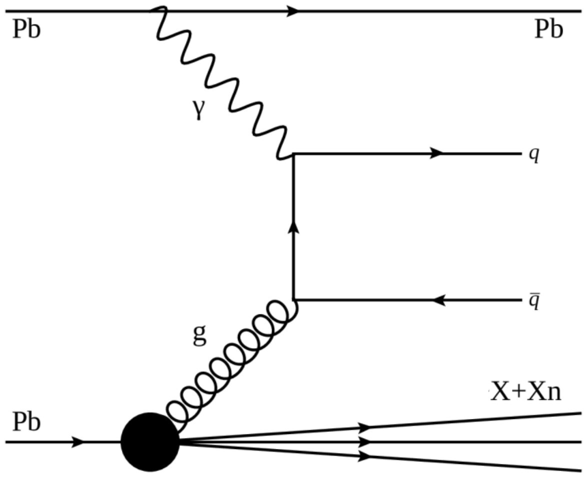

Proxy for Q^2

$$H_T = \sum_i p_T^i$$

$$z_\gamma = \frac{M_{jets} e^{+y_{jets}}}{\sqrt{s_{NN}}}$$

$$x_A = \frac{M_{jets} e^{-y_{jets}}}{\sqrt{s_{NN}}}$$

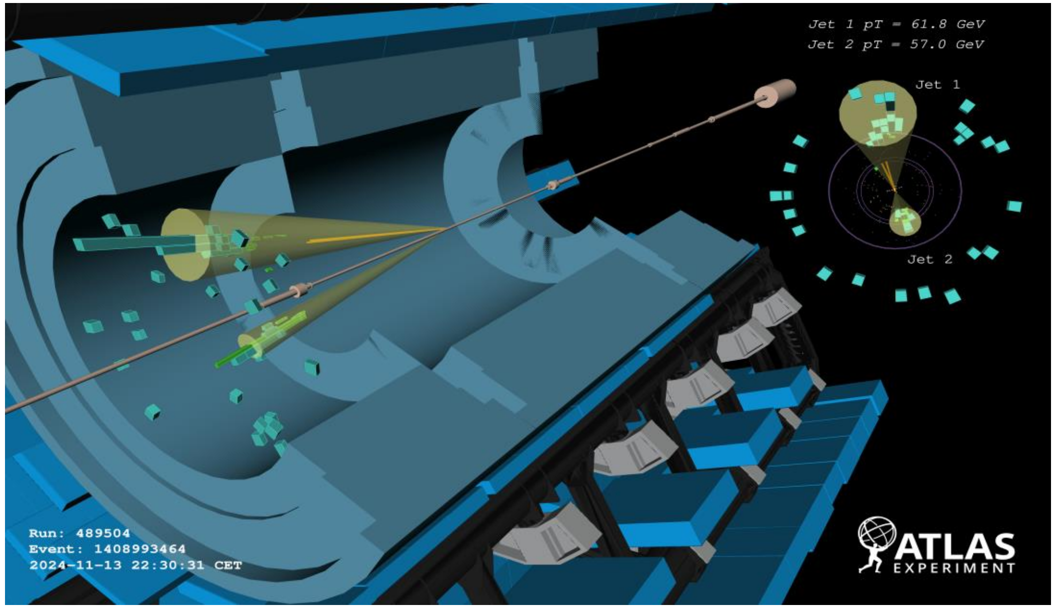

$$p_T^{avg} = \frac{p_T^1 + p_T^2}{2}$$

$$x_p = \frac{2 p_T^{avg} \cosh(y^*) e^{+y_b}}{\sqrt{s}}$$

$$x_{Pb} = \frac{2 p_T^{avg} \cosh(y^*) e^{-y_b}}{\sqrt{s}}$$

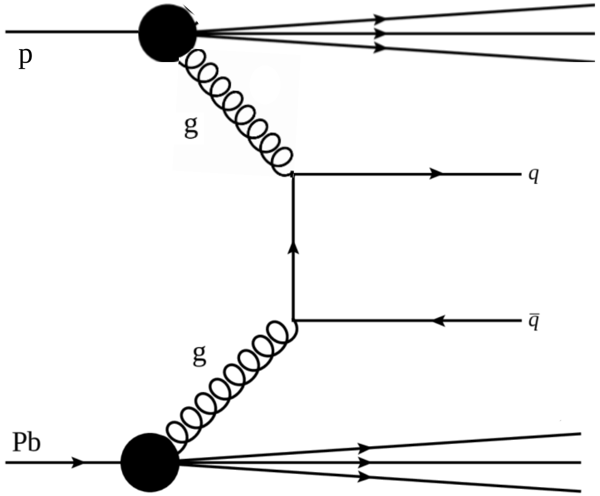

$$y_b = \frac{y_1 + y_2}{2}$$

$$y^* = \frac{|y_1 - y_2|}{2}$$

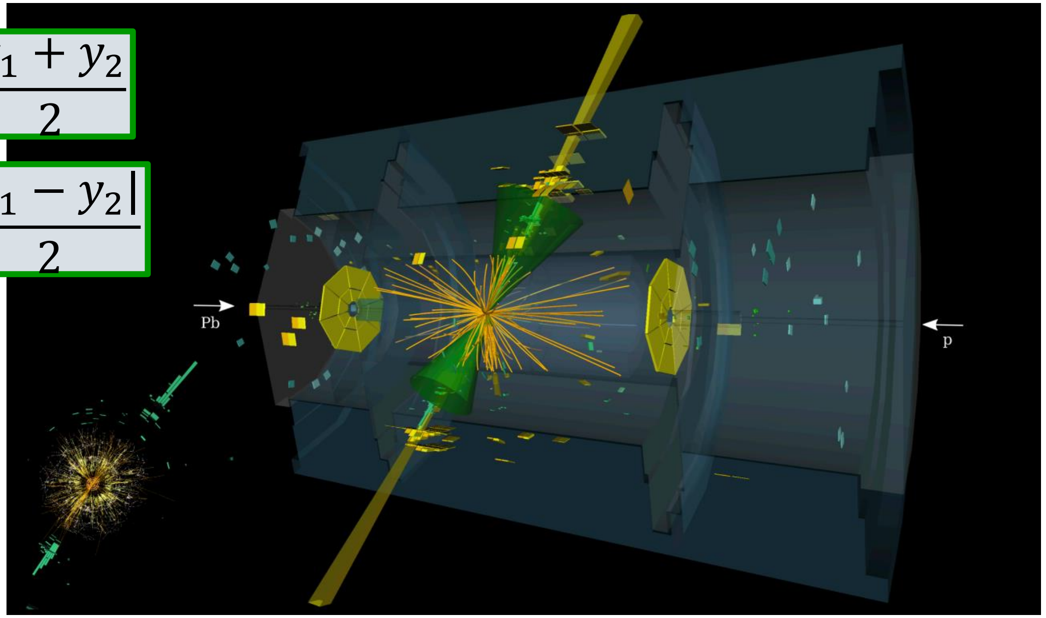

Dijet Measurements in Two Collision Systems

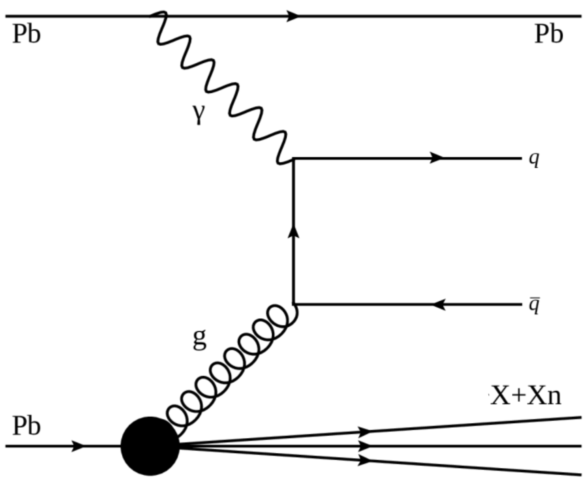

Proxy for Q^2

$$H_T = \sum_i p_T^i$$

Probe parton energy fraction

$$z_\gamma = \frac{M_{jets} e^{+y_{jets}}}{\sqrt{s_{NN}}}$$

$$x_A = \frac{M_{jets} e^{-y_{jets}}}{\sqrt{s_{NN}}}$$

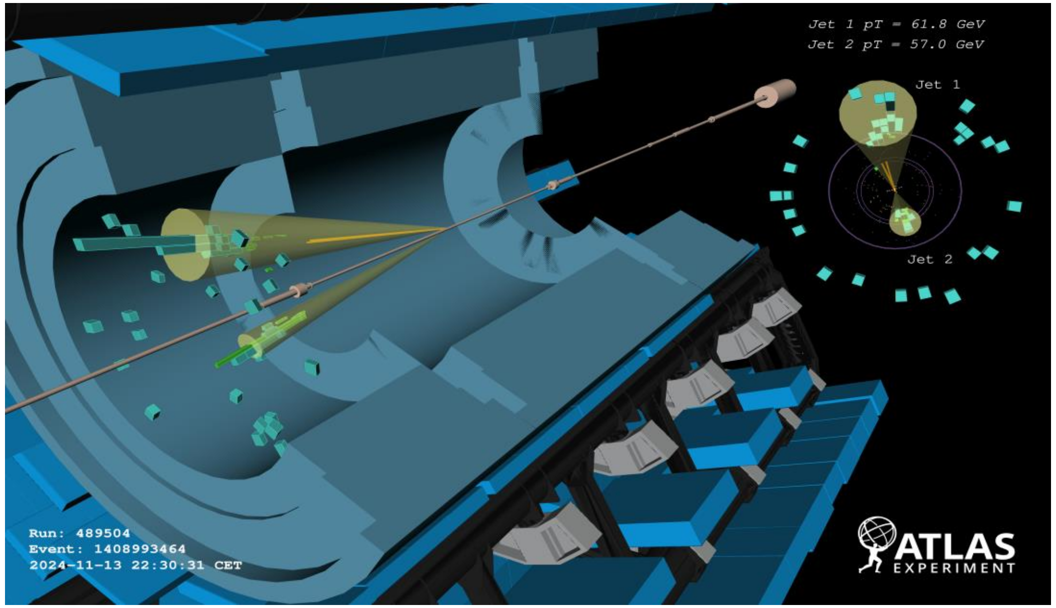

$$p_T^{avg} = \frac{p_T^1 + p_T^2}{2}$$

$$x_p = \frac{2 p_T^{avg} \cosh(y^*) e^{+y_b}}{\sqrt{s}}$$

$$x_{Pb} = \frac{2 p_T^{avg} \cosh(y^*) e^{-y_b}}{\sqrt{s}}$$

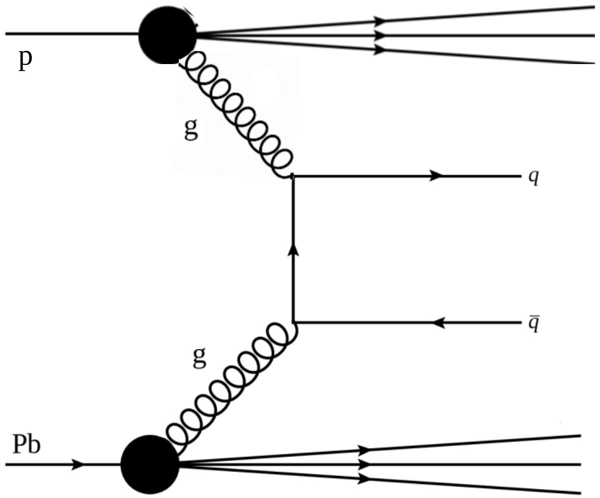

$$y_b = \frac{y_1 + y_2}{2}$$

$$y^* = \frac{|y_1 - y_2|}{2}$$

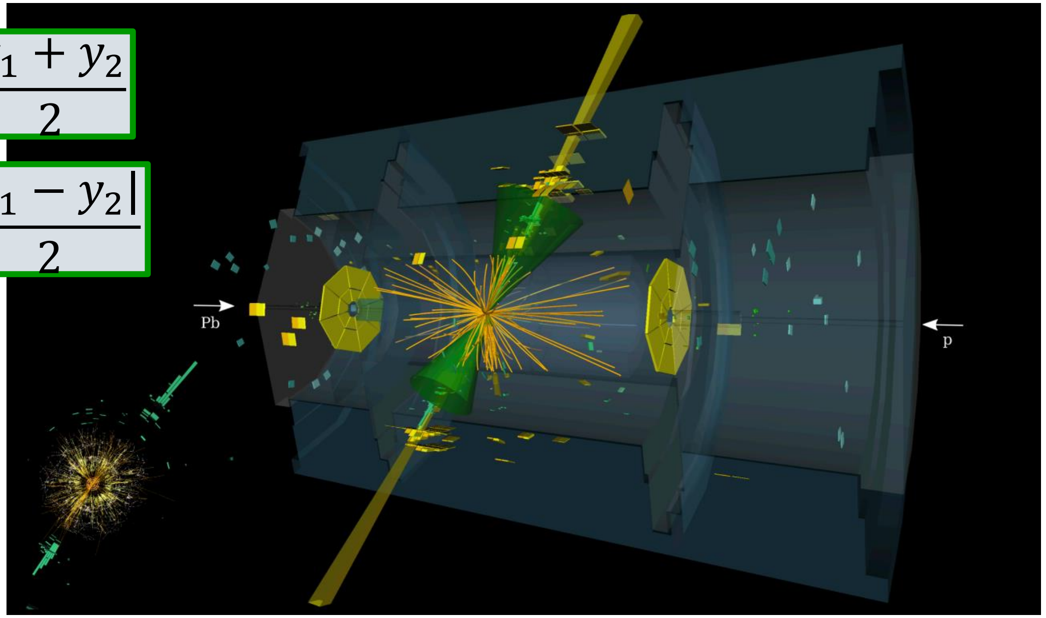

Dijet Measurements in Two Collision Systems

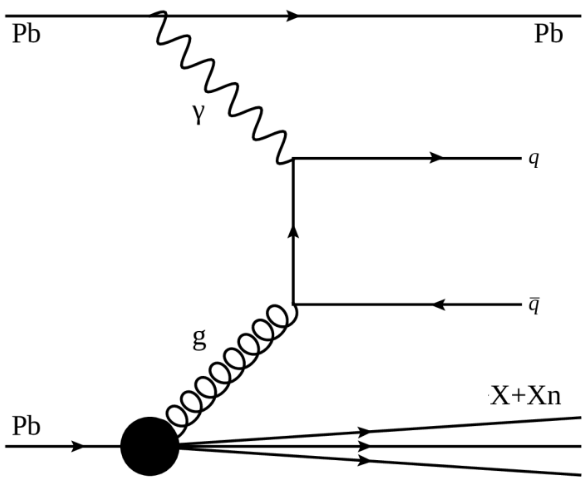

Proxy for Q^2

$$H_T = \sum_i p_T^i$$

Probe parton energy fraction

$$z_\gamma = \frac{M_{jets} e^{+y_{jets}}}{\sqrt{s_{NN}}}$$

Target parton energy fraction

$$x_A = \frac{M_{jets} e^{-y_{jets}}}{\sqrt{s_{NN}}}$$

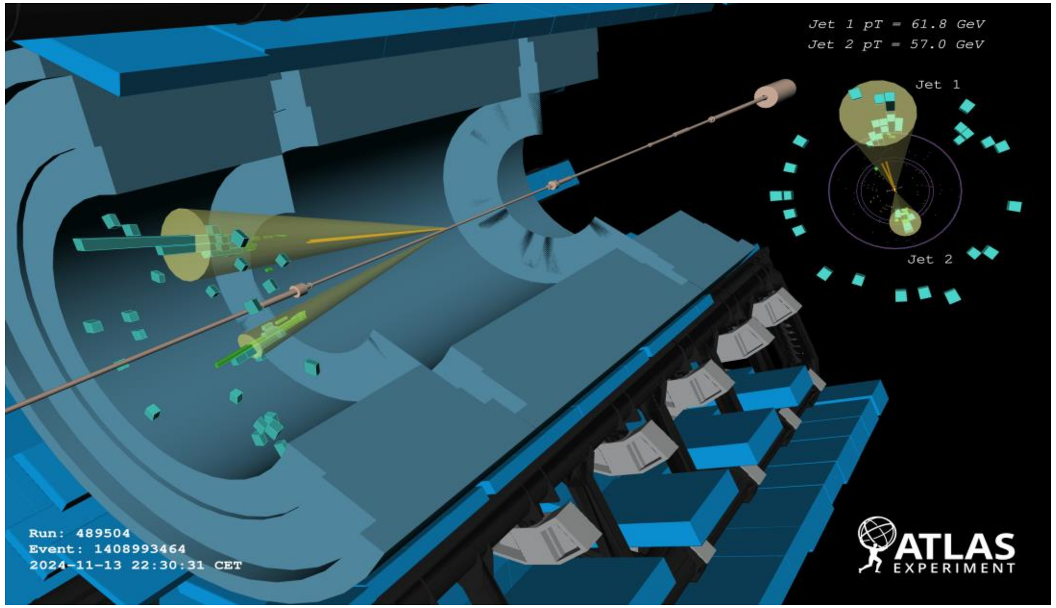

$$p_T^{avg} = \frac{p_T^1 + p_T^2}{2}$$

$$x_p = \frac{2p_T^{avg} \cosh(y^*) e^{+y_b}}{\sqrt{s}}$$

$$x_{Pb} = \frac{2p_T^{avg} \cosh(y^*) e^{-y_b}}{\sqrt{s}}$$

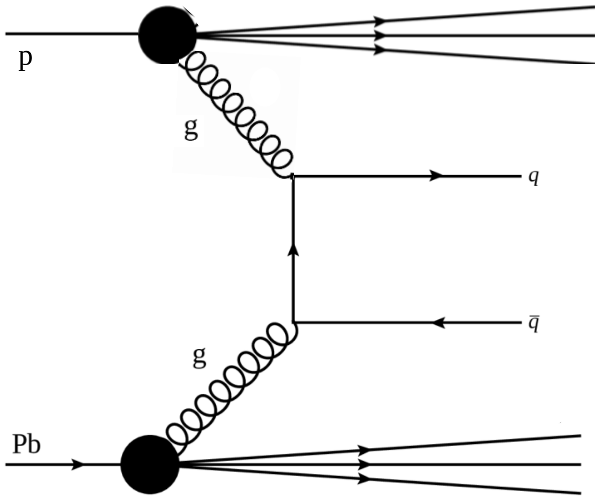

$$y_b = \frac{y_1 + y_2}{2}$$

$$y^* = \frac{|y_1 - y_2|}{2}$$

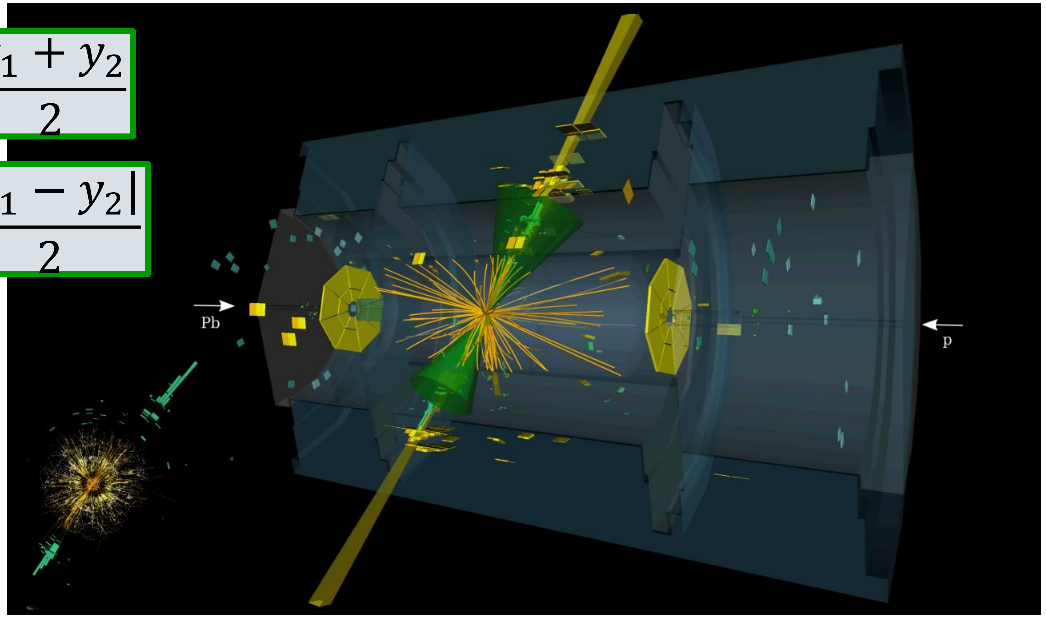

Centrality-Dependence in p+Pb

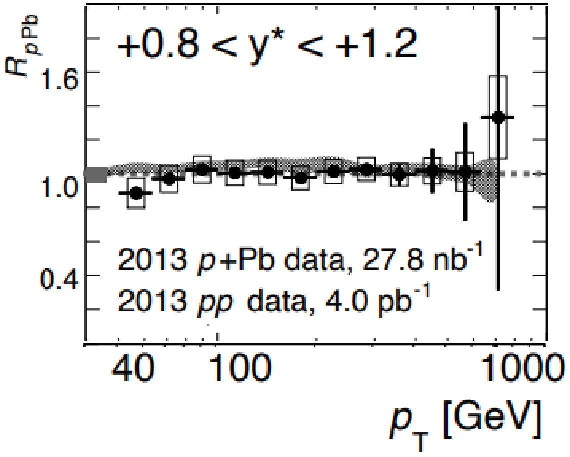

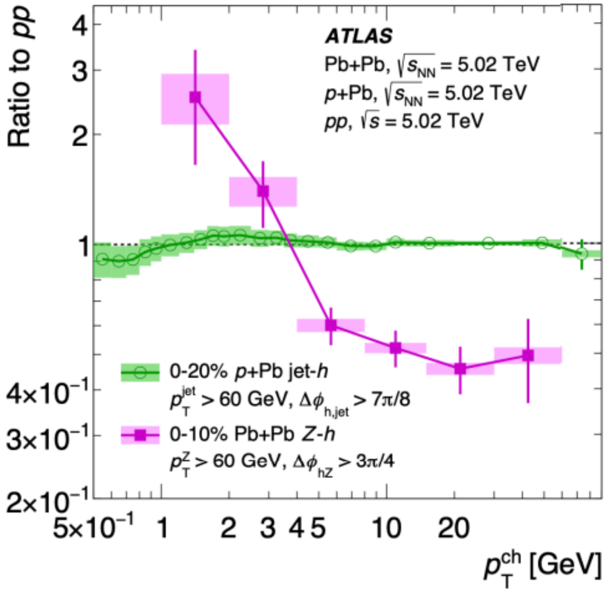

- Strong evidence supports the claim there is no jet quenching p+Pb collisions.
  - Tight constraints from ATLAS, arXiv:2206.01138
- Variation with centrality is an initial, not final state effect!

Centrality-Dependence in p+Pb

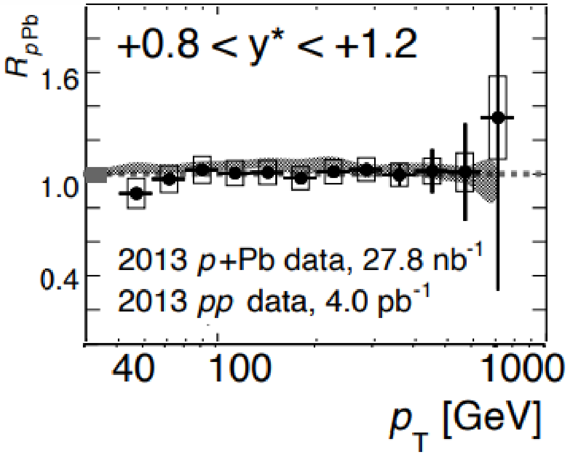

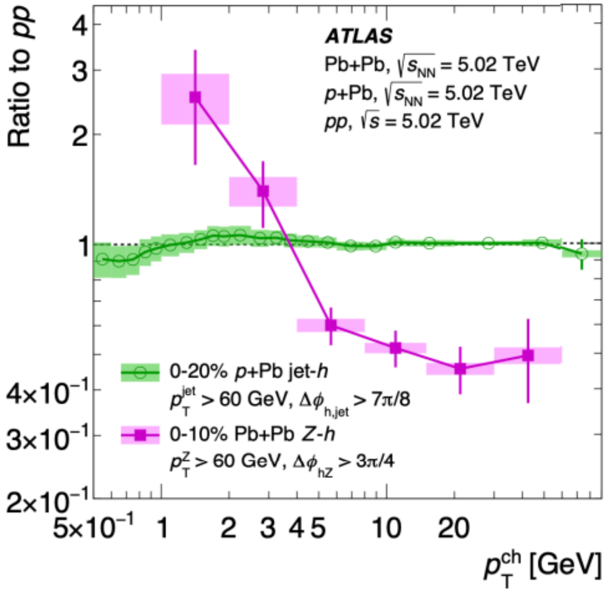

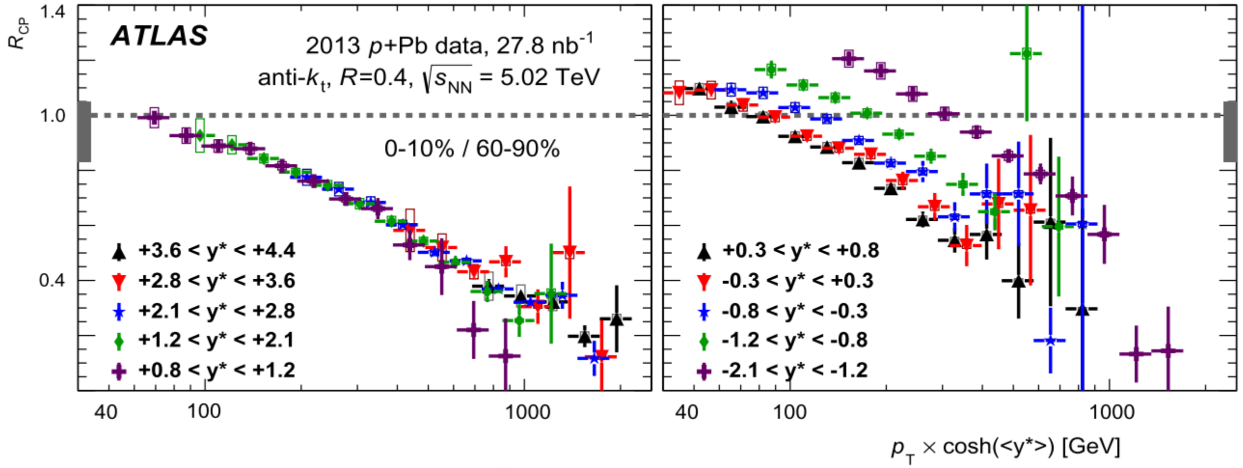

- Strong evidence supports the claim there is no jet quenching p+Pb collisions.
  - Tight constraints from ATLAS, arXiv:2206.01138
- Variation with centrality is an initial, not final state effect!

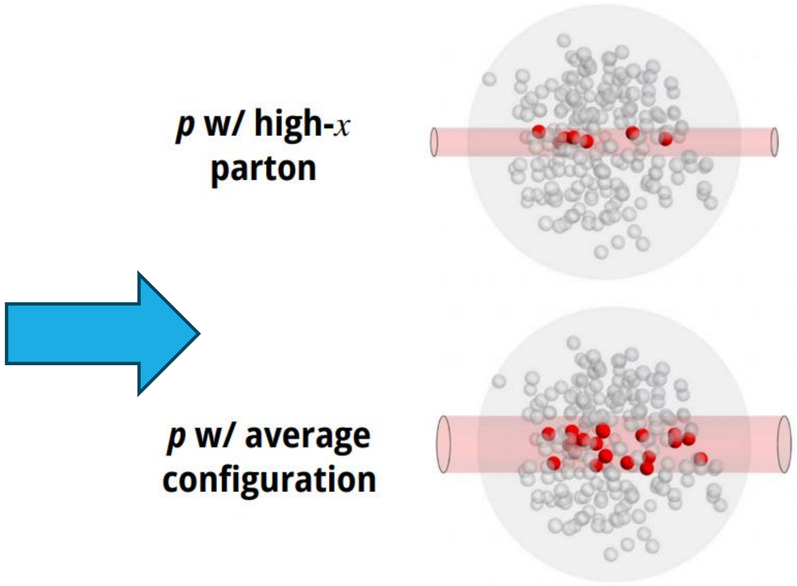

This effect has been quite successfully described through a framework of color fluctuations.

Proton probes containing a high-x parton have smaller than average size (color transparency).

Sketch from Alvioli et al., arXiv:1709.04993

Centrality-Dependence in p+Pb

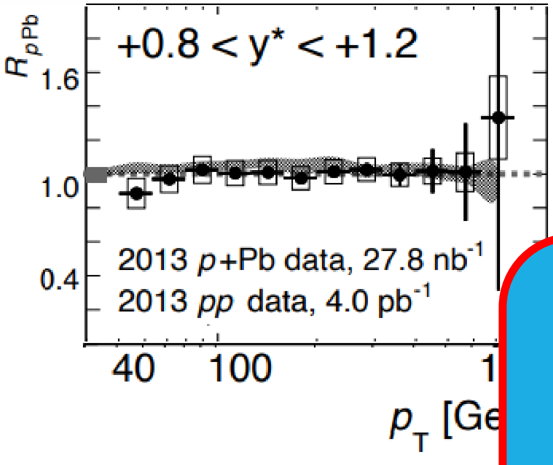

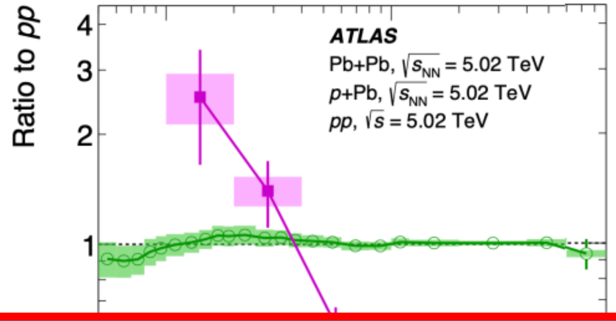

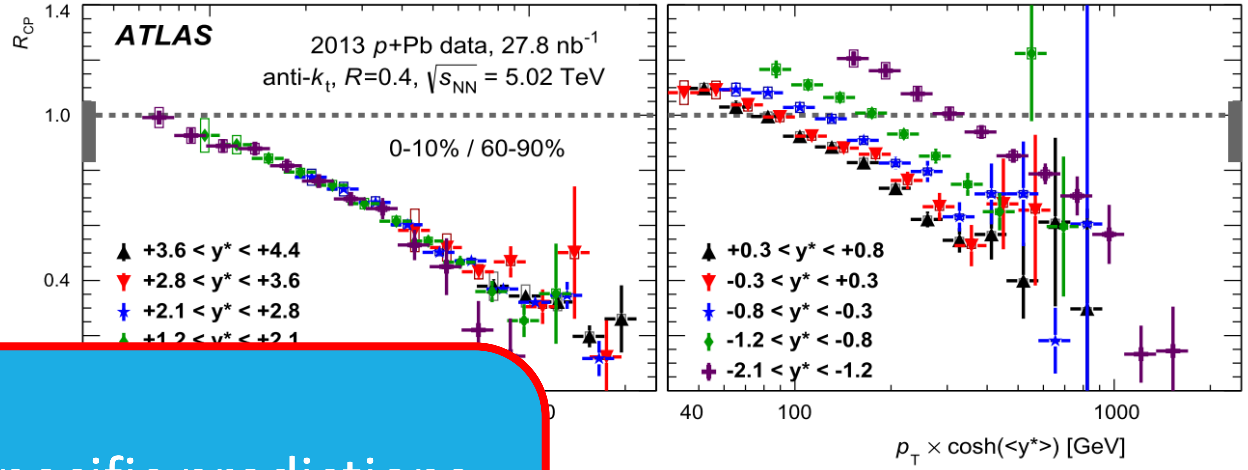

Color transparency makes specific predictions about dependence on x_p, not x_{Pb}. Dijets can probe this effect in unprecedented detail!

- Strong evidence supp quenching p+Pb collisions.
  - Tight constraints from ATLAS, arXiv:2206.01138
- Variation with centrality is an initial, not final state effect!

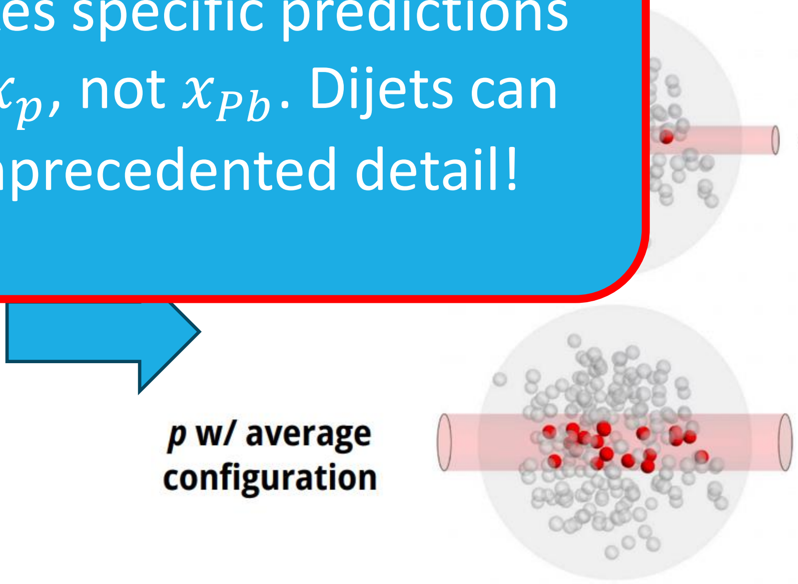

This effect has been quite successfully described through a framework of color fluctuations.

Proton probes containing a high-x parton have smaller than average size (color transparency).

Sketch from Alvioli et al., arXiv:1709.04993

Mapping Results to Parton Kinematics

$$y^* = \frac{|y_1 - y_2|}{2}$$

$$y_b = \frac{y_1 + y_2}{2}$$

$$x_p = \frac{2p_T^{avg}\cosh(y^*)e^{+y_b}}{\sqrt{s}}$$

$$x_{Pb} = \frac{2p_T^{avg}\cosh(y^*)e^{-y_b}}{\sqrt{s}}$$

$$R_{CP}^{\frac{0-10\%}{60-90\%}}(p_T^{avg}, y_b, y^*) = \frac{\frac{1}{< T_{AB}^{0-10\%} >}\frac{1}{N_{evt}^{0-10\%}}\frac{dN_{dijet}^{0-10\%}}{dp_T^{avg}dy_b dy^*}}{\frac{1}{< T_{AB}^{60-90\%} >}\frac{1}{N_{evt}^{60-90\%}}\frac{dN_{dijet}^{60-90\%}}{dp_T^{avg}dy_b dy^*}}$$

R_{CP}: Ratio of yields with high vs. low event activity

Mapping Results to Parton Kinematics

$$y^* = \frac{|y_1 - y_2|}{2}$$

$$y_b = \frac{y_1 + y_2}{2}$$

$$x_p = \frac{2p_T^{avg}\cosh(y^*)e^{+y_b}}{\sqrt{s}}$$

$$x_{Pb} = \frac{2p_T^{avg}\cosh(y^*)e^{-y_b}}{\sqrt{s}}$$

$$R_{CP}^{\frac{0-10\%}{60-90\%}}(p_T^{avg}, y_b, y^*) = \frac{\frac{1}{< T_{AB}^{0-10\%} >}\frac{1}{N_{evt}^{0-10\%}}\frac{dN_{dijet}^{0-10\%}}{dp_T^{avg}dy_b dy^*}}{\frac{1}{< T_{AB}^{60-90\%} >}\frac{1}{N_{evt}^{60-90\%}}\frac{dN_{dijet}^{60-90\%}}{dp_T^{avg}dy_b dy^*}}$$

R_{CP}: Ratio of yields with high vs. low event activity

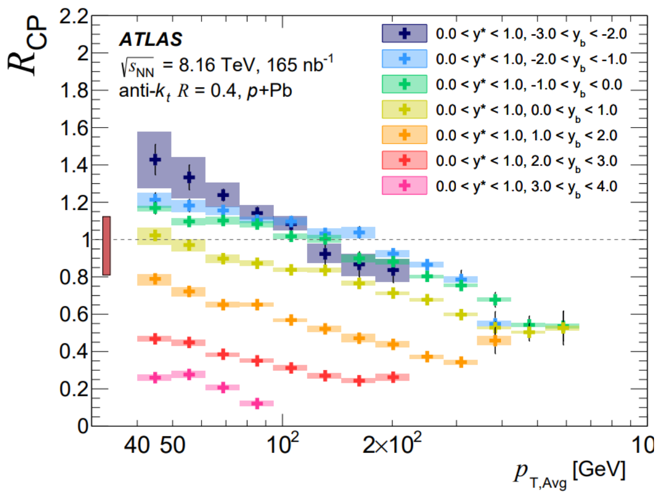

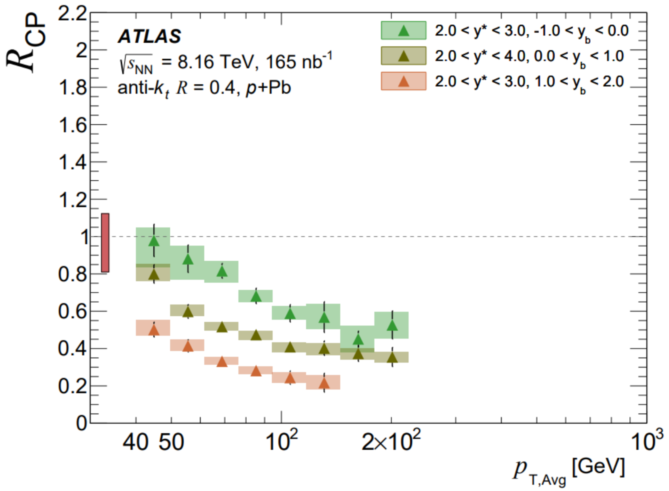

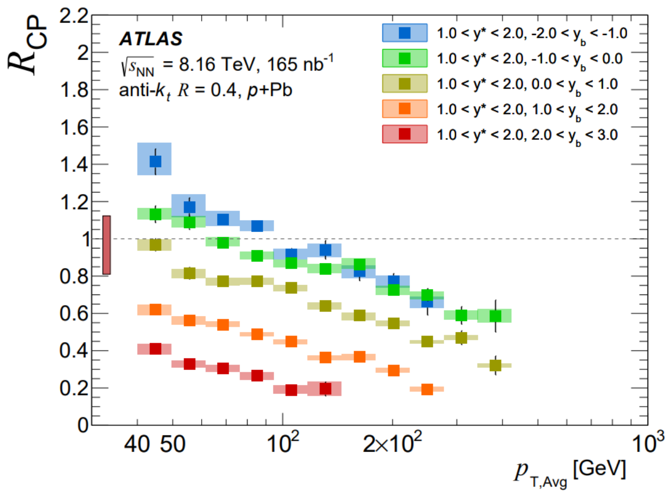

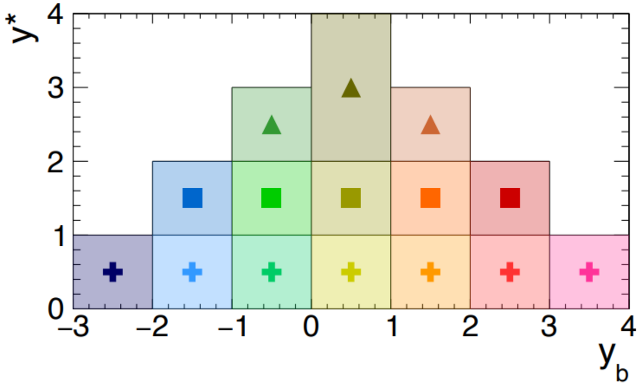

Mapping Results to Parton Kinematics

$$y^* = \frac{|y_1 - y_2|}{2}$$

$$y_b = \frac{y_1 + y_2}{2}$$

$$x_p = \frac{2p_T^{avg}\cosh(y^*)e^{+y_b}}{\sqrt{s}}$$

$$x_{Pb} = \frac{2p_T^{avg}\cosh(y^*)e^{-y_b}}{\sqrt{s}}$$

$$R_{CP}^{\frac{0-10\%}{60-90\%}}(p_T^{avg}, y_b, y^*) = \frac{\frac{1}{< T_{AB}^{0-10\%} >}\frac{1}{N_{evt}^{0-10\%}}\frac{dN_{dijet}^{0-10\%}}{dp_T^{avg}dy_b dy^*}}{\frac{1}{< T_{AB}^{60-90\%} >}\frac{1}{N_{evt}^{60-90\%}}\frac{dN_{dijet}^{60-90\%}}{dp_T^{avg}dy_b dy^*}}$$

R_{CP}: Ratio of yields with high vs. low event activity

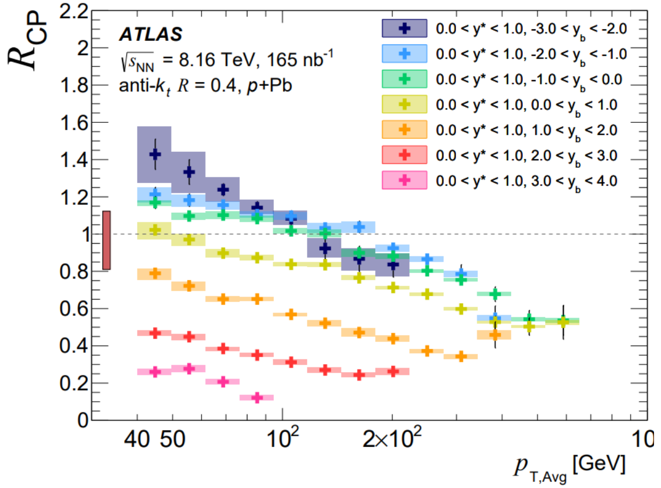

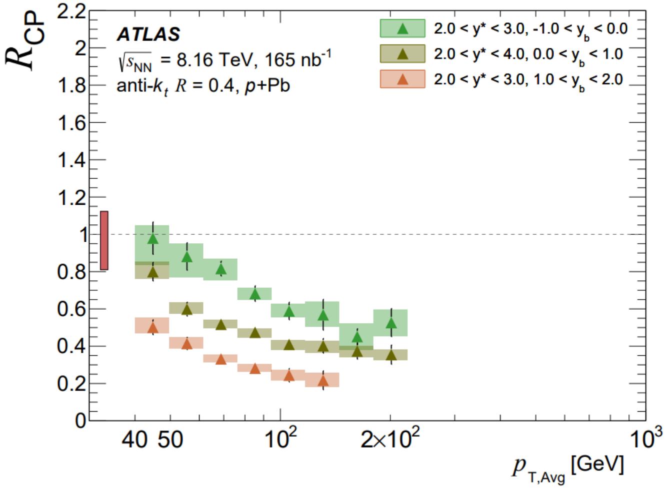

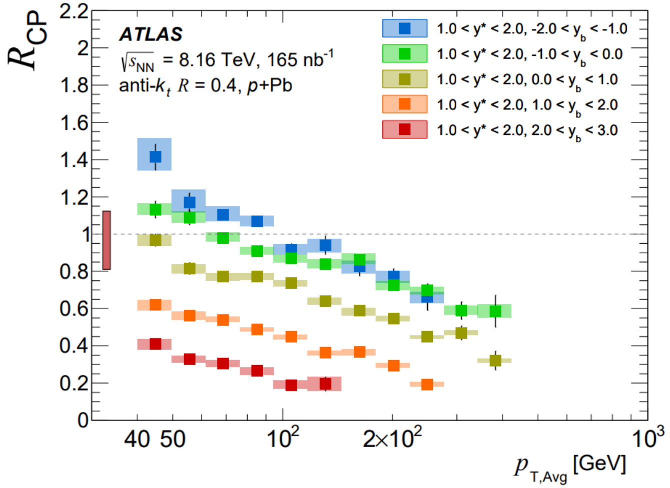

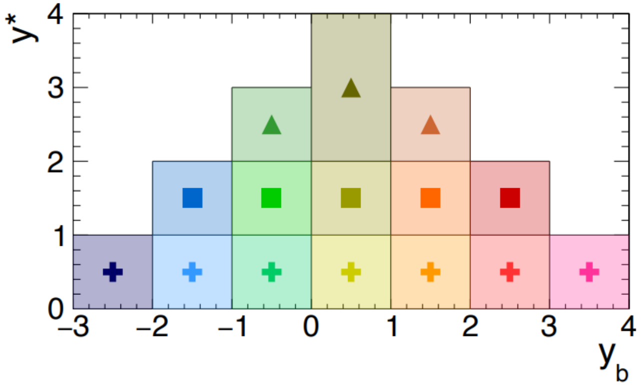

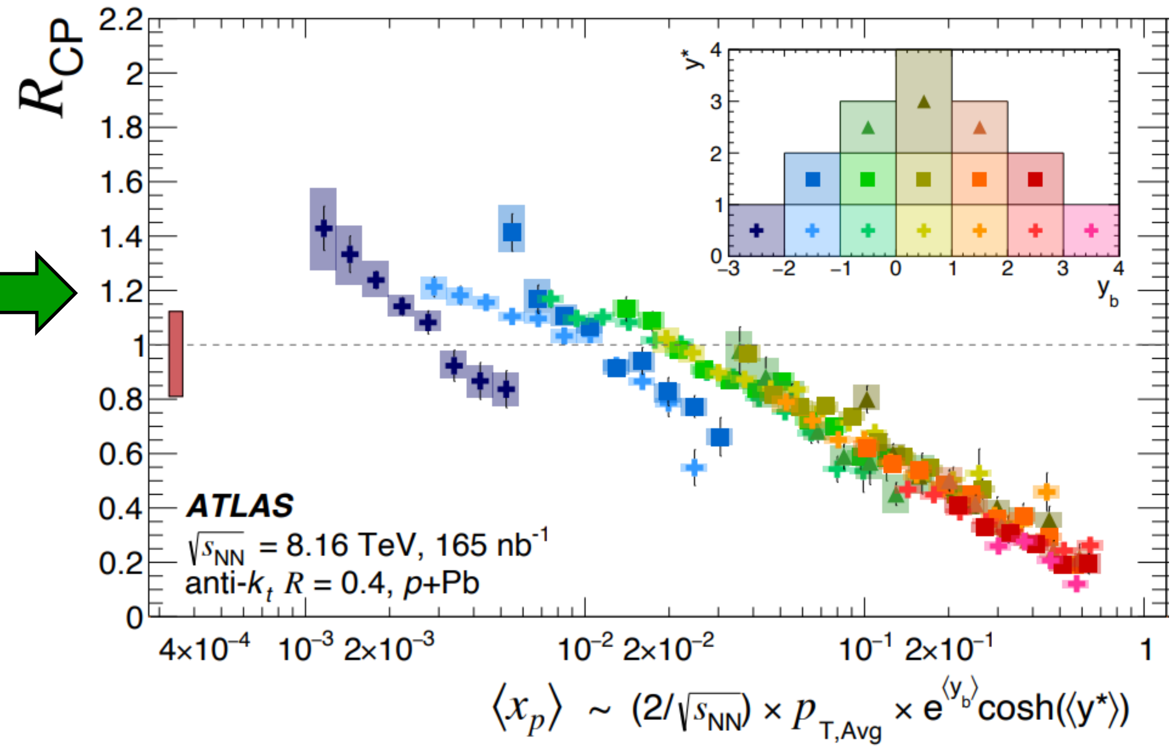

P+Pb Dijet Results: Trends in R_{CP}

More details available in poster by R. Longo

Credit: R. Longo

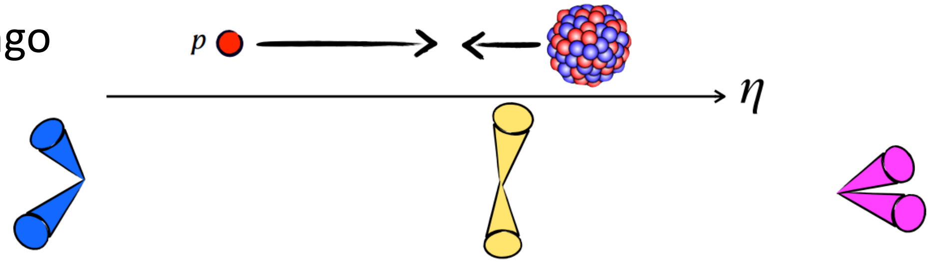

$$x_p = \frac{2p_T^{avg}\cosh(y^*)e^{+y_b}}{\sqrt{s}}$$

$$x_{Pb} = \frac{2p_T^{avg}\cosh(y^*)e^{-y_b}}{\sqrt{s}}$$

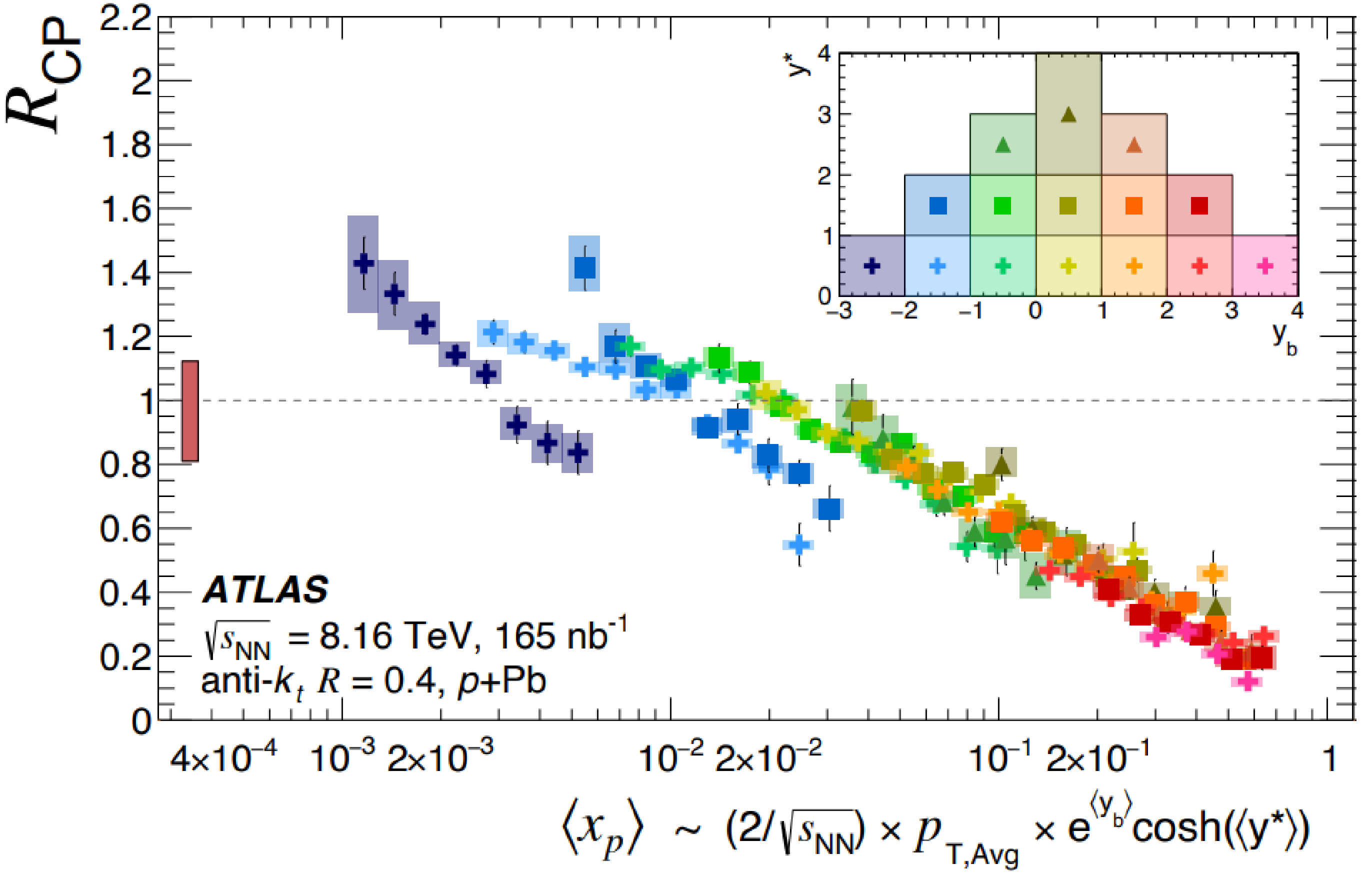

P+Pb Dijet Results: Trends in R_{CP}

More details available in poster by R. Longo

Credit: R. Longo

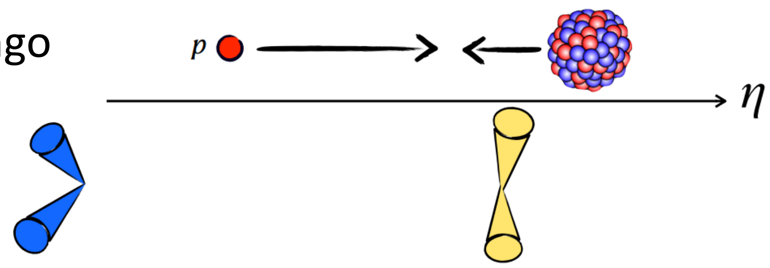

$$x_p = \frac{2p_T^{avg}\cosh(y^*)e^{+y_b}}{\sqrt{s}}$$

$$x_{Pb} = \frac{2p_T^{avg}\cosh(y^*)e^{-y_b}}{\sqrt{s}}$$

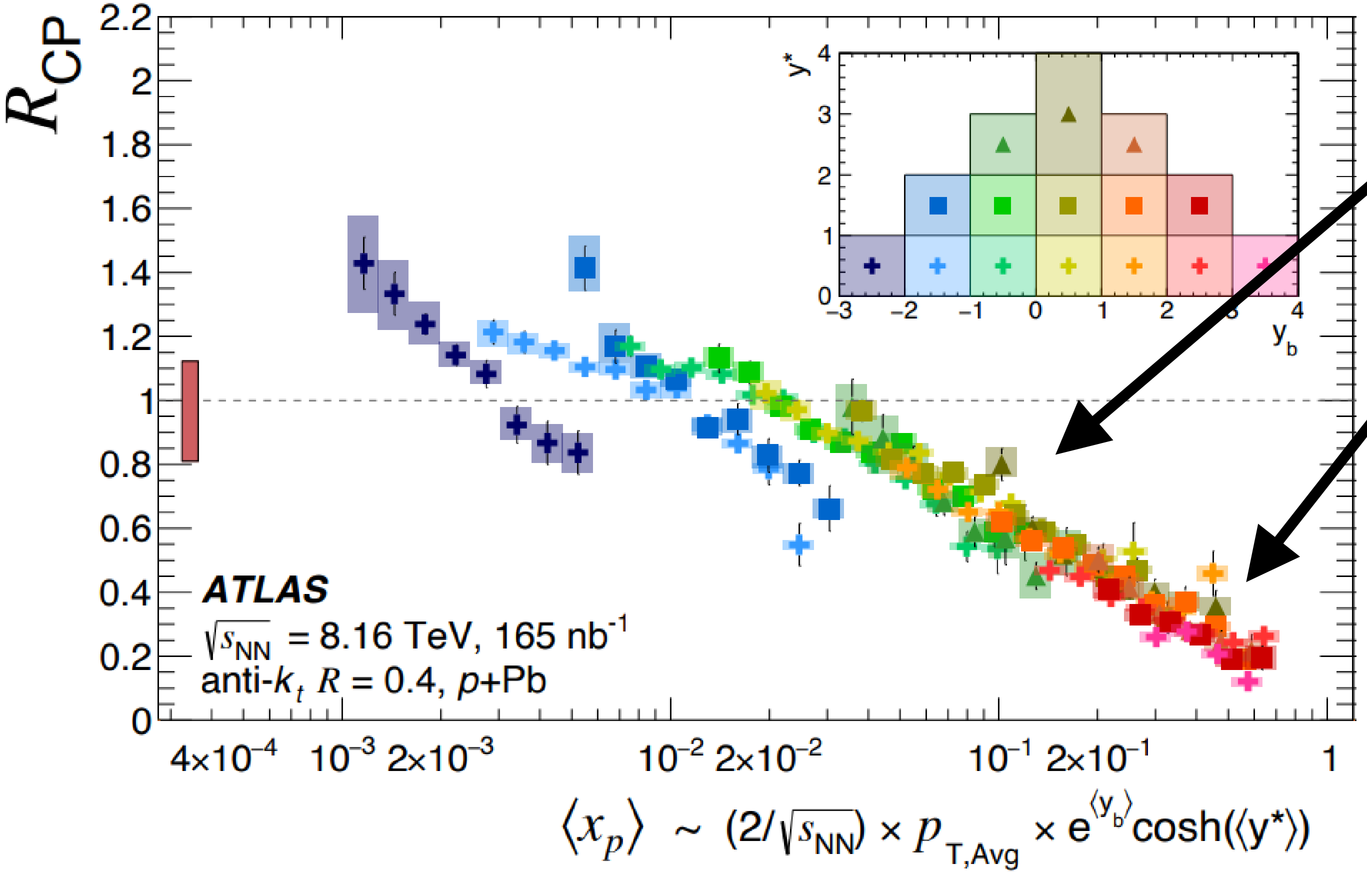

The expected log-linear decrease with x_p from **color transparency** is observed in the valence region.

The very strong suppression at the highest values of x_p is also consistent with this expectation.

P+Pb Dijet Results: Trends in R_{CP}

More details available in poster by R. Longo

Credit: R. Longo

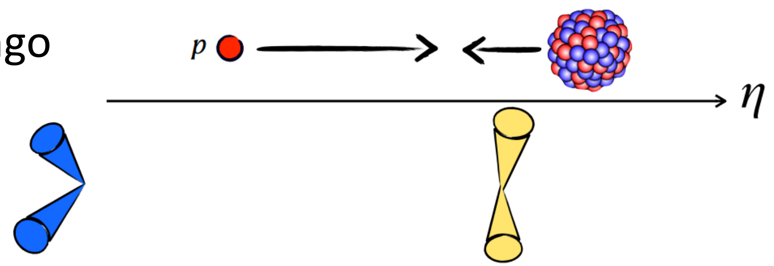

$$x_p = \frac{2p_T^{avg}\cosh(y^*)e^{+y_b}}{\sqrt{s}}$$

$$x_{Pb} = \frac{2p_T^{avg}\cosh(y^*)e^{-y_b}}{\sqrt{s}}$$

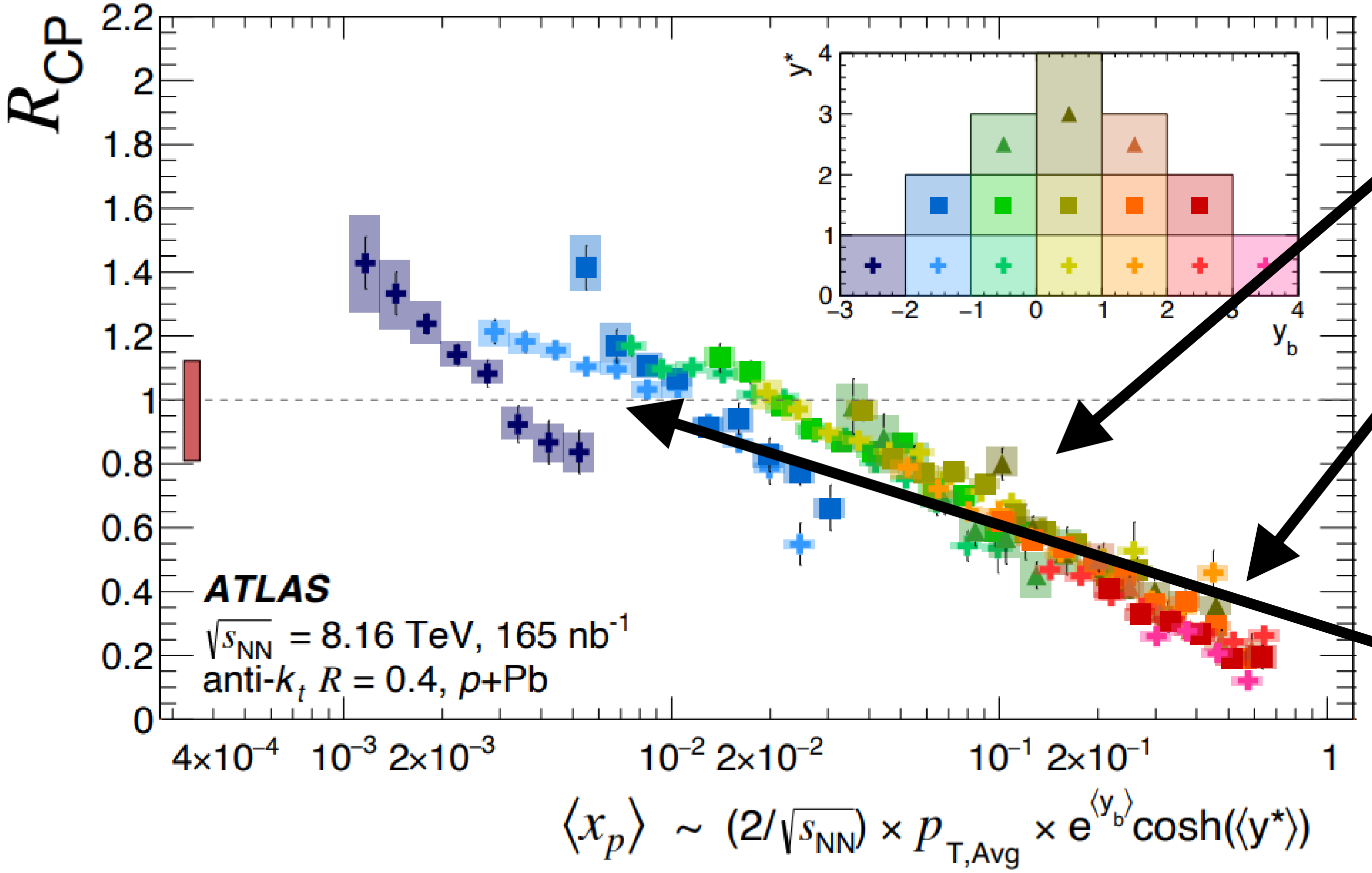

The expected log-linear decrease with x_p from **color transparency** is observed in the valence region.

The very strong suppression at the highest values of x_p is also consistent with this expectation.

The log-linear trend appears to break down in the low-x_p region

P+Pb Dijet Results: Trends in R_{CP}

More details available in poster by R. Longo

Credit: R. Longo

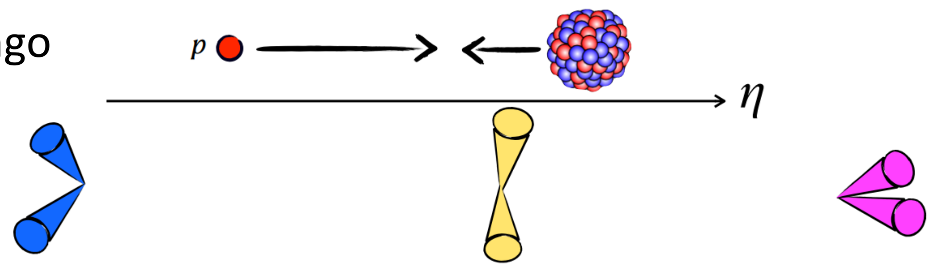

$$x_p = \frac{2p_T^{avg}\cosh(y^*)e^{+y_b}}{\sqrt{s}}$$

$$x_{Pb} = \frac{2p_T^{avg}\cosh(y^*)e^{-y_b}}{\sqrt{s}}$$

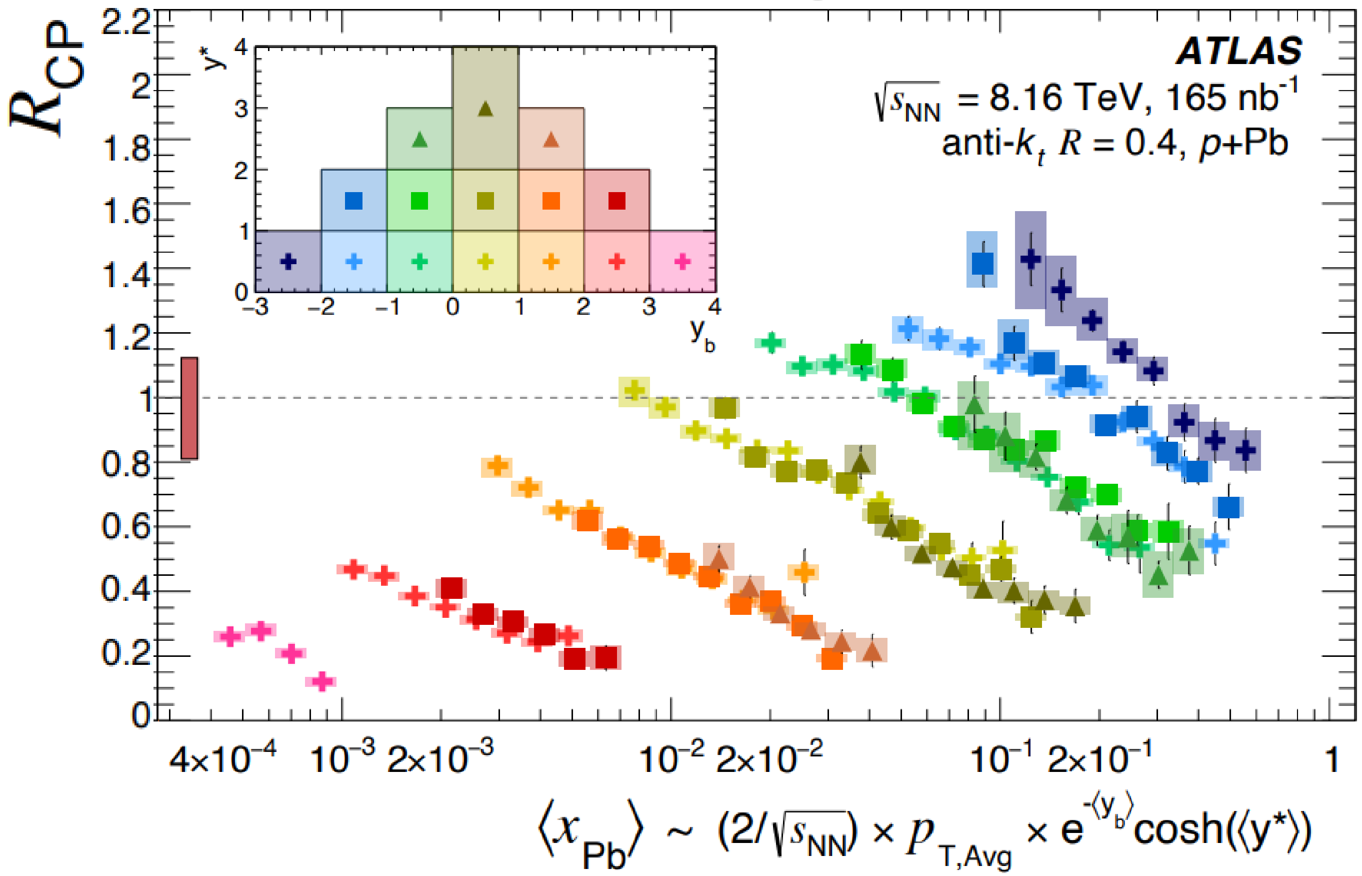

P+Pb Dijet Results: Trends in R_{CP}

More details available in poster by R. Longo

Credit: R. Longo

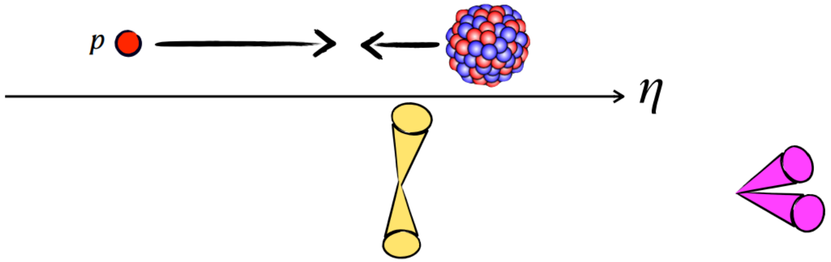

$$x_p = \frac{2p_T^{avg}\cosh(y^*)e^{+y_b}}{\sqrt{s}}$$

$$x_{Pb} = \frac{2p_T^{avg}\cosh(y^*)e^{-y_b}}{\sqrt{s}}$$

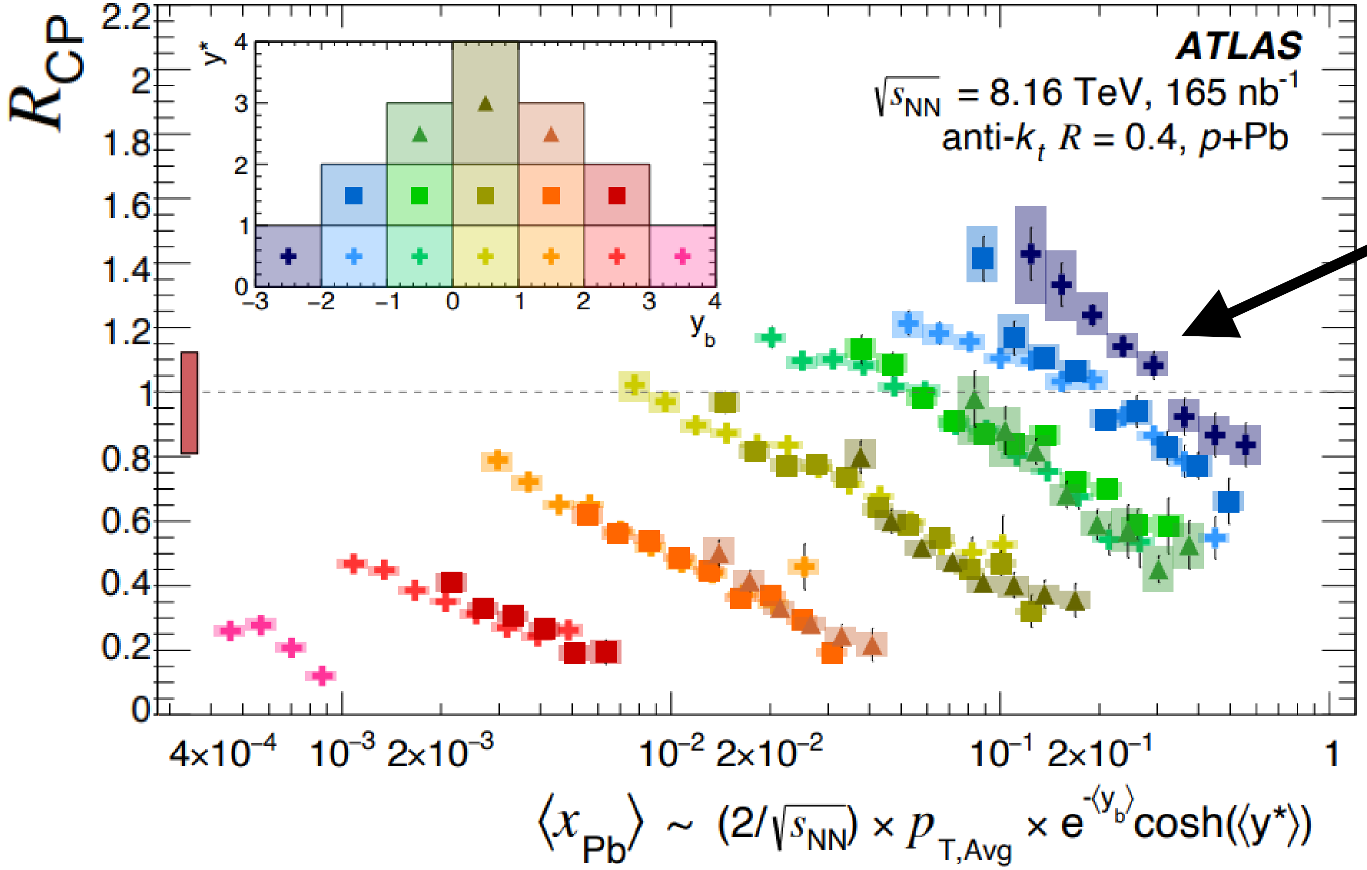

The trend with R_{CP} is much less consistent in x_{Pb} than in x_p .

Suppression depends on y_b and $p_{T,Avg}$ without a clear trend in x_{Pb}.

Nuclear PDFs at Low-x

- Nuclear Parton Distribution Functions (nPDFs) are important for precision measurements of a number of physical observables.

- They are poorly constrained at low-x and intermediate Q^2 due to a lack of available data.
  - 100 GeV² $< Q^2 <$ 1000 GeV² has very little constraint.
  - Nuclear shadowing at low-x in this region is of particular theoretical interest.

- Photo-nuclear jet production provides a clean probe of this kinematic region, similar to DIS:
  - Proposal by [Strikman, Vogt, and White (2005)]
  - Test of sensitivity (right) by [Helenius (2018)]

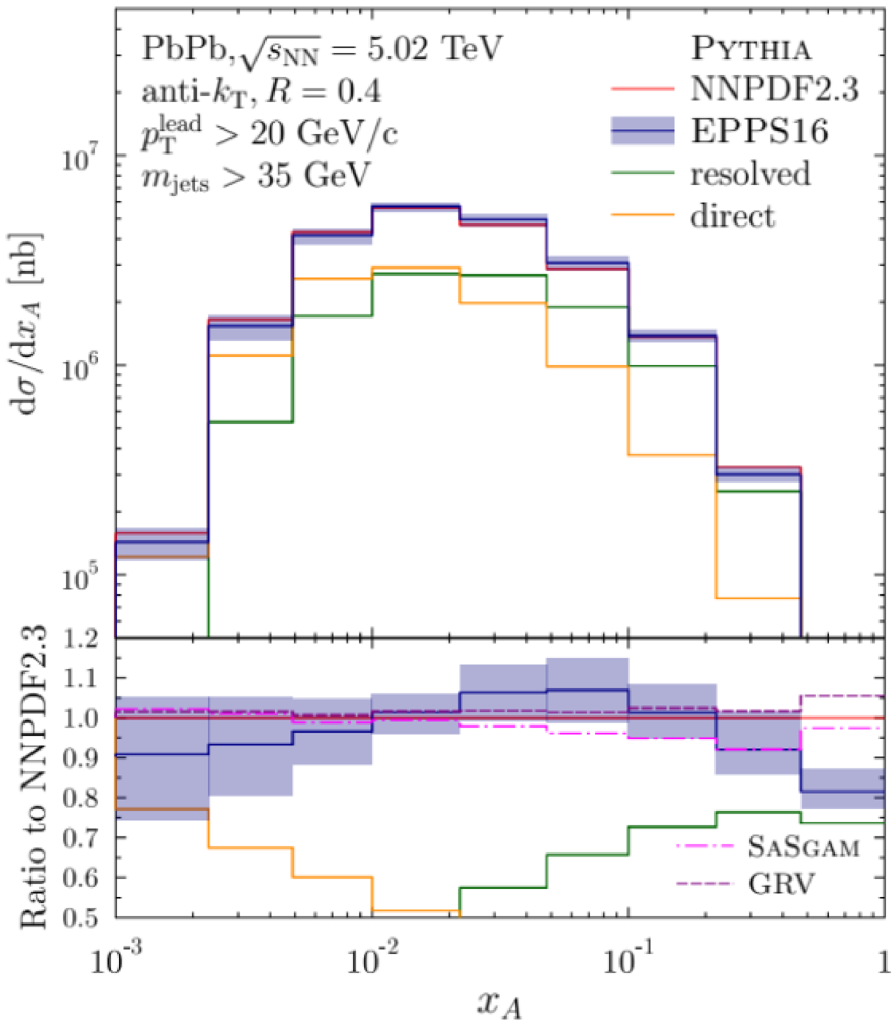

Photonuclear Jet Event Selections

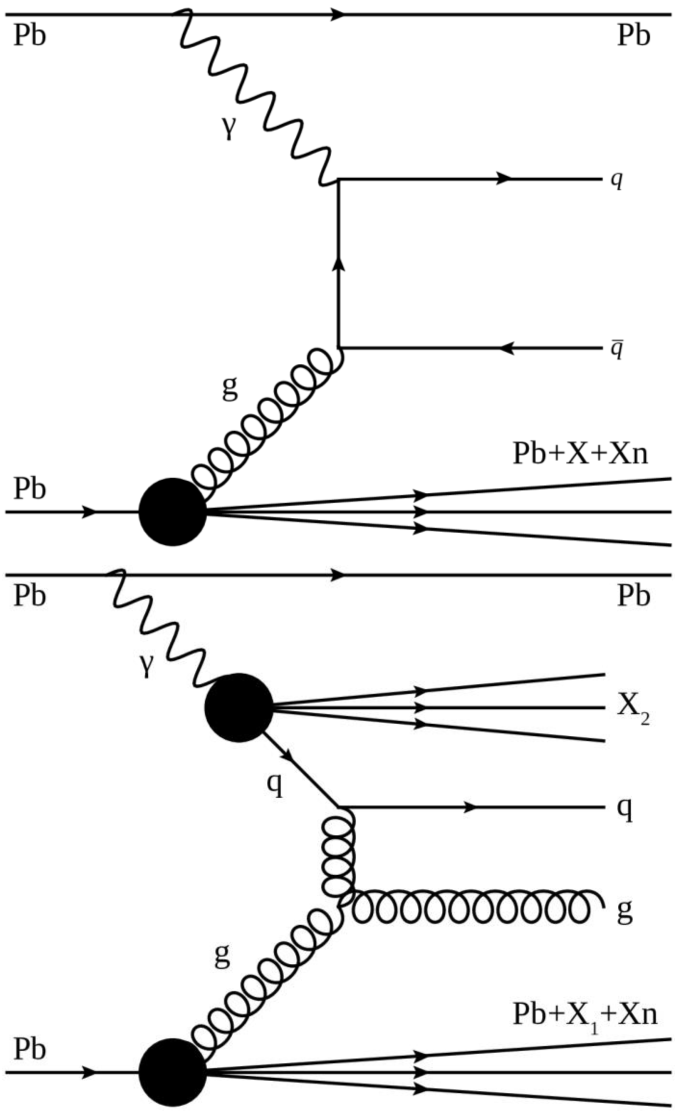

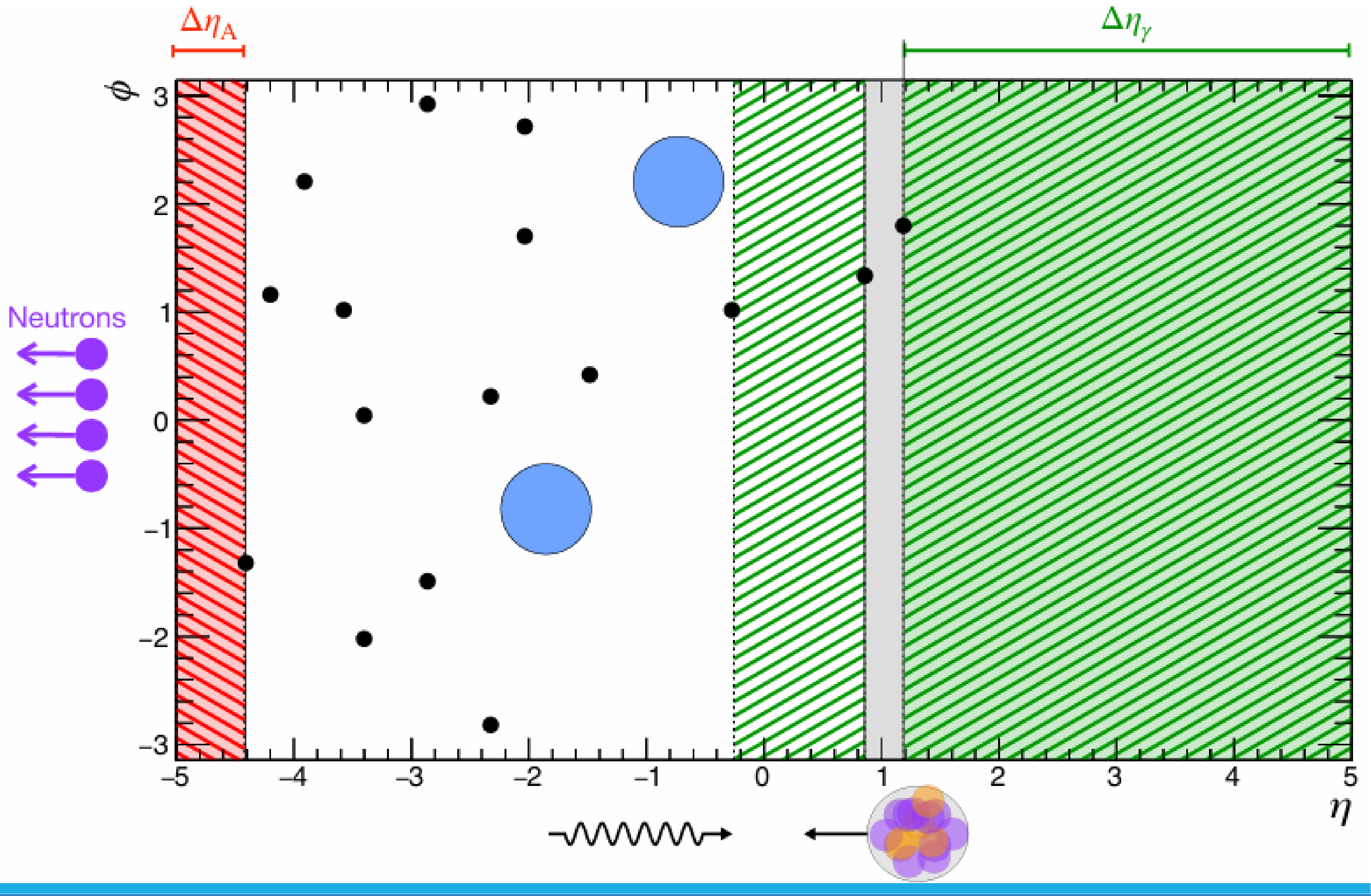

Selecting Photo-nuclear Jet Events

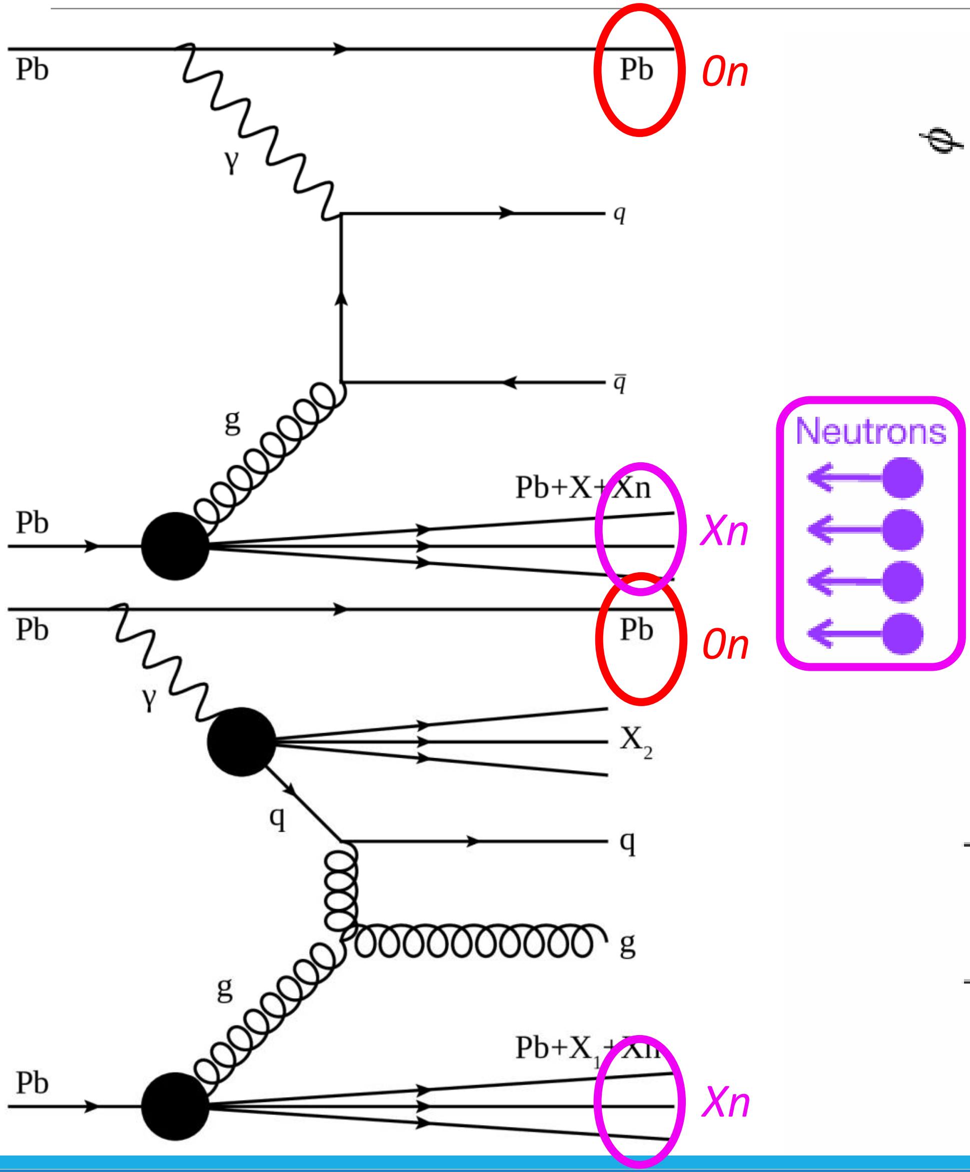

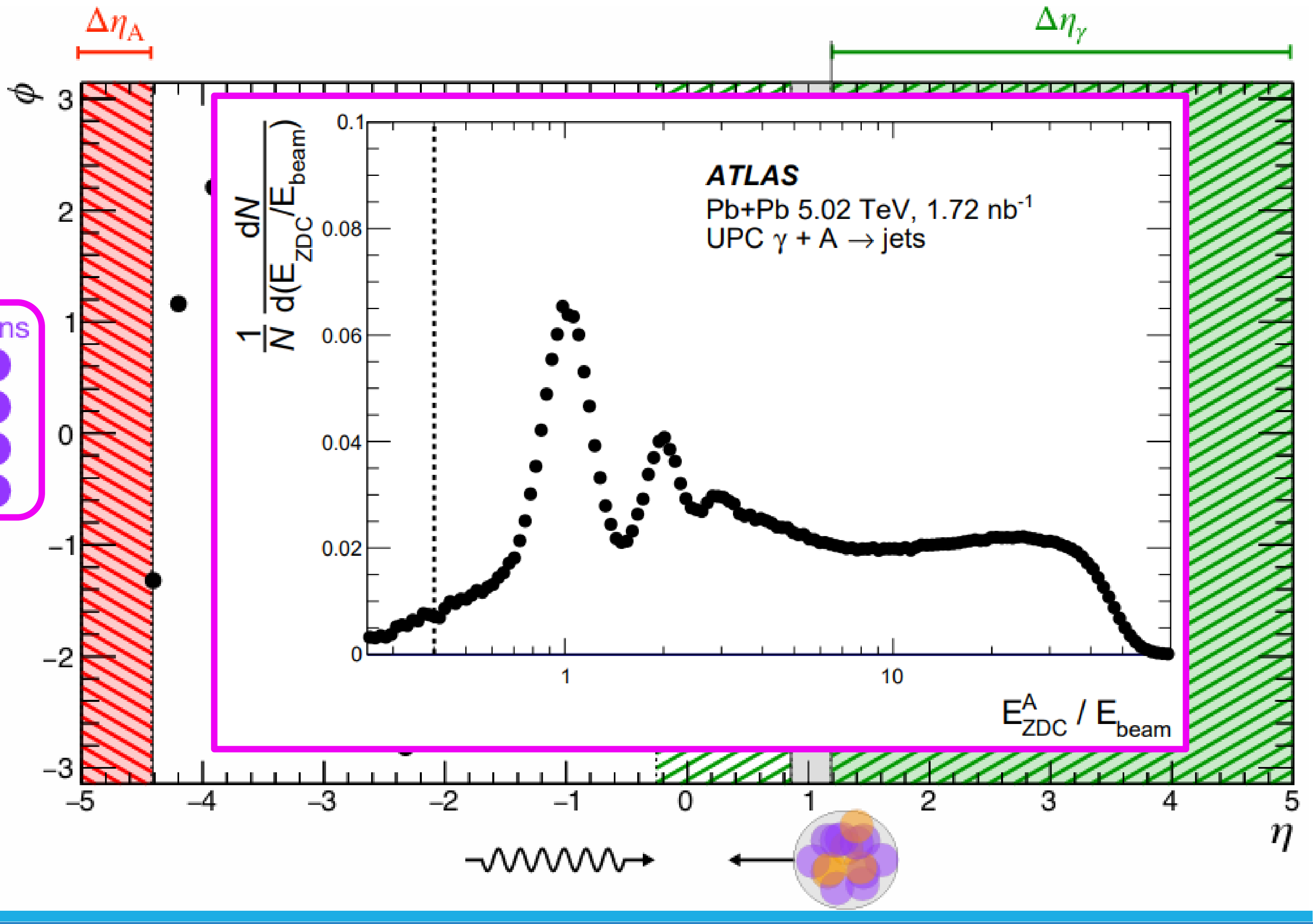

Selecting Photo-nuclear Jet Events

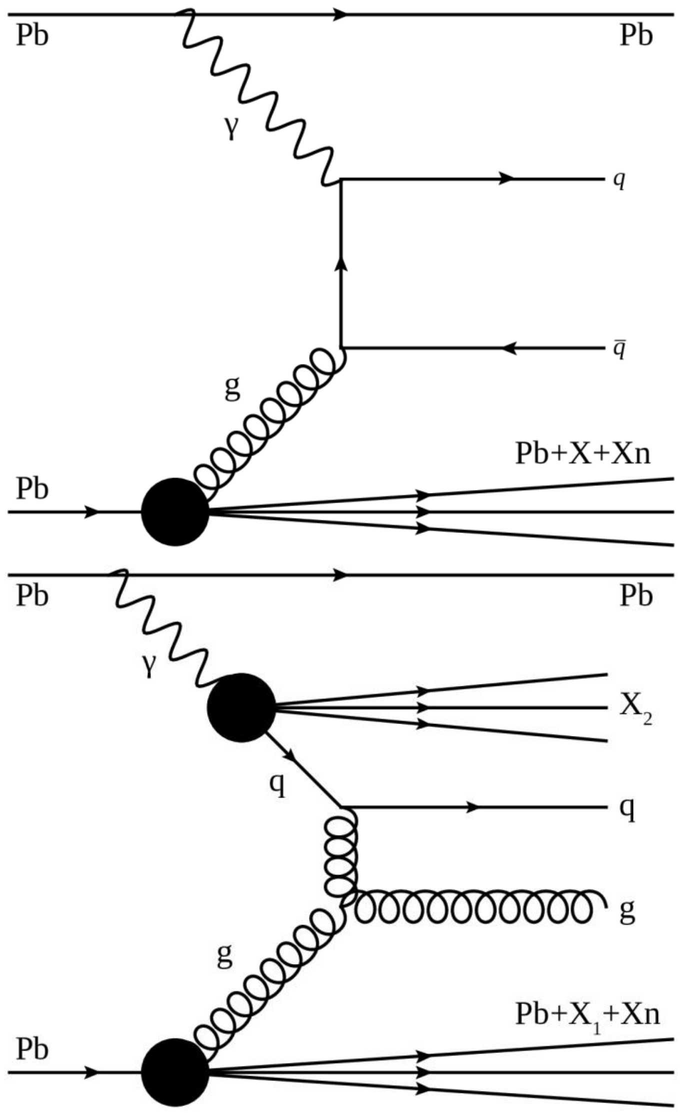

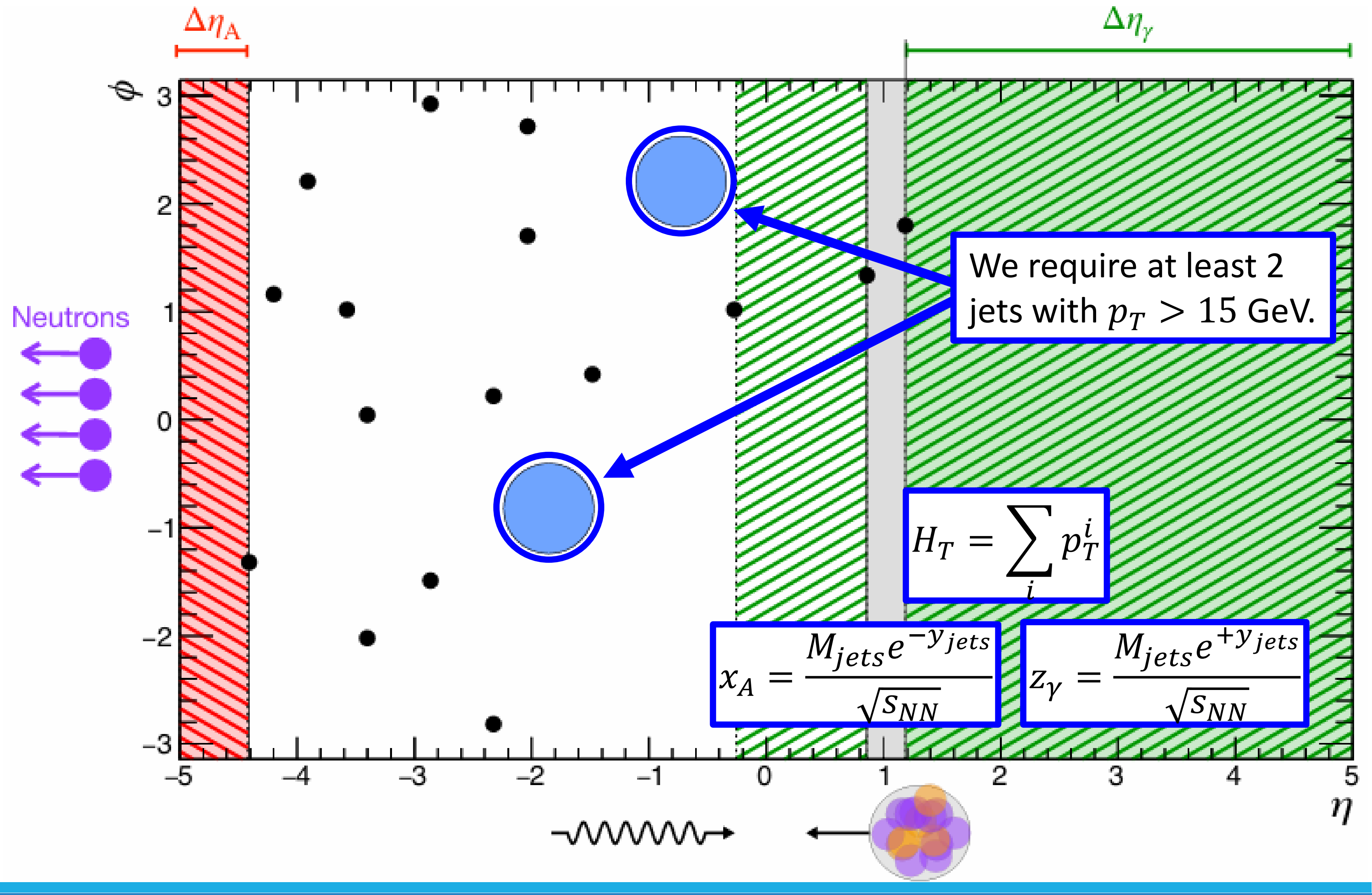

Selecting Photo-nuclear Jet Events

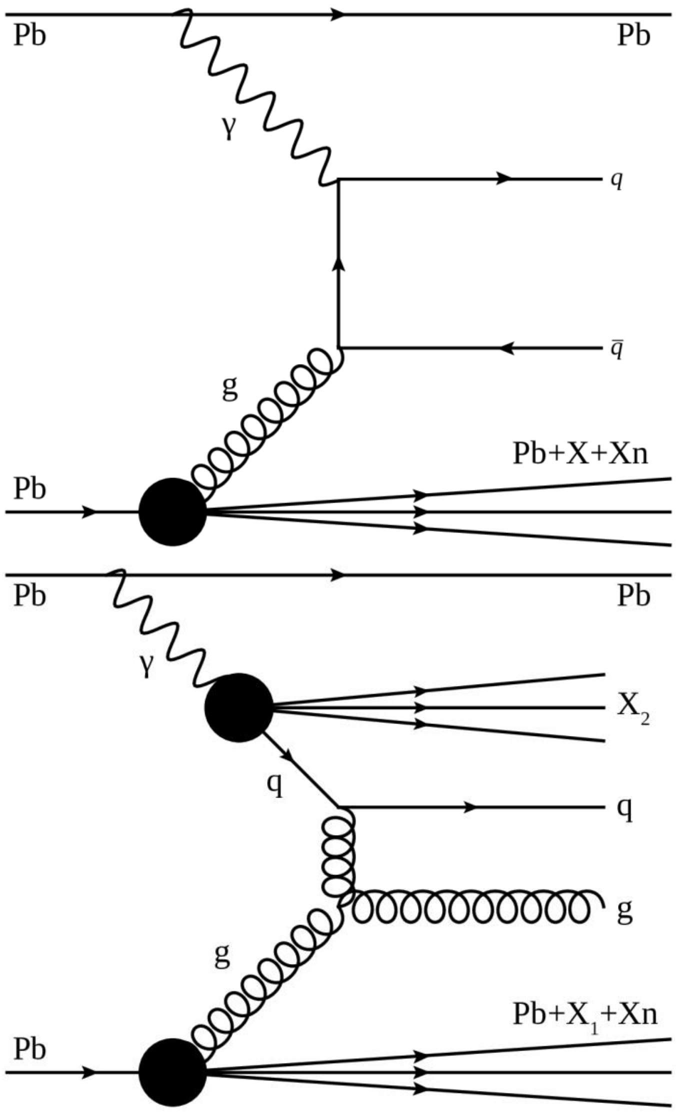

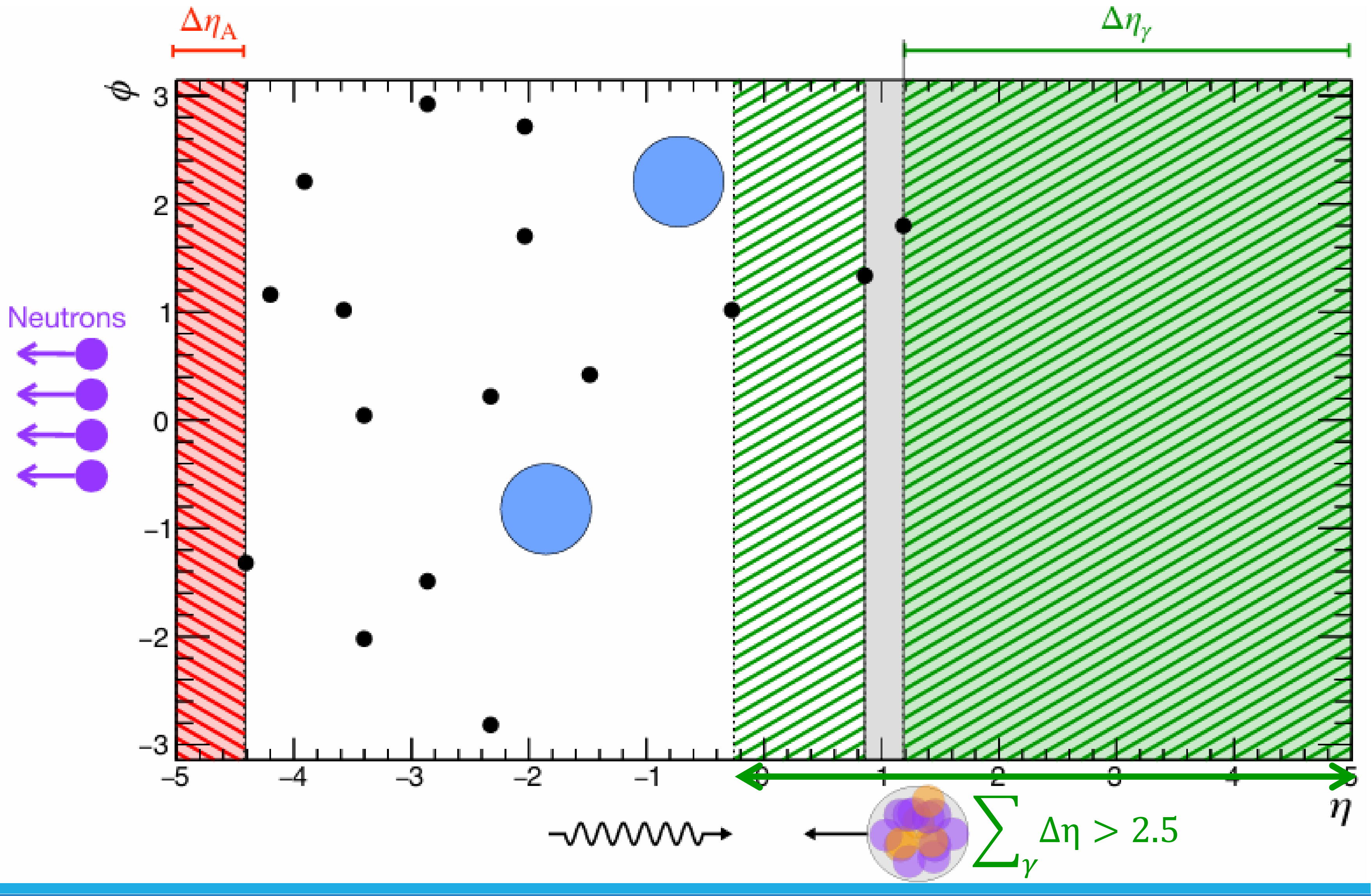

Photonuclear Event Selections

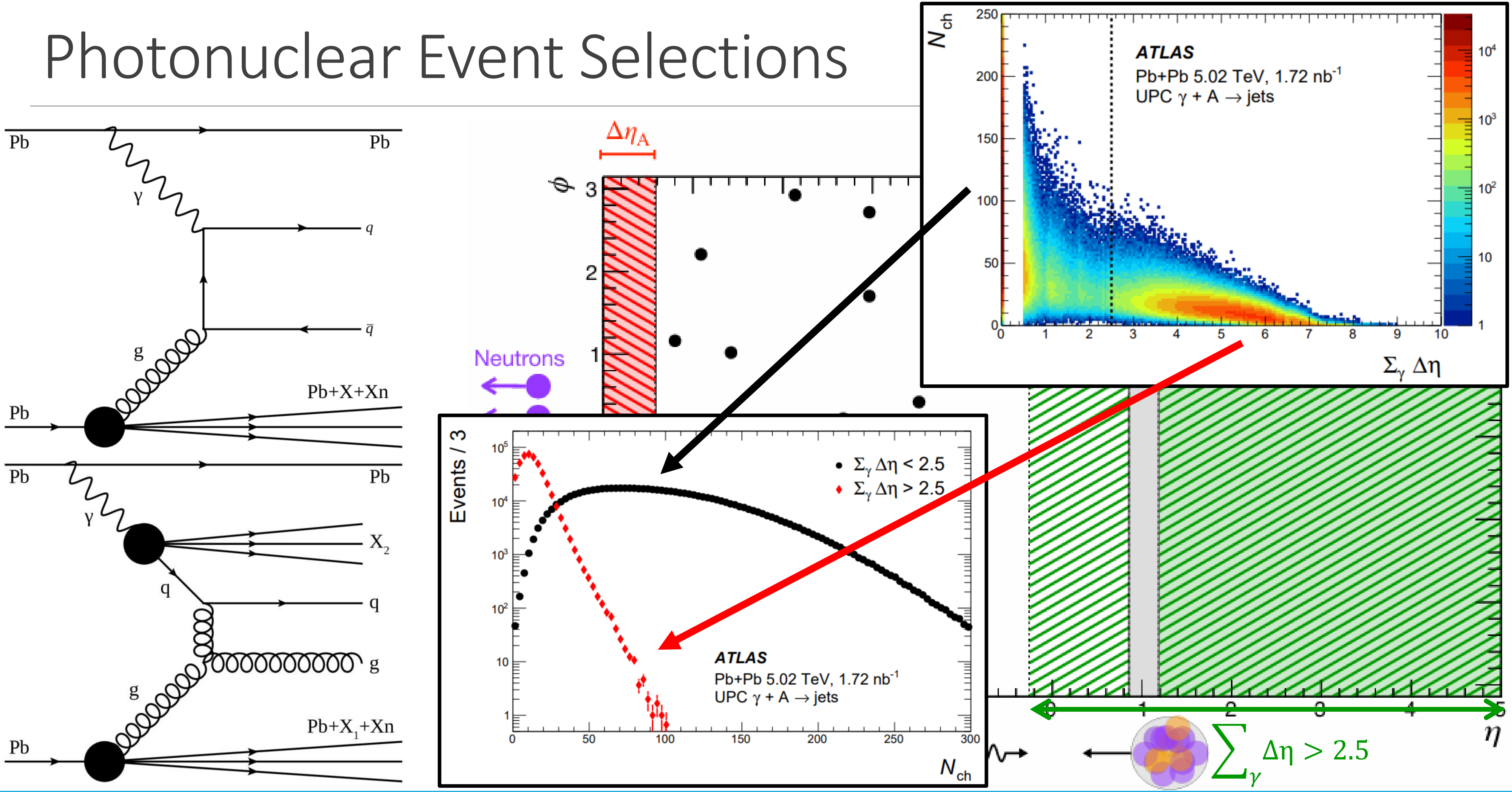

Gap Selections and Photon Structure

$$z_\gamma = \frac{M_{jets} e^{+y_{jets}}}{\sqrt{s_{NN}}}$$

Template fit studies of $\sum_\gamma \Delta\eta$ provide two pieces of information:

- The efficiency and background contamination rates of different gap selections
- The relative proportion of direct and resolved events

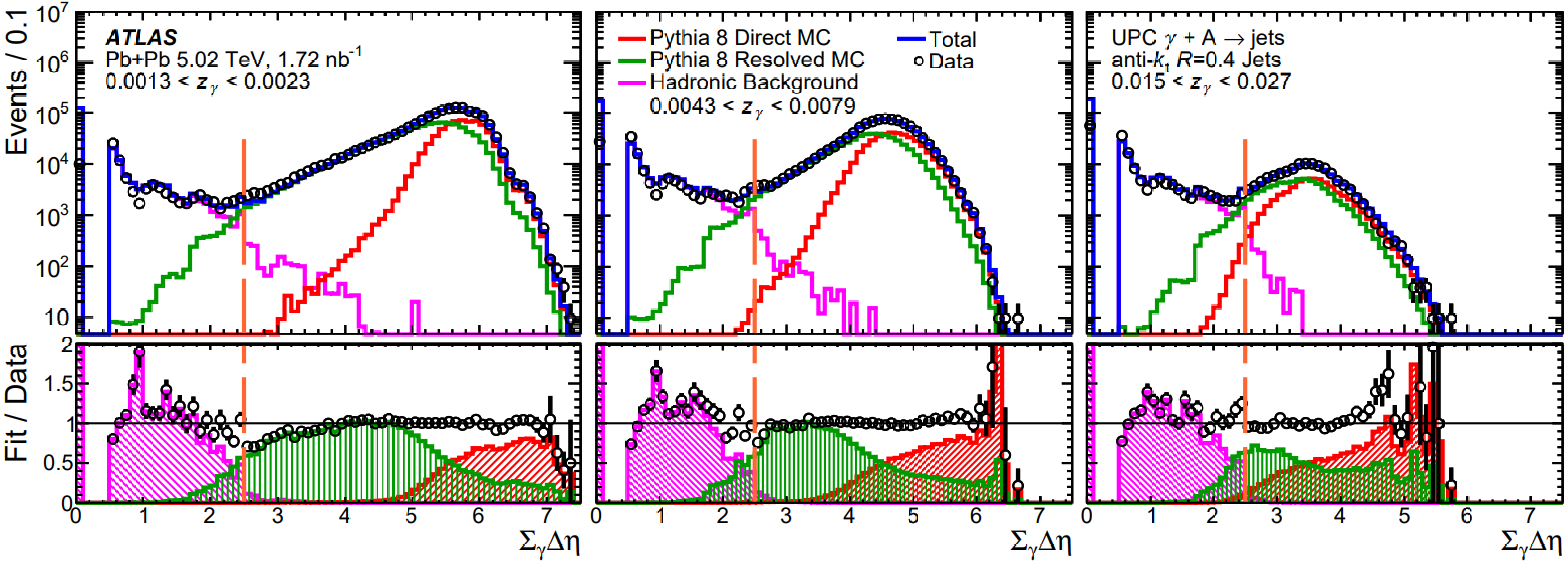

Gap Selections and Photon Structure

$$H_T = \sum_i p_T^i$$

$$z_\gamma = \frac{M_{jets} e^{+y_{jets}}}{\sqrt{s_{NN}}}$$

- The selection we apply (red) maintains a sufficient level of signal purity.

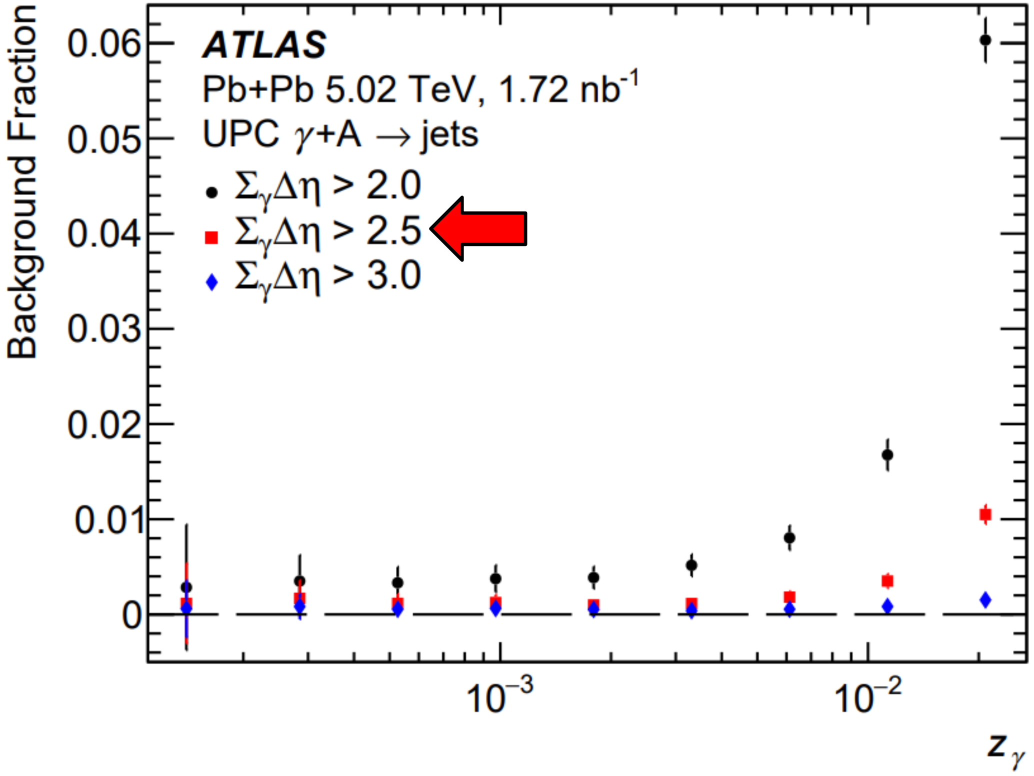

Gap Selections and Photon Structure

$$H_T = \sum_i p_T^i \qquad z_\gamma = \frac{M_{jets} e^{+y_{jets}}}{\sqrt{s_{NN}}}$$

- The selection we apply (red) maintains a sufficient level of signal purity.
- The direct fraction differs between data and theory at low H_T but is modeled well at high H_T.

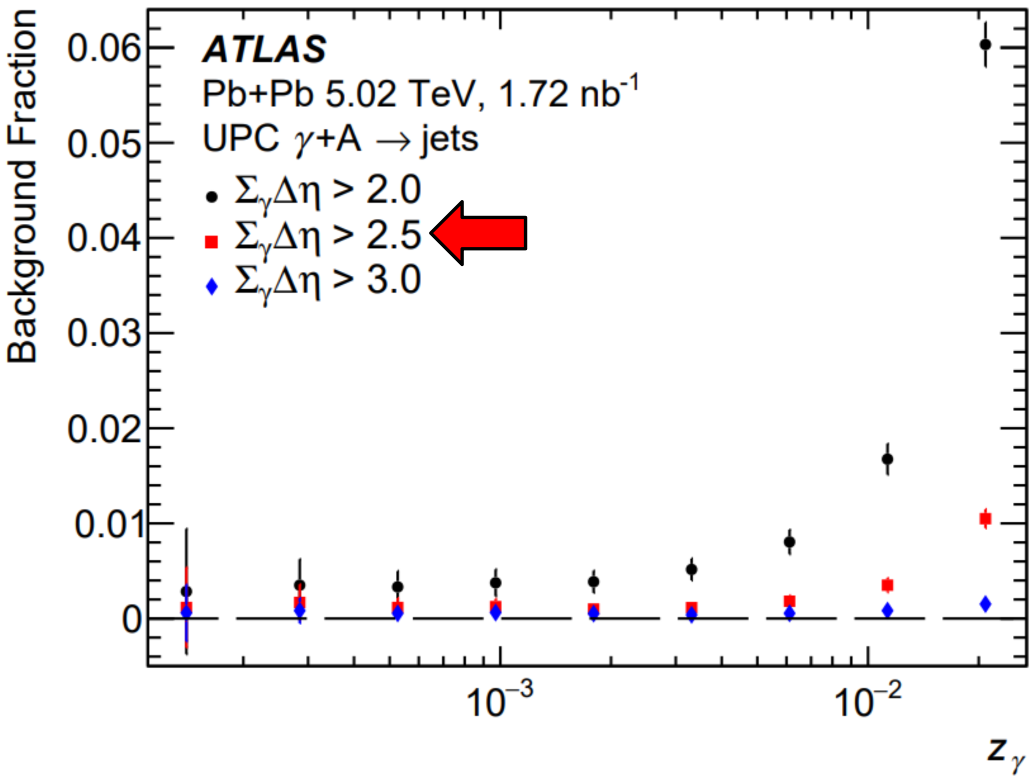

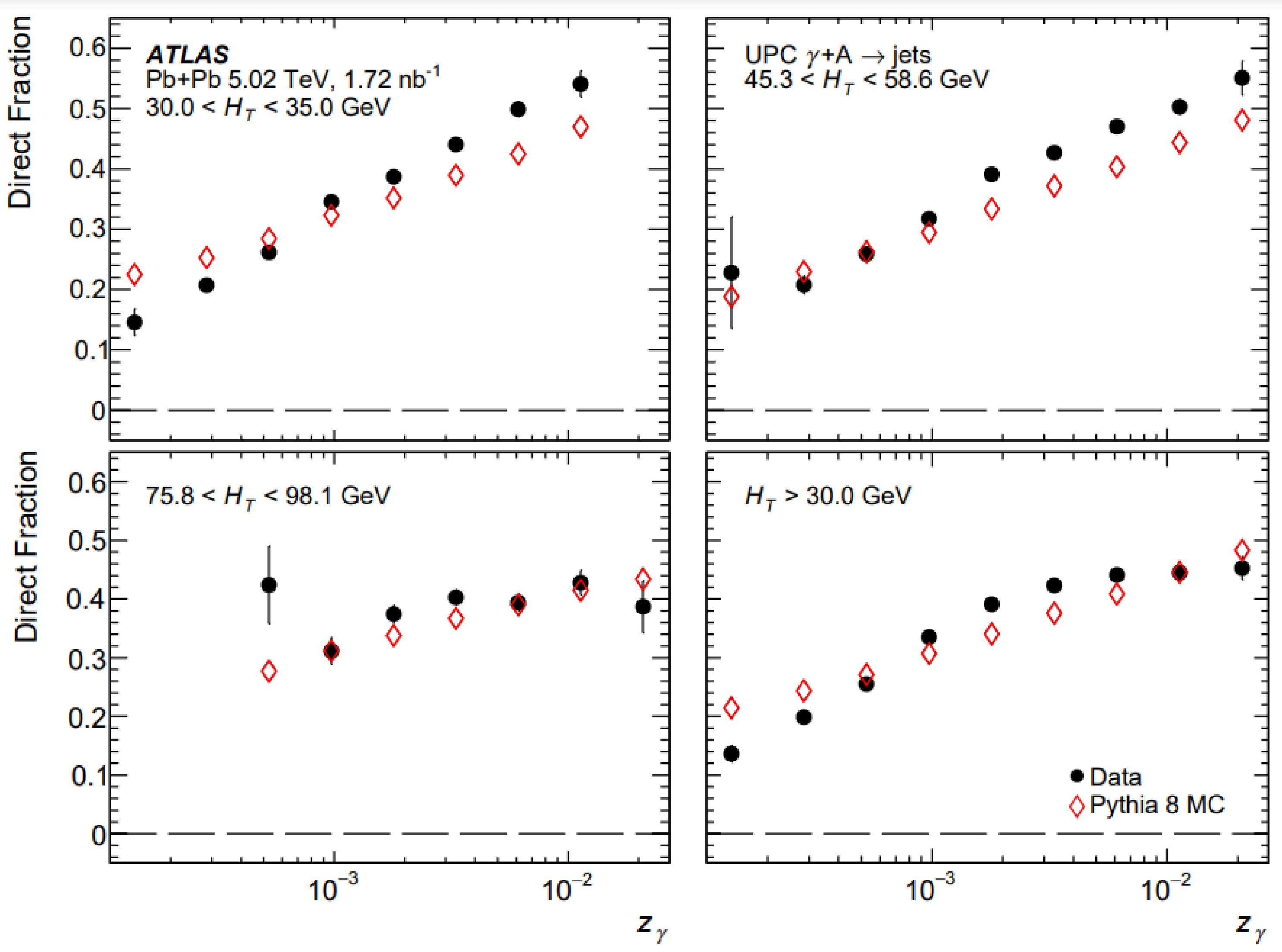

A New Calibration for Jets in UPC

- Due to the unique environment of UPCs, an entirely new jet calibration was derived specifically for this measurement.
- This result extends lower in jet p_T than any previous ATLAS measurement.
  - This coverage was made possible through the development of new techniques for studying the absolute energy scale at low p_T.
- Methodology for measuring jets in UPC is useful for the EIC program, and some dominant uncertainties (MC modeling) are shared!

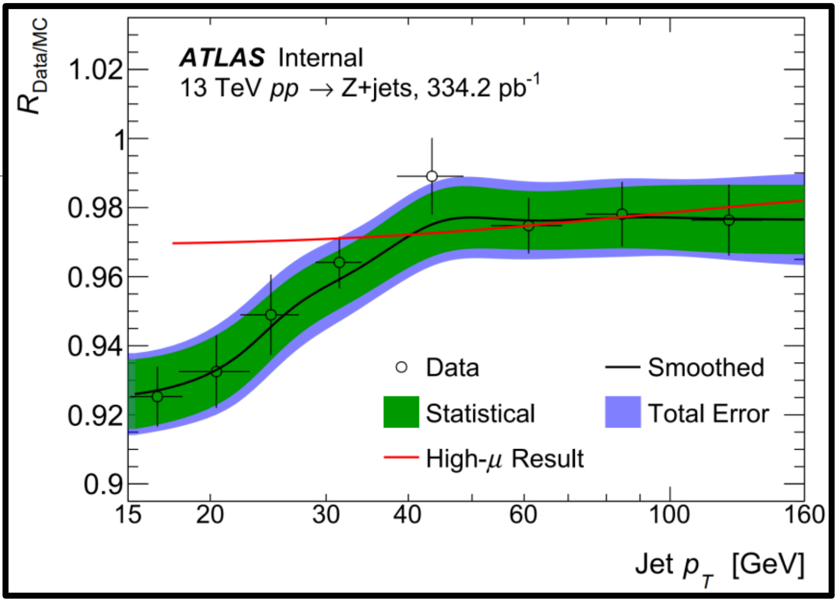

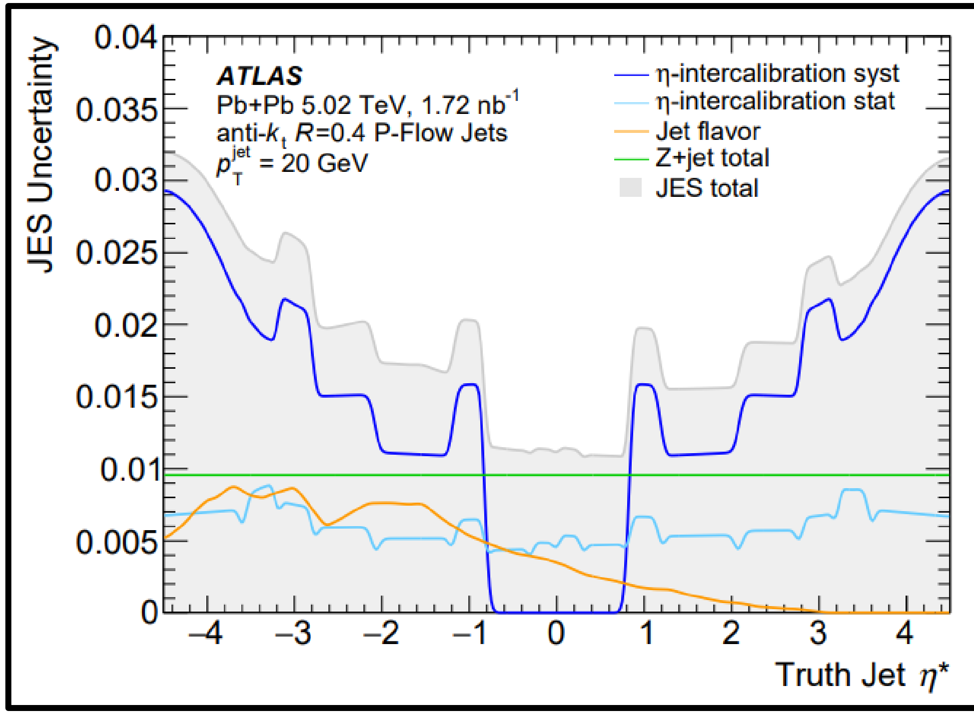

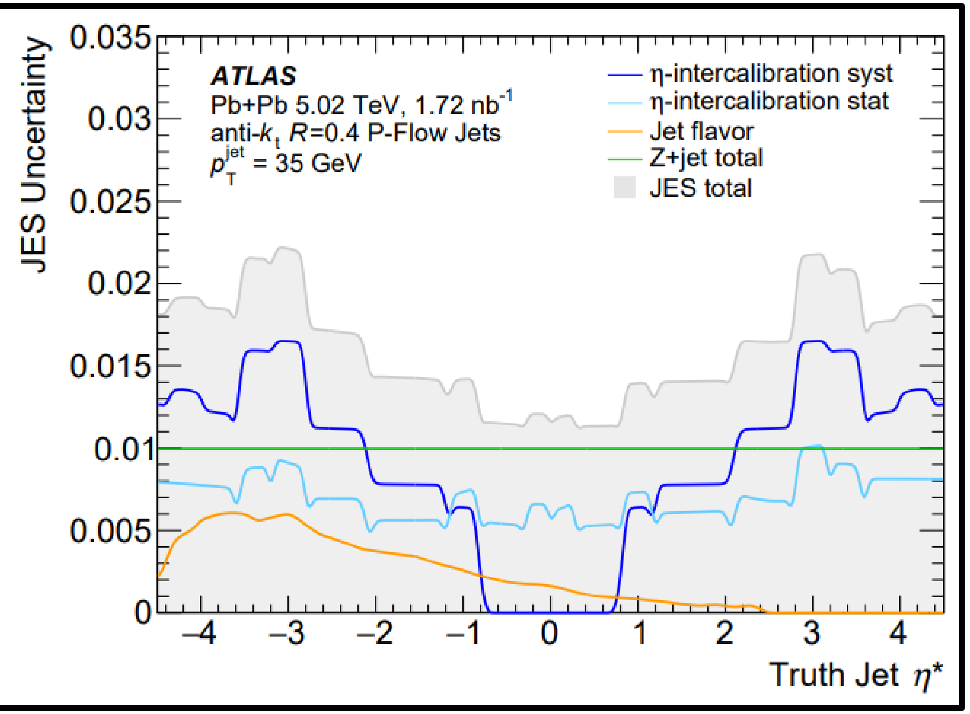

Systematic Uncertainties

Systematic uncertainties are the key limiting factor in our sensitivity to nuclear PDFs.

The jet energy scale and resolution uncertainties are typically 5-10%.

Systematic uncertainties are also evaluated on the unfolding and event selections.

Full treatment of correlated uncertainties helps to provide substantially more information on nPDFs.

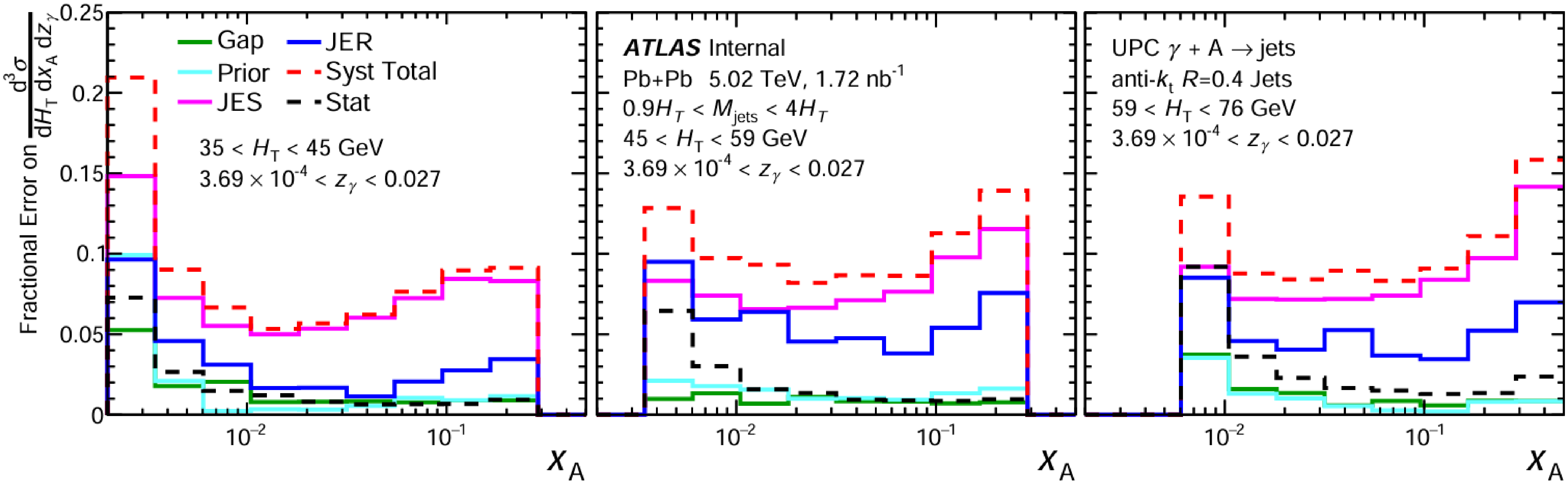

An Aside: Nuclear Break-up

- Our typical picture of an ultra-peripheral heavy-ion collision involves two nuclei with some large separation, $b > 2R_A$.
  - $E_\gamma \propto 1/b \rightarrow$ Biases towards lower impact-parameter collisions
  - Much higher probability of breakup of the photon-emitting nucleus due to additional EM interactions

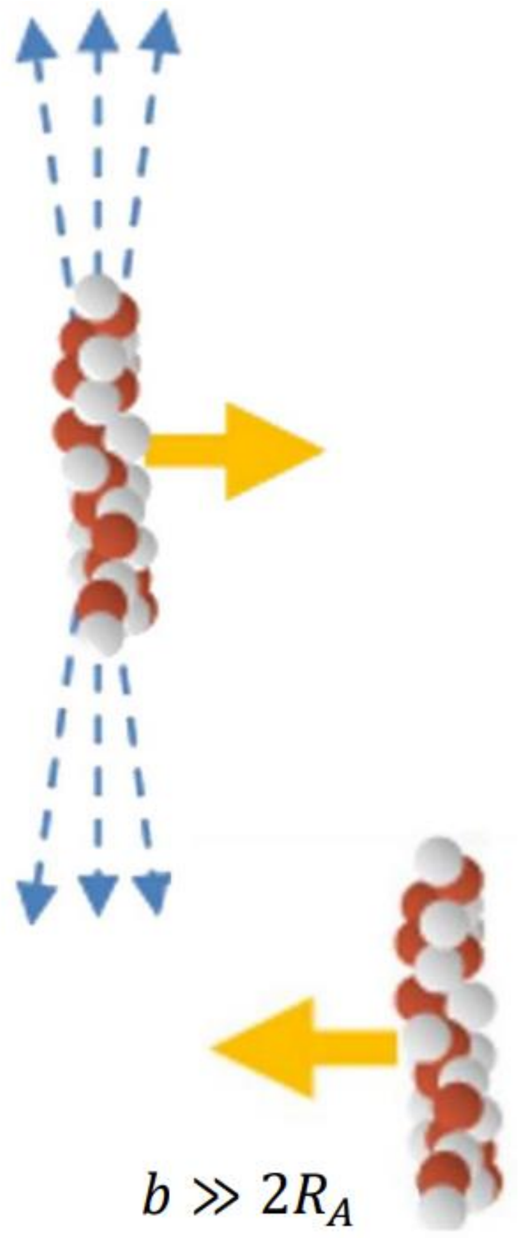

An Aside: Nuclear Break-up

- Our typical picture of an ultra-peripheral heavy-ion collision involves two nuclei with some large separation, b > $2R_A$.
  - $E_\gamma \propto 1/b \rightarrow$ Biases towards lower impact-parameter collisions
  - Much higher probability of breakup of the photon-emitting nucleus due to additional EM interactions

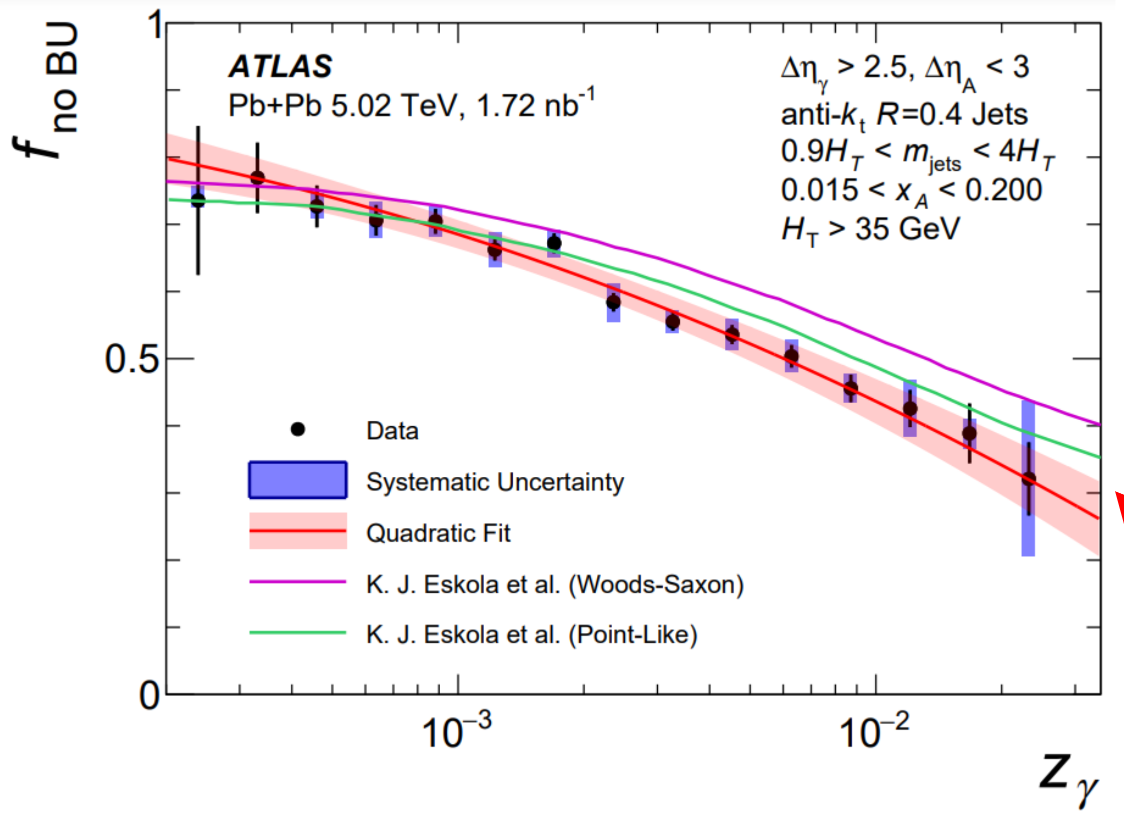

$$f_{\text{no BU}} \equiv \frac{d\sigma/dz_\gamma|_{0nXn}}{d\sigma/dz_\gamma|_{XnXn} + d\sigma/dz_\gamma|_{0nXn}}$$

The measured breakup is used to correct the theory predictions when comparing to data.

Theoretical modeling predicts the rate quite well! (arXiv:2404.09731)

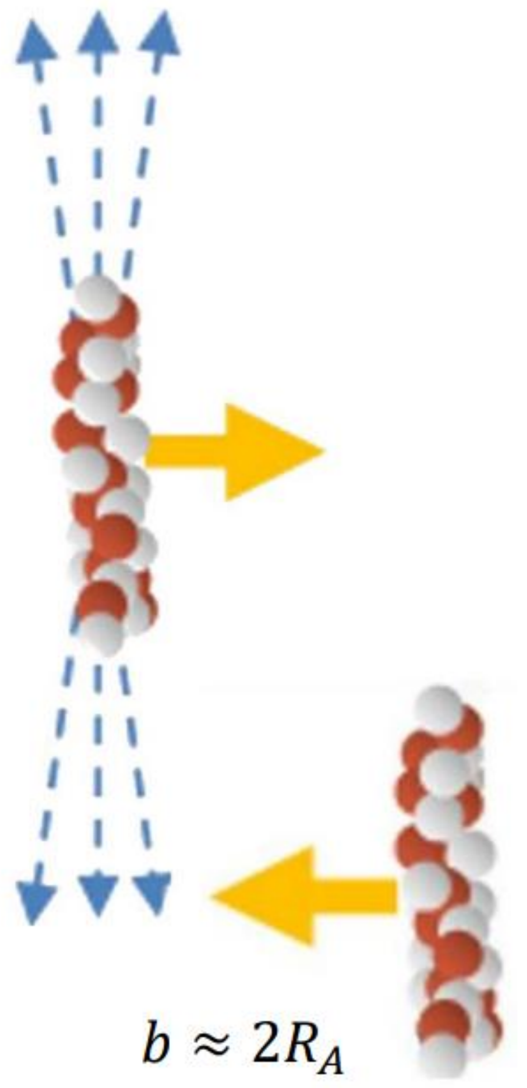

UPC Jets: Scanning in Photon Energy

$$H_T = \sum_i p_T^i \qquad x_A = \frac{M_{jets} e^{-y_{jets}}}{\sqrt{s_{NN}}} \qquad z_\gamma = \frac{M_{jets} e^{+y_{jets}}}{\sqrt{s_{NN}}}$$

The x_A distribution has substantial acceptance effects in z_γ.

Selecting on photon energy removes this bias, allowing for a more direct measurement of nPDFs.

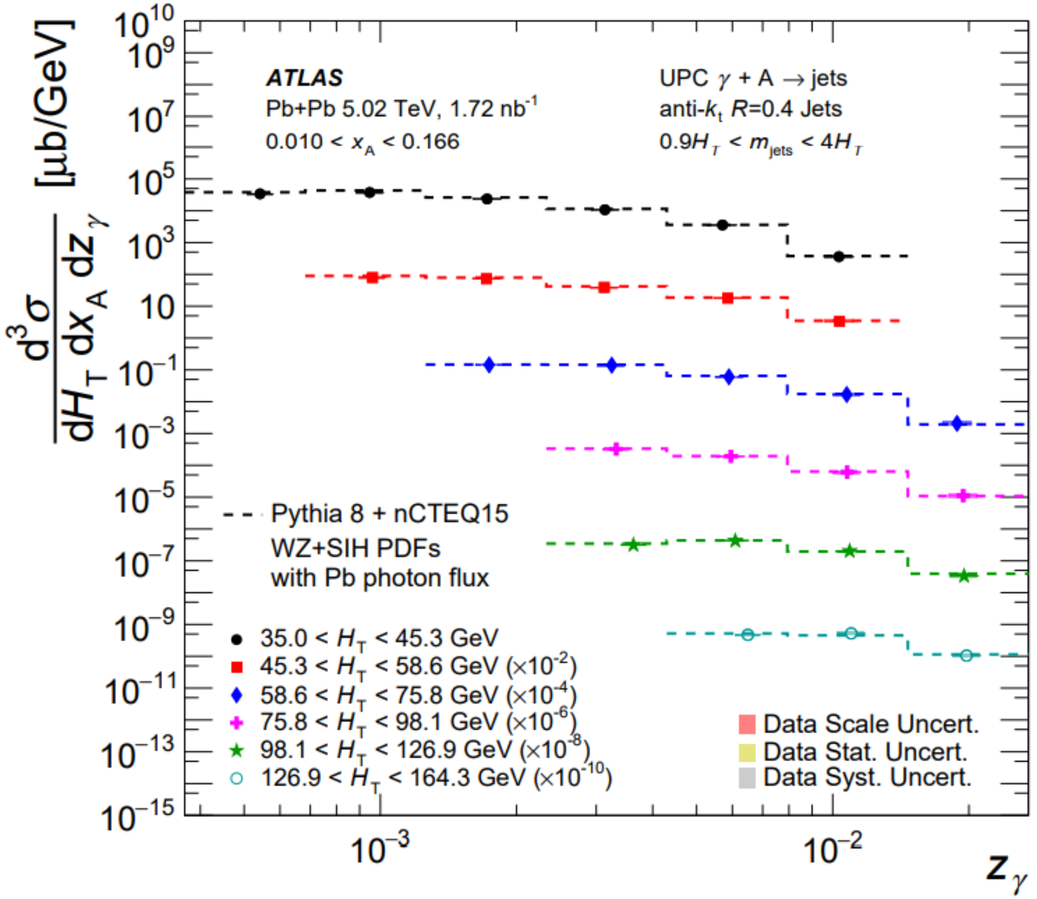

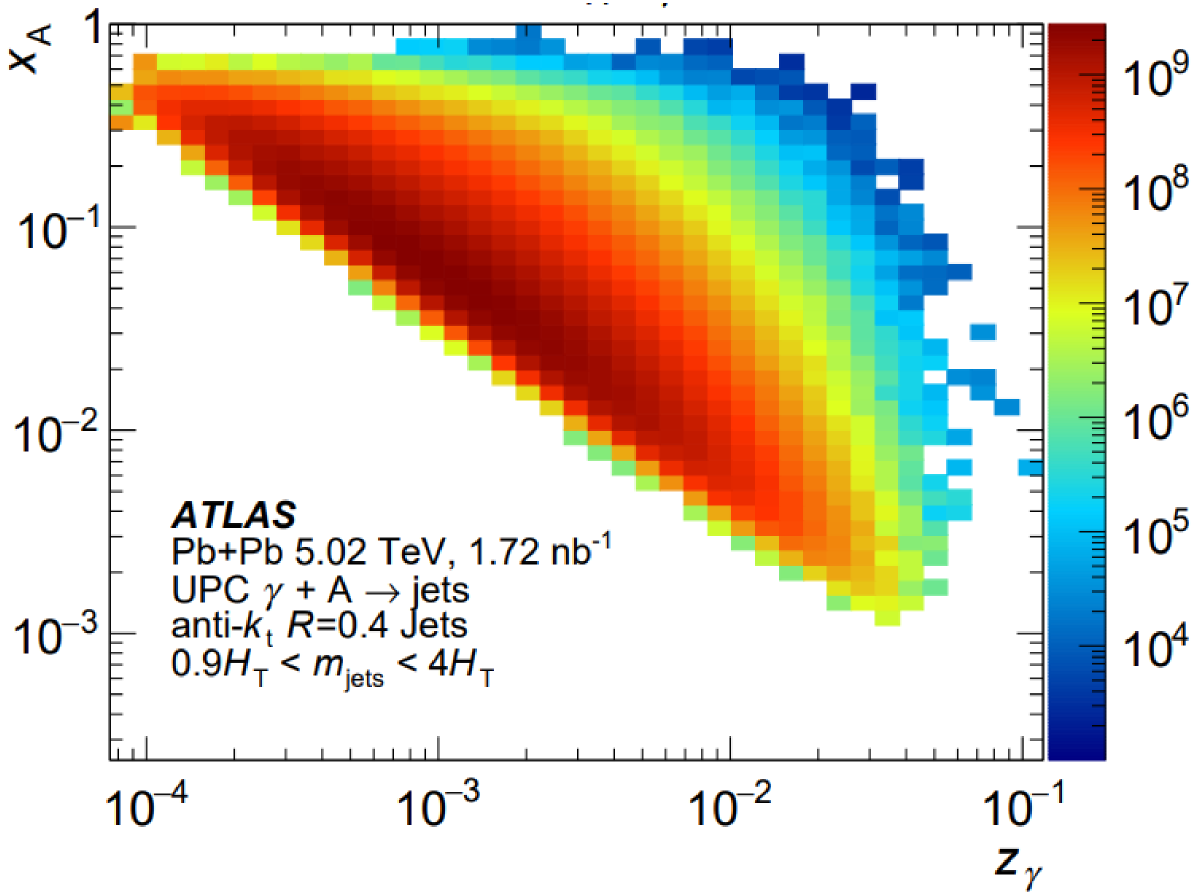

UPC Jets: Scanning in Photon Energy

$$H_T = \sum_i p_T^i \qquad x_A = \frac{M_{jets} e^{-y_{jets}}}{\sqrt{s_{NN}}} \qquad z_\gamma = \frac{M_{jets} e^{+y_{jets}}}{\sqrt{s_{NN}}}$$

The x_A distribution has substantial acceptance effects in z_γ.

Selecting on photon energy removes this bias, allowing for a more direct measurement of nPDFs.

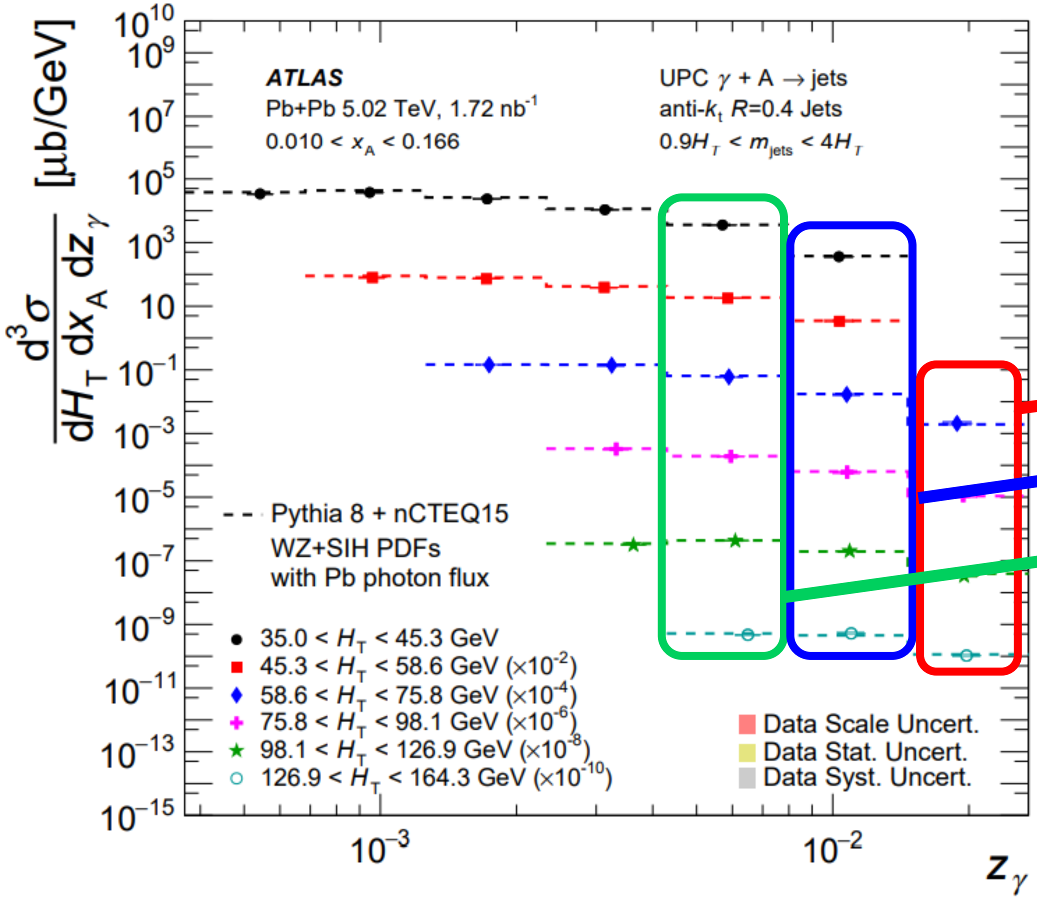

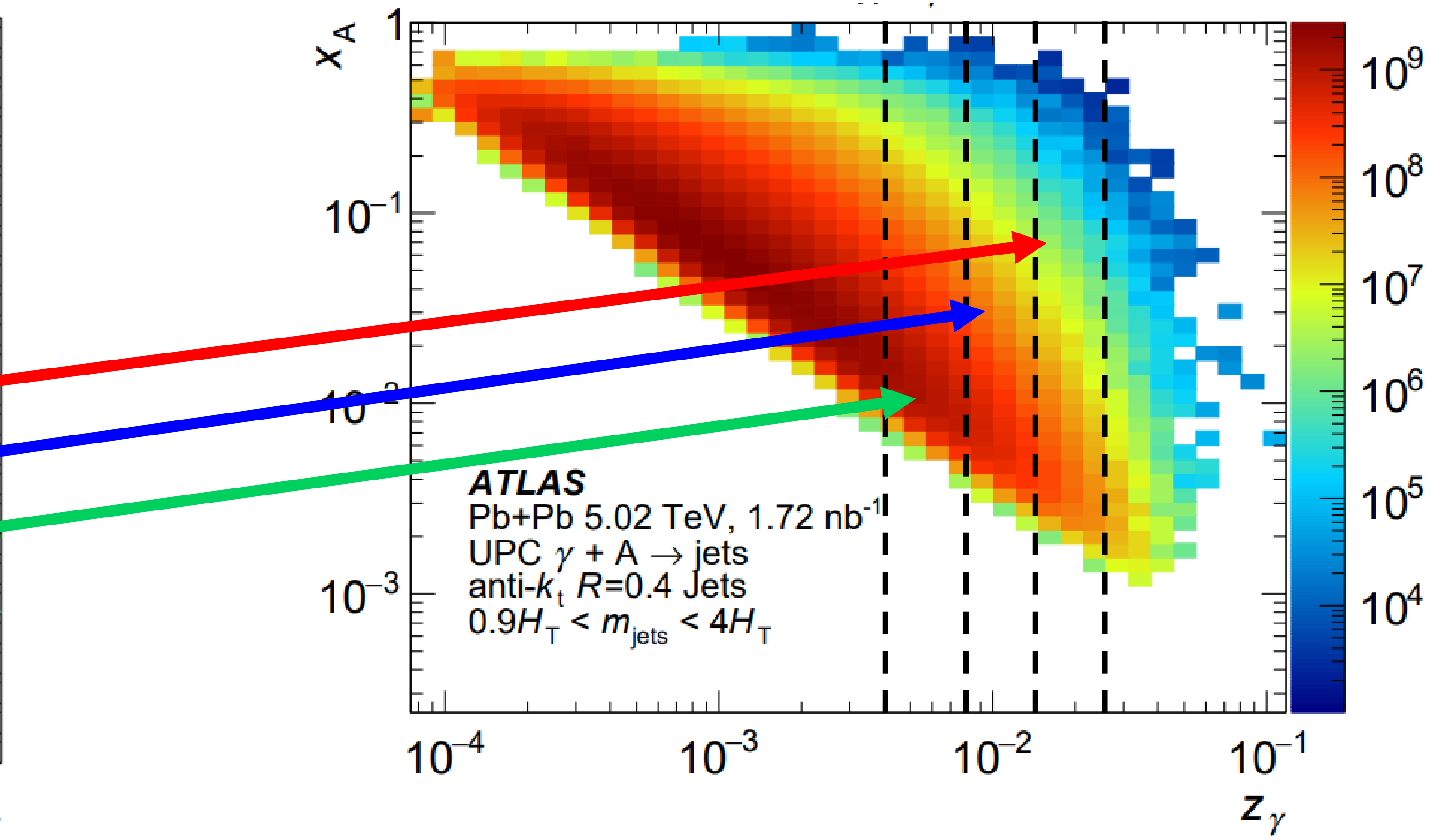

Measured Cross-Sections

$H_T = \sum_i p_T^i$ | $x_A = \frac{M_{jets} e^{-y_{jets}}}{\sqrt{s_{NN}}}$ | $z_\gamma = \frac{M_{jets} e^{+y_{jets}}}{\sqrt{s_{NN}}}$

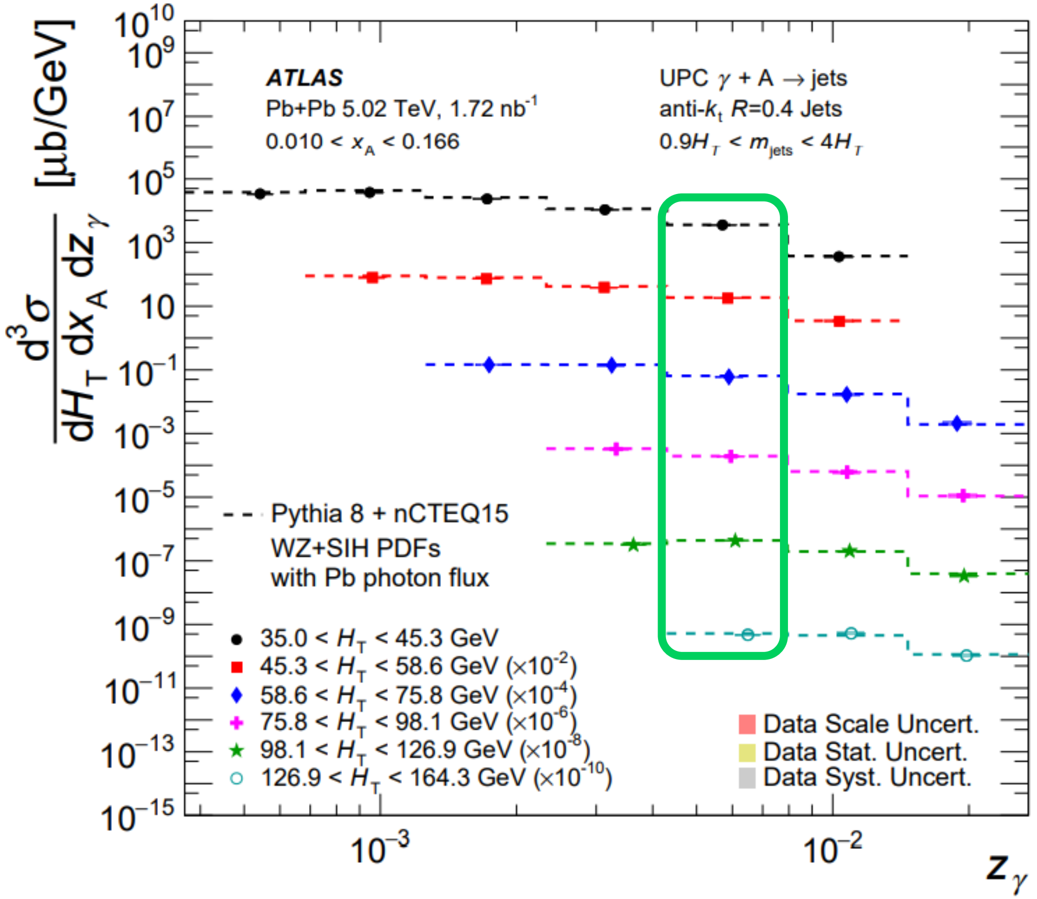

Photon Energy

$0.004 < z_\gamma < 0.008$

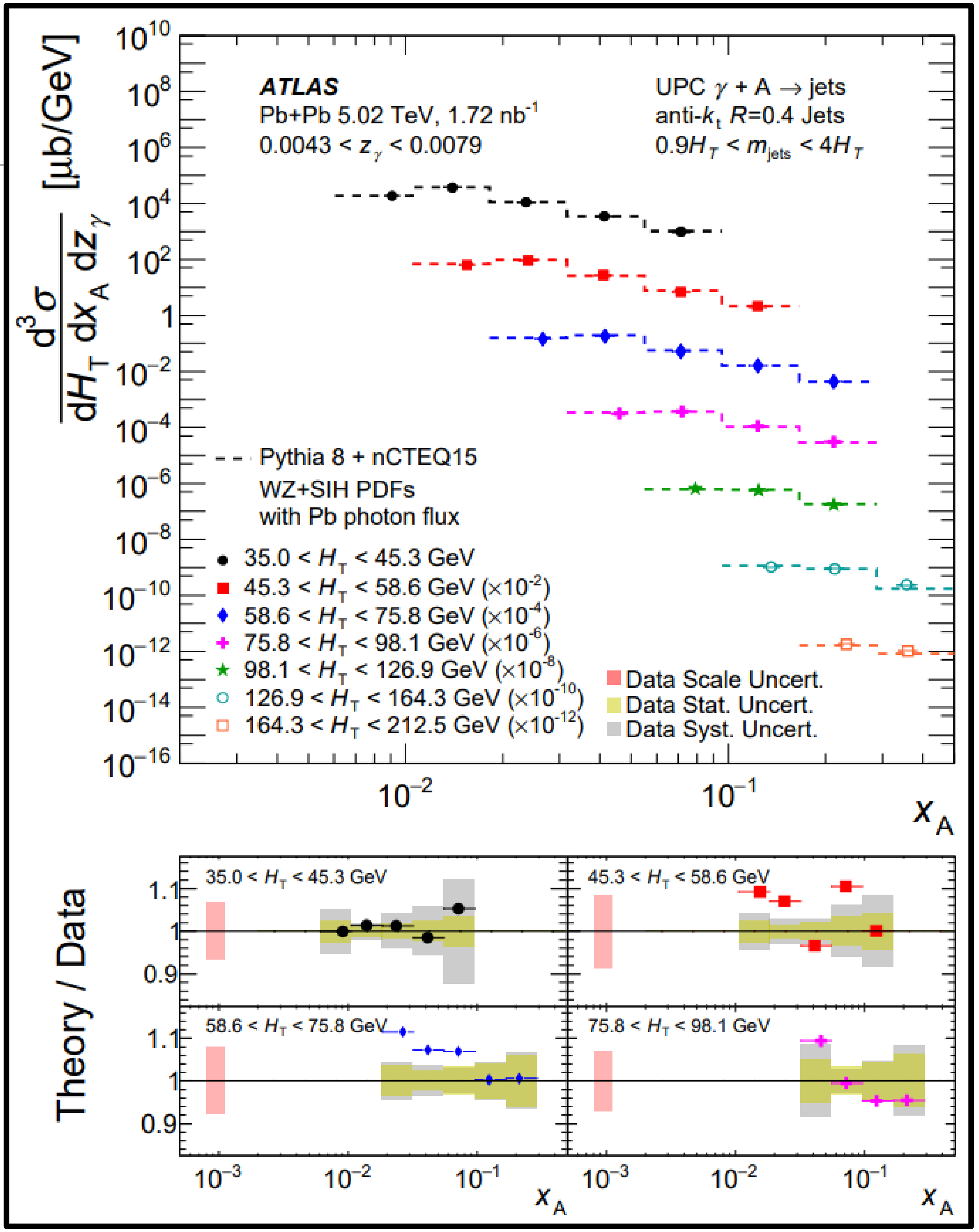

Measured Cross-Sections

$$H_T = \sum_i p_T^i \qquad x_A = \frac{M_{jets} e^{-y_{jets}}}{\sqrt{s_{NN}}} \qquad z_\gamma = \frac{M_{jets} e^{+y_{jets}}}{\sqrt{s_{NN}}}$$

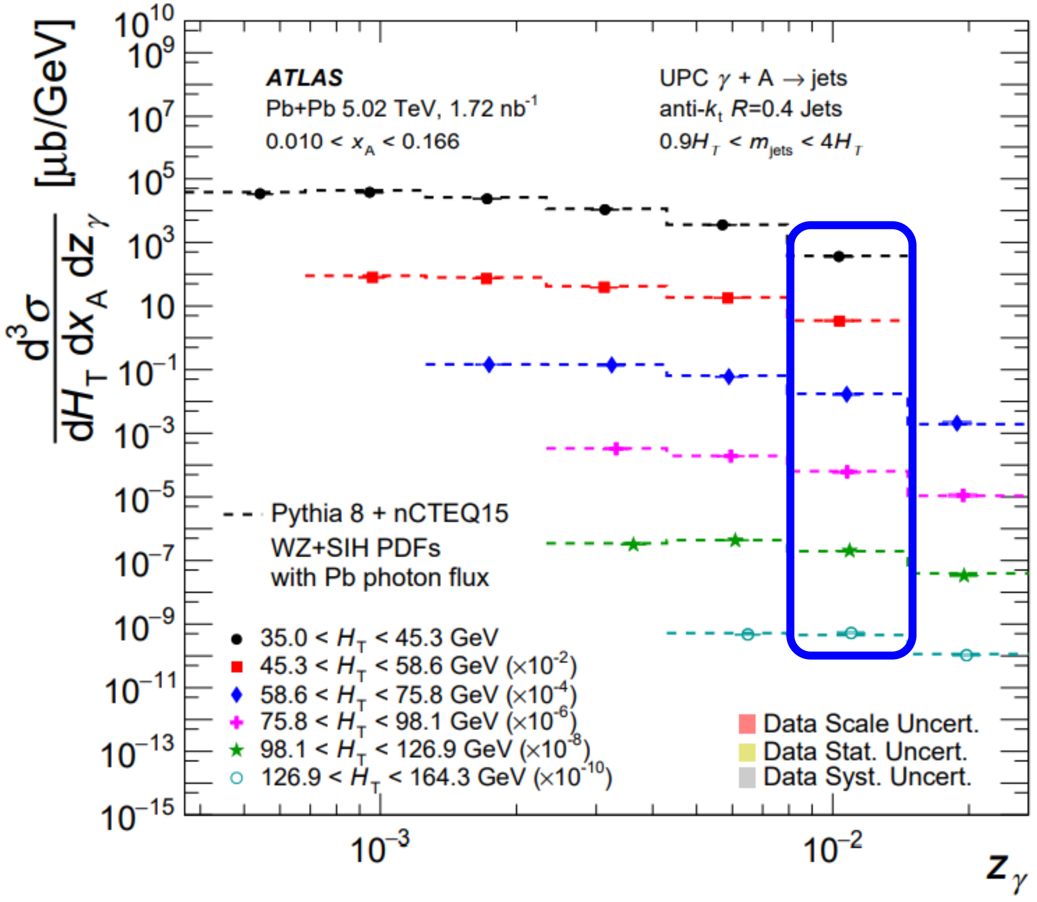

Photon Energy

$0.008 < z_\gamma < 0.015$

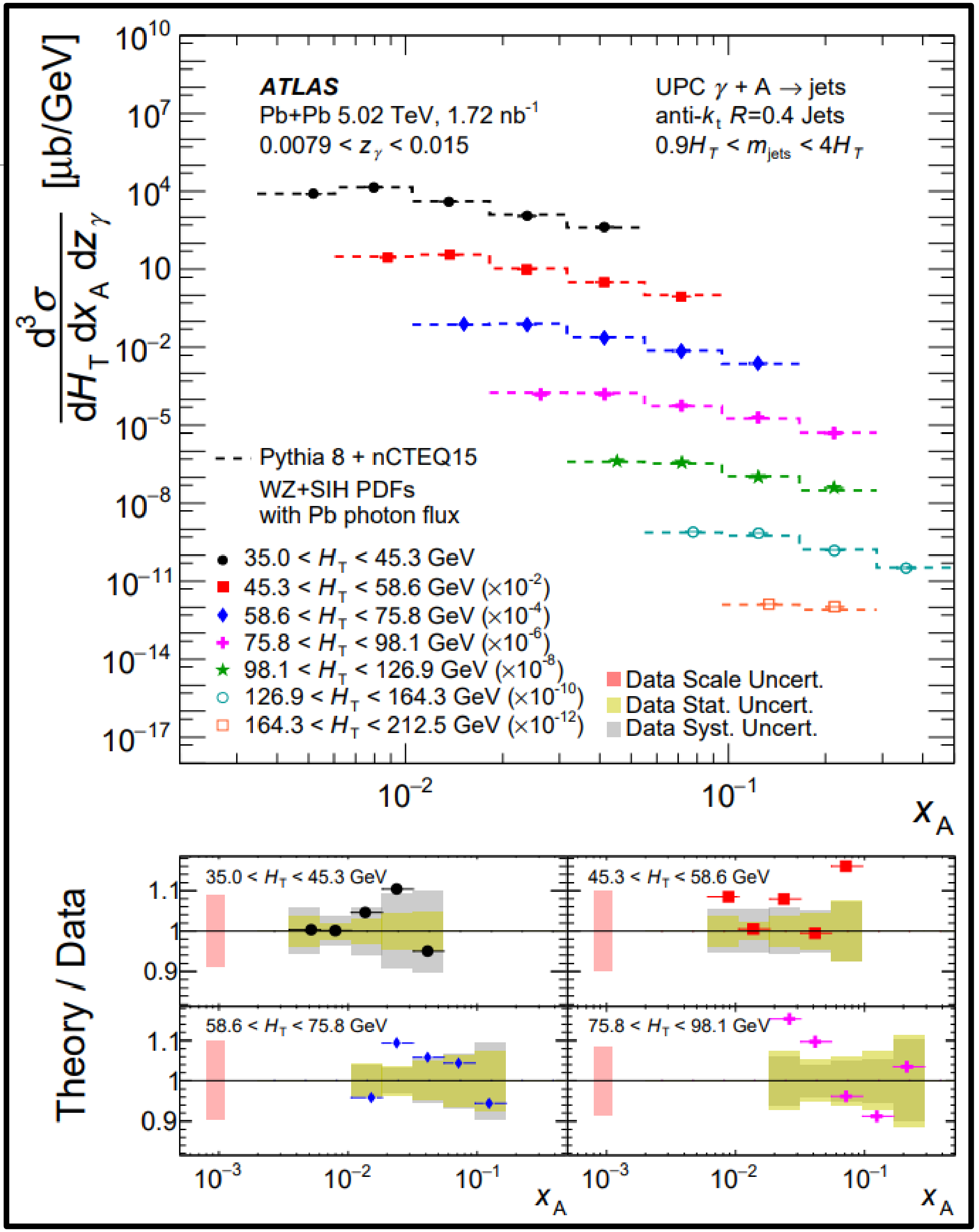

Measured Cross-Sections

$$H_T = \sum_i p_T^i \qquad x_A = \frac{M_{jets} e^{-y_{jets}}}{\sqrt{s_{NN}}} \qquad z_\gamma = \frac{M_{jets} e^{+y_{jets}}}{\sqrt{s_{NN}}}$$

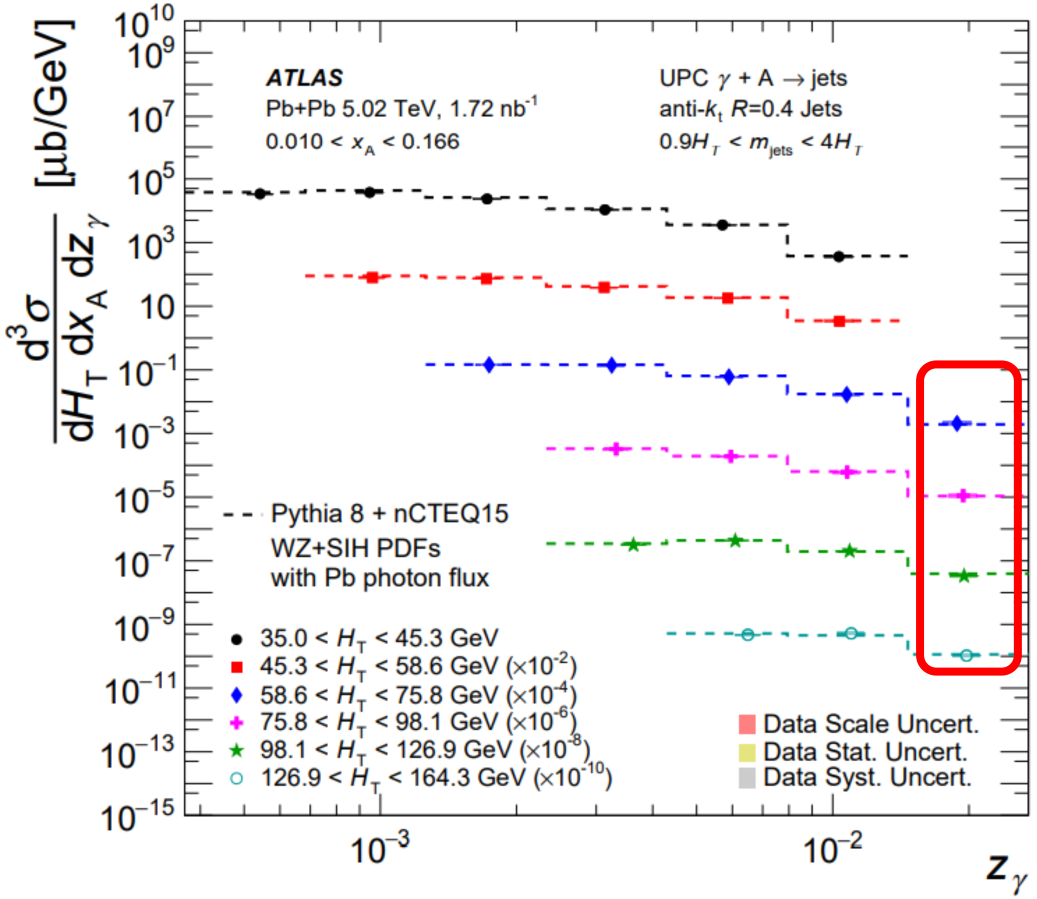

Photon Energy

$0.015 < z_\gamma < 0.027$

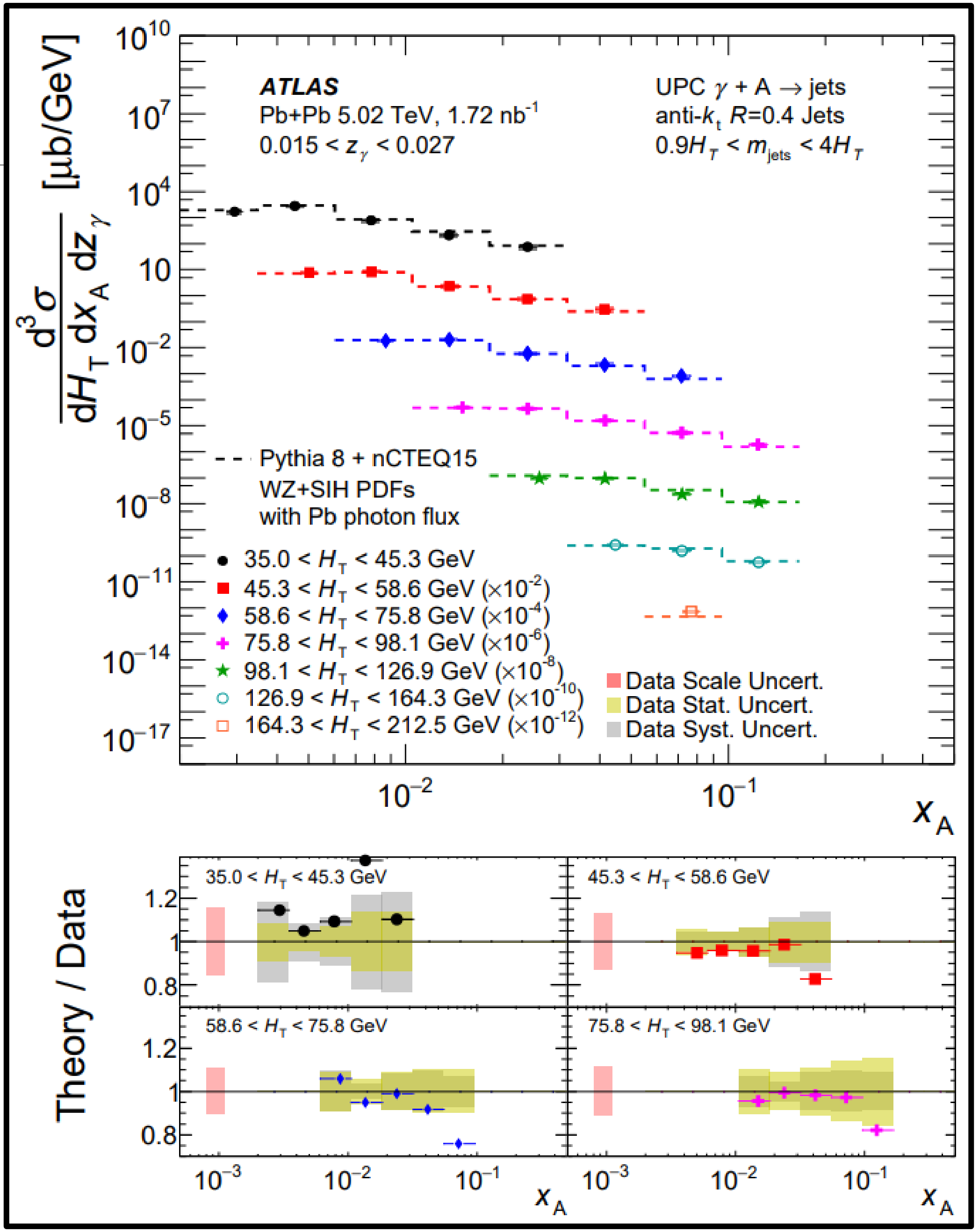

Measured Cross-Sections

$$H_T = \sum_i p_T^i$$ $$x_A = \frac{M_{jets} e^{-y_{jets}}}{\sqrt{s_{NN}}}$$ $$z_\gamma = \frac{M_{jets} e^{+y_{jets}}}{\sqrt{s_{NN}}}$$

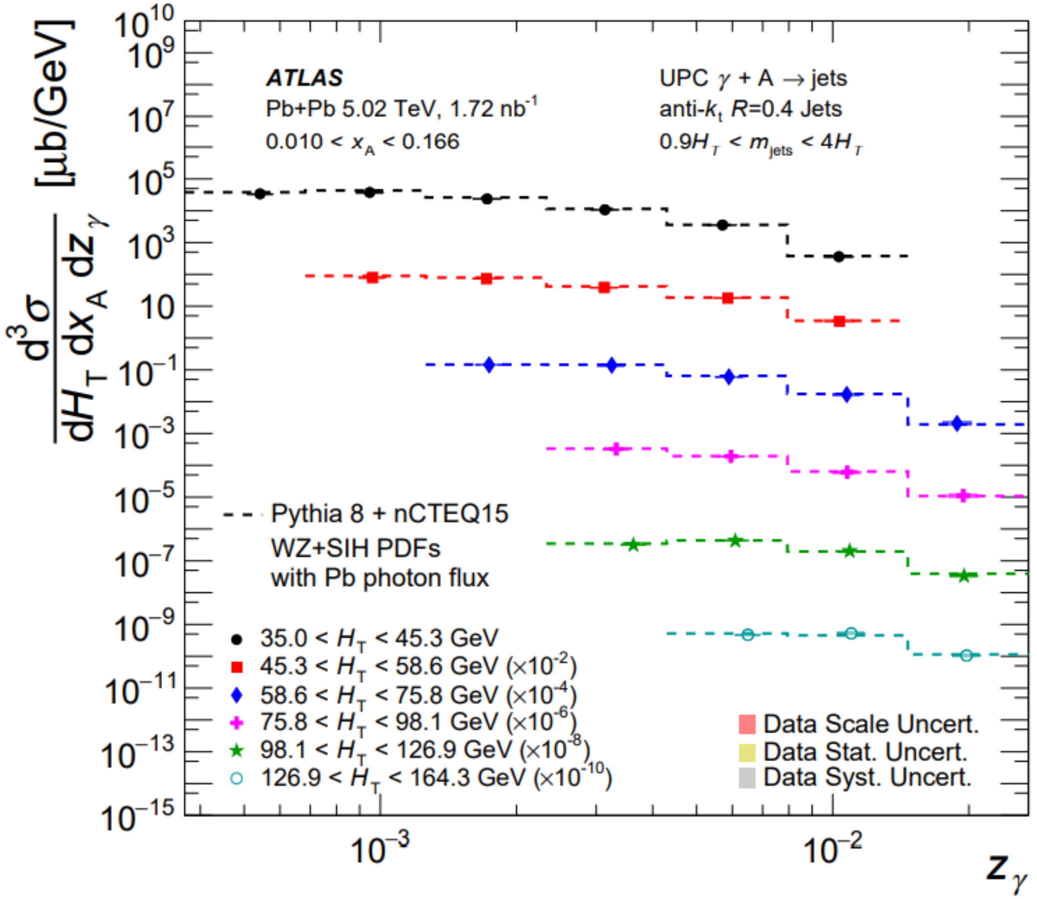

Photon Energy

$3.7 \times 10^{-4} < z_\gamma < 0.027$

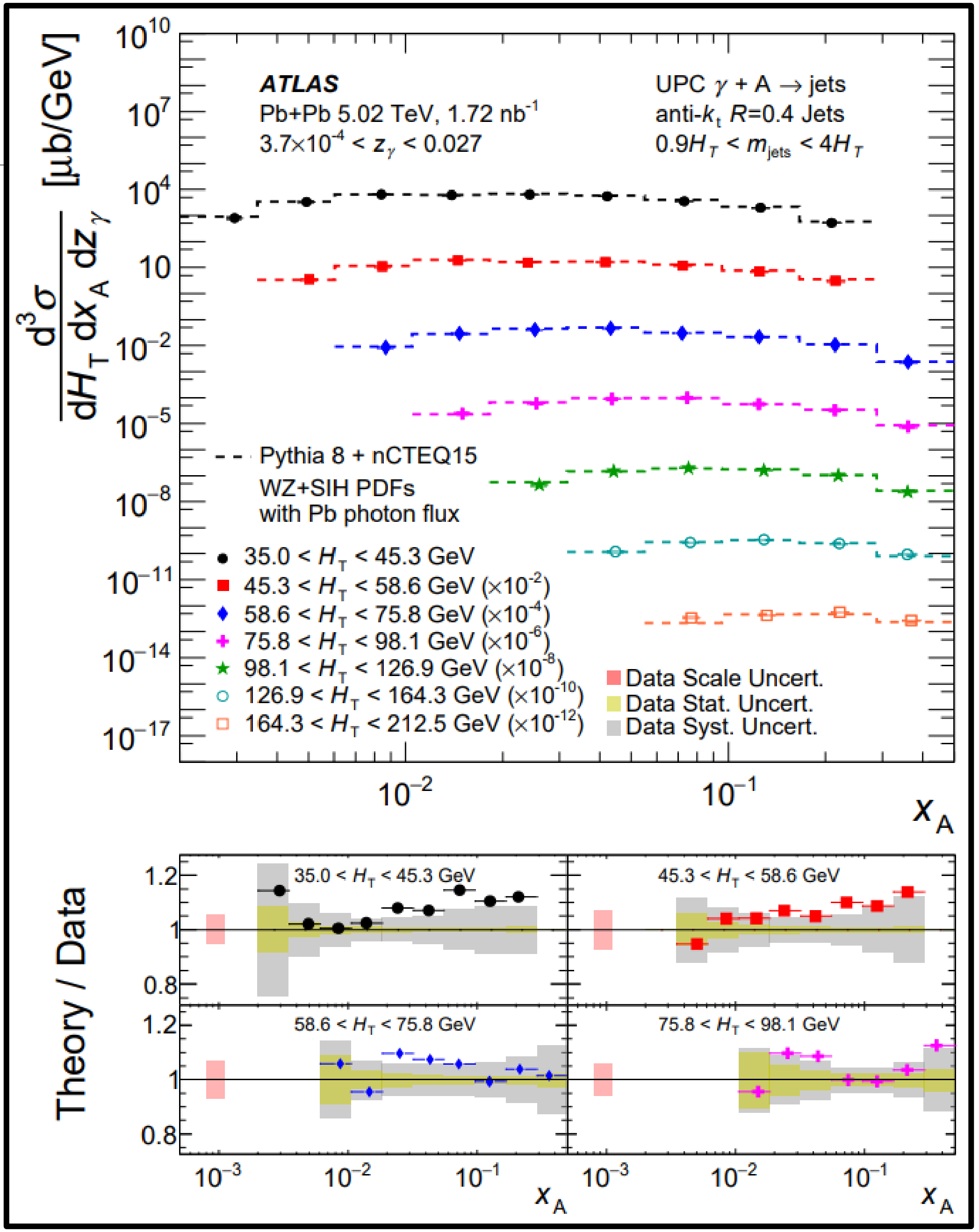

nPDF Theory Comparisons

$H_T = \sum_i p_T^i$ $x_A = \frac{M_{jets} e^{-y_{jets}}}{\sqrt{s_{NN}}}$ $z_\gamma = \frac{M_{jets} e^{+y_{jets}}}{\sqrt{s_{NN}}}$

- Comparing to additional nPDF fits can provide some insight for how well these data agree with existing predictions.
- Generally, the agreement is best with nCTEQ and TUJU.
  - One should be careful not to overly interpret these results, especially the normalization, without an NLO comparison.
- There is a clear tension between fits with larger modifications (nNNPDF, EPPS) and smaller modifications (nCTEQ, TUJU), especially at low H_T.
  - These tensions primarily impact the size of shadowing and anti-shadowing effects.
  - Little can be said about the EMC effect in these results, due to the limited coverage at high-x_A.

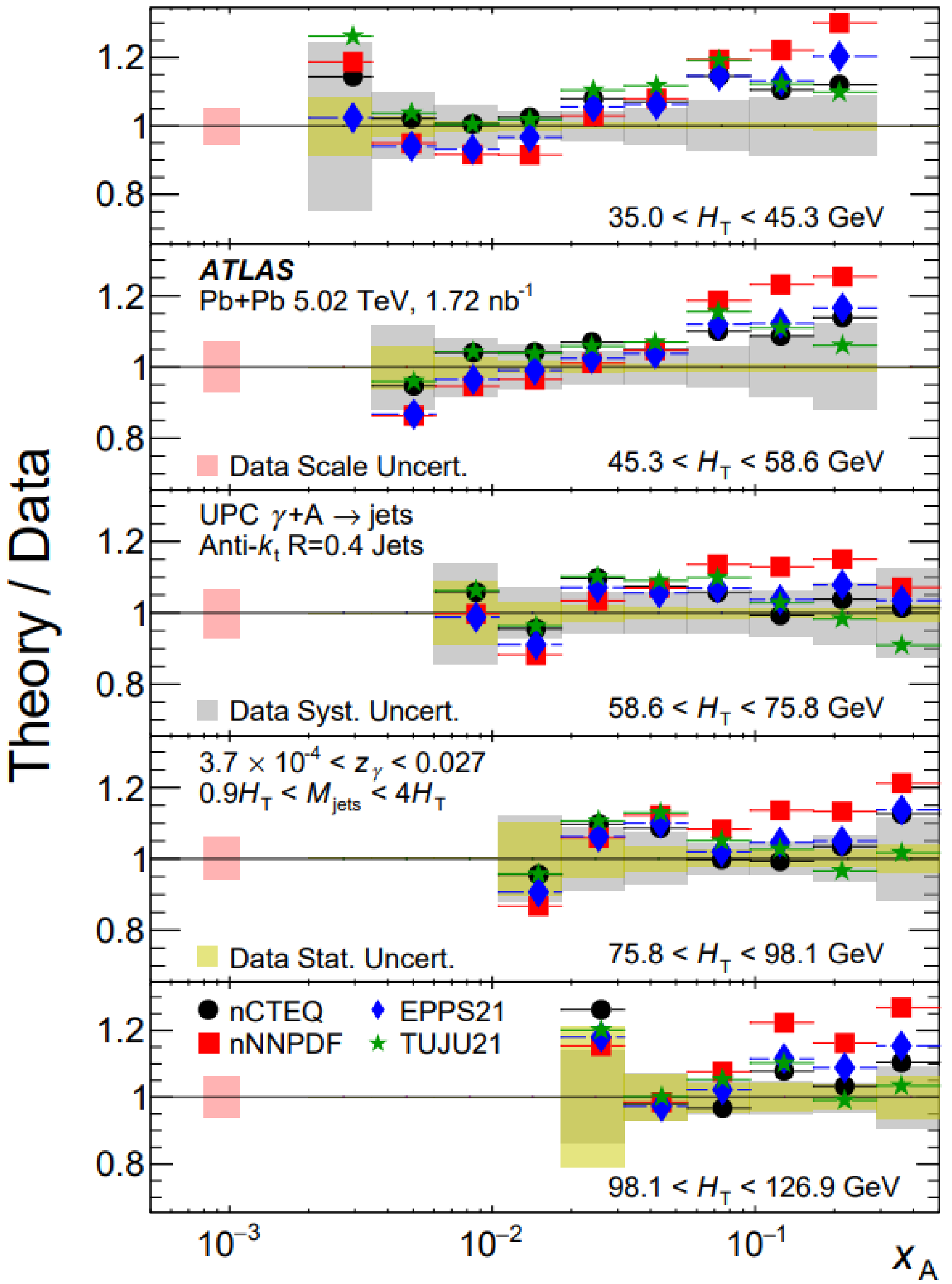

Conclusions: nPDF Coverage

- The results from this measurement provide substantially improved coverage of the <u>intermediate-Q^2 region</u>, for a <u>wide range of x values</u>.
- These results are fully inclusive, and after correction for nuclear break-up, the measured cross-sections <u>agree well with existing nPDFs</u> using LO+PS calculations.
- With the full treatment of correlated systematic uncertainty, these data will have <u>substantial constraining power</u> for nPDFs.

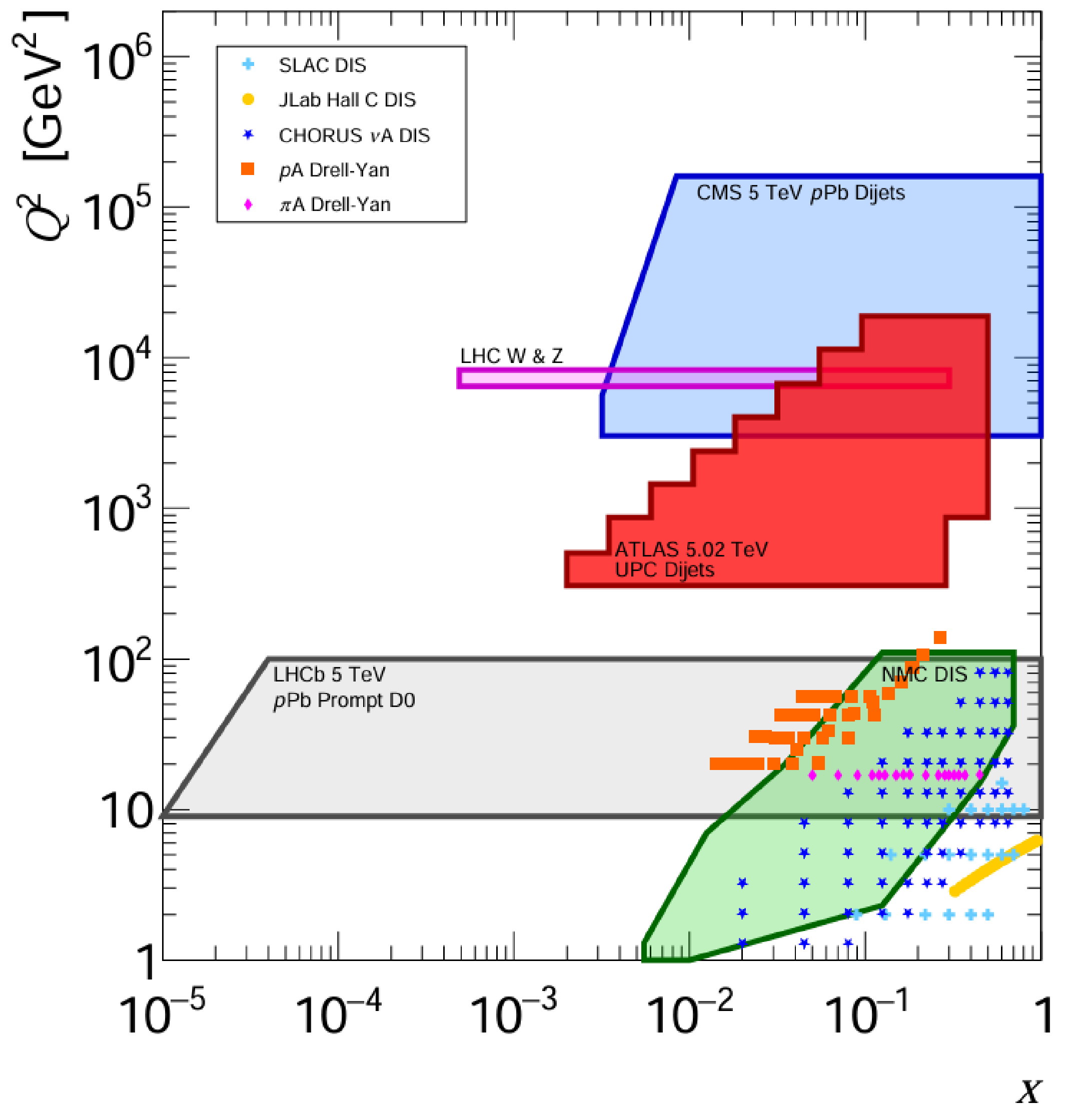

Conclusions: Connection to the EIC

- The results from this measurement provide substantially improved coverage of the intermediate-Q^2 region, for a wide range of x values.
- These results are fully inclusive, and after correction for nuclear break-up, the measured cross-sections agree well with existing nPDFs using LO+PS calculations.
- With the full treatment of correlated systematic uncertainty, these data will have substantial constraining power for nPDFs.

- In addition to measuring a region of phase space with little other data, this measurement also bridges projected EIC coverage and LHC data.
  - These data overlap in coverage with both high-Q^2 LHC measurements and project EIC coverage.
- By overlapping both regions, this data can help provide both a baseline for DIS measurements at the EIC and a direct connection to other measurements at the LHC.

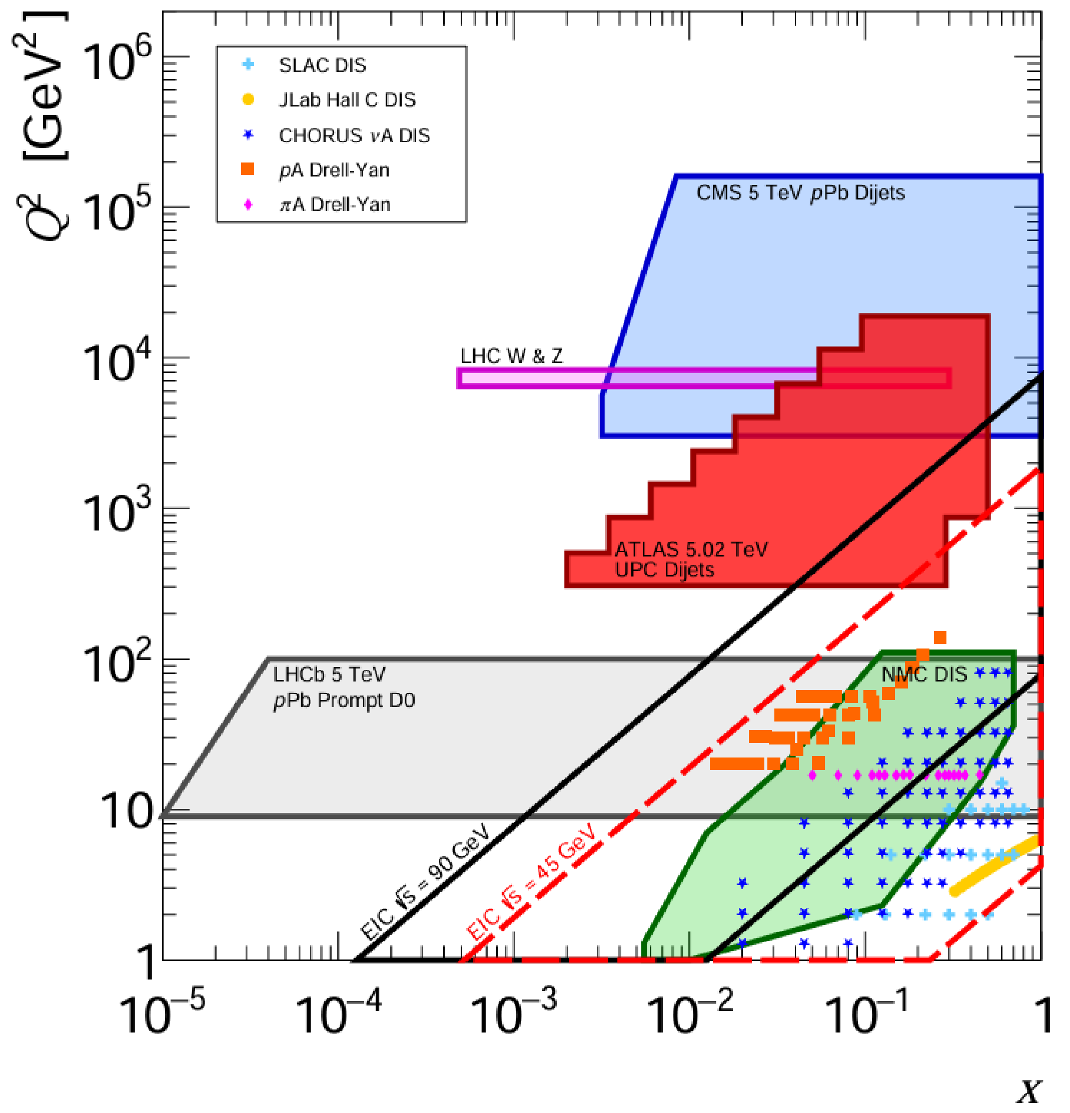

Summary

- ATLAS jet measurements provide several novel approaches to constrain initial-state effects in nuclear collisions.
    - Dijet production in *p*+Pb demonstrates the impact of color transparency on processes with a hadronic probe.
    - UPC dijet production provides a novel approach to measure nPDFs with high precision and much less sensitivity to initial state effects.
- These UPC jet results are a key first step in a rapidly expanding program of inclusive photonuclear processes at the LHC.

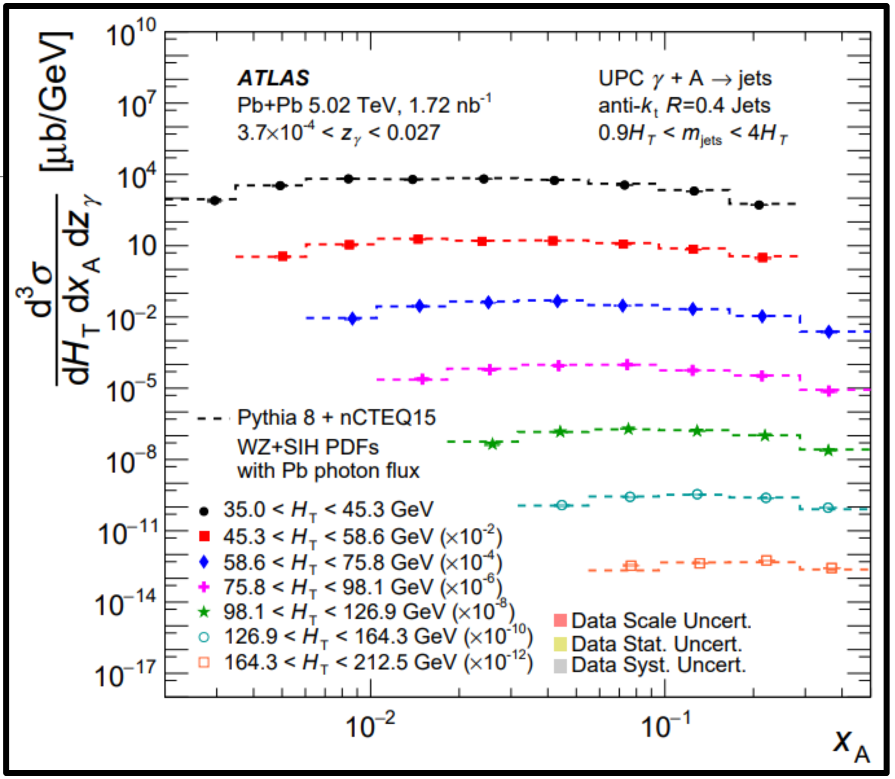

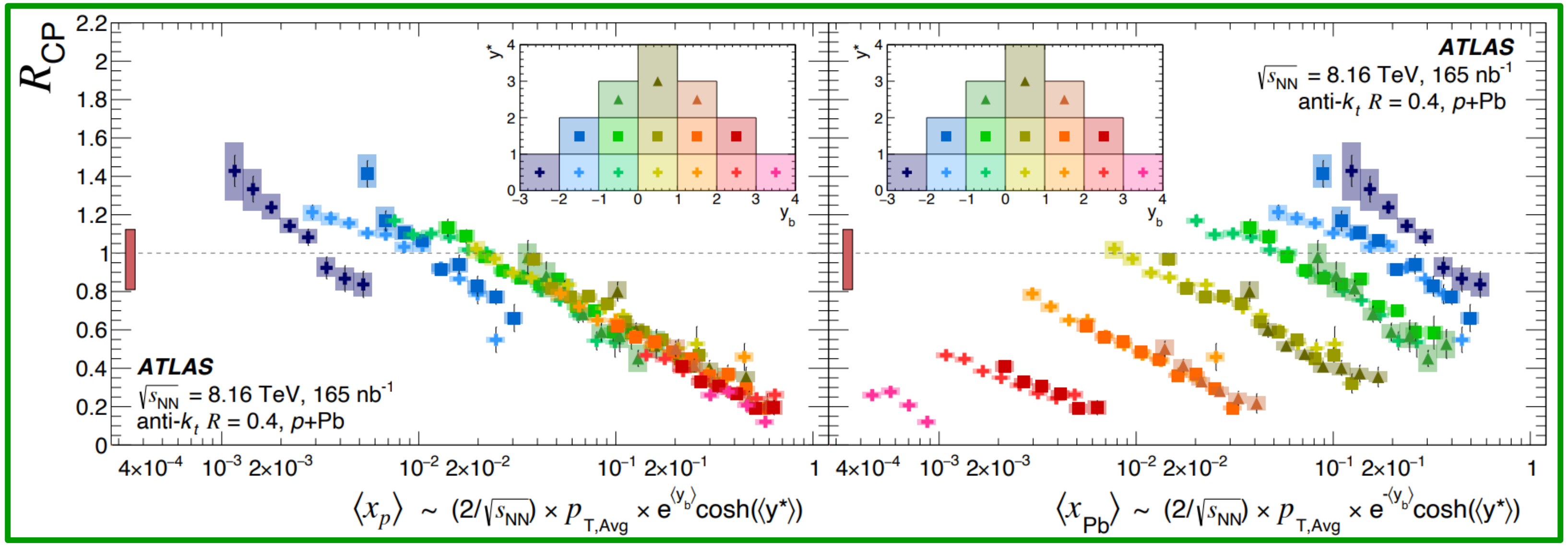

These results already provide some key inputs for interpreting early physics results of the EIC!

Backup

The ATLAS Detector

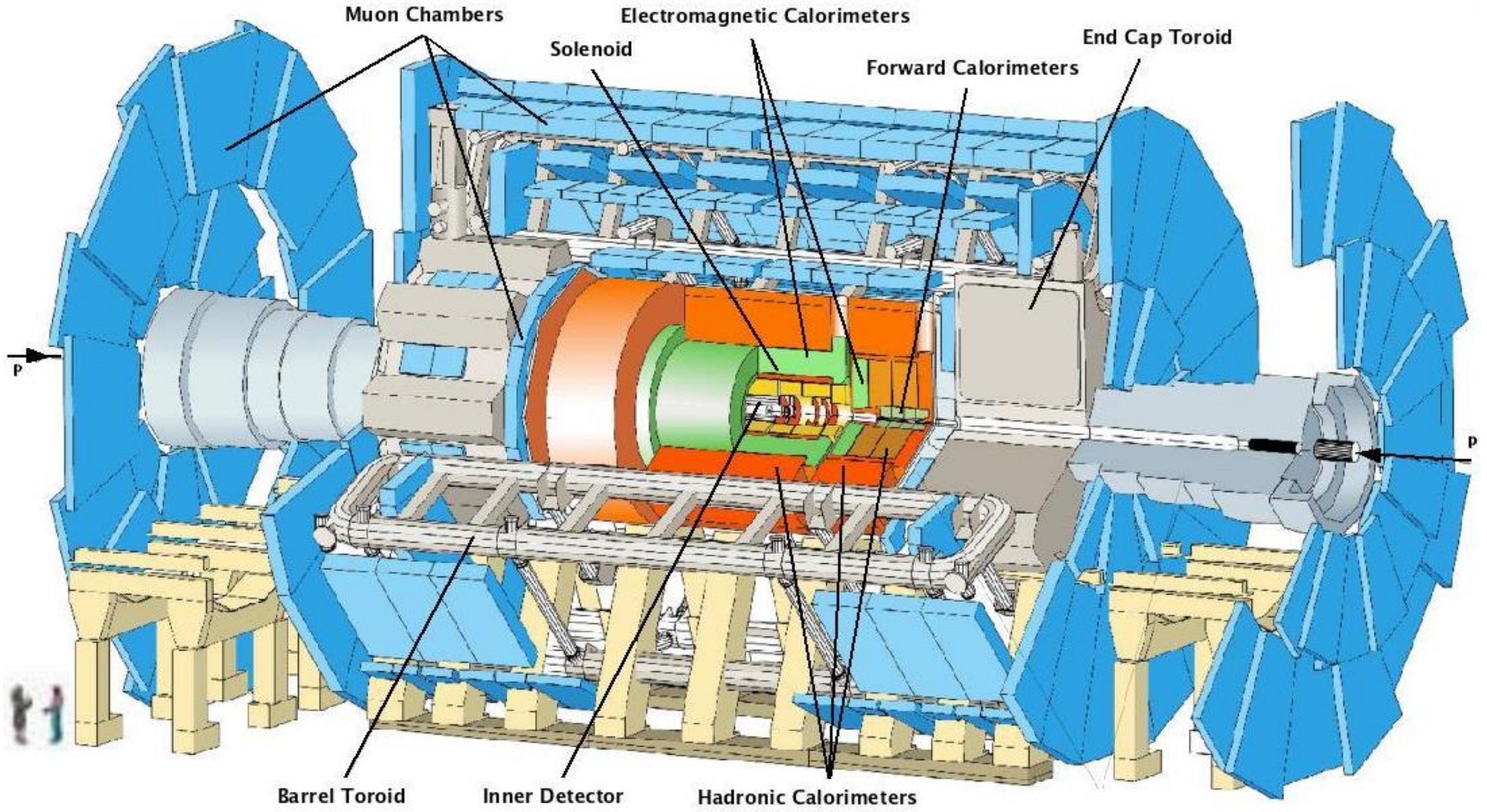

Acceptance and Observables: p+Pb Dijets

$$p_{T,avg} = \frac{p_T^1 + p_T^2}{2}$$ $$y^* = \frac{|y_1 - y_2|}{2}$$ $$y_b = \frac{y_1 + y_2}{2}$$ → $$x_p = \frac{2p_T^{avg}\cosh(y^*)e^{+y_b}}{\sqrt{s}}$$ $$x_{Pb} = \frac{2p_T^{avg}\cosh(y^*)e^{-y_b}}{\sqrt{s}}$$

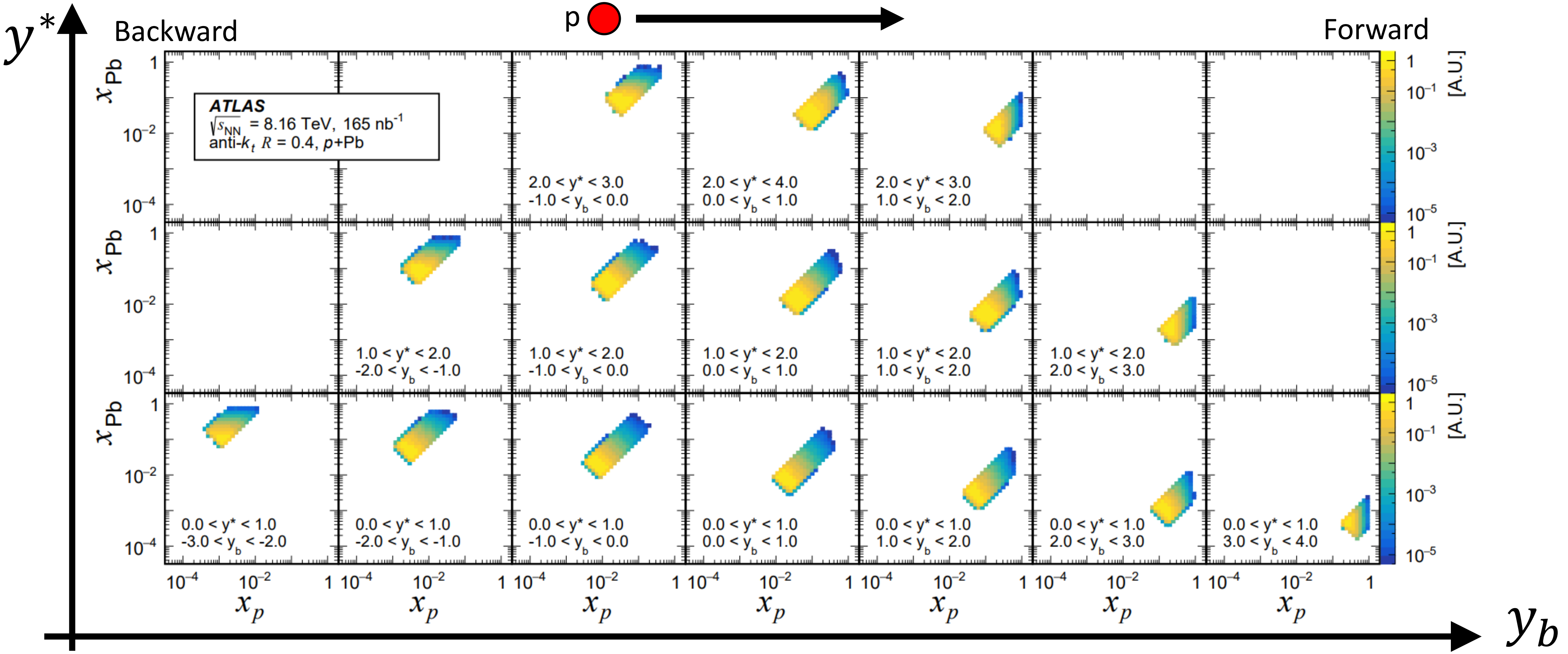

P+Pb Dijet Results in p_T^{avg}, y_b, y^*

$$p_{T,avg} = \frac{p_T^1 + p_T^2}{2} \qquad y^* = \frac{|y_1 - y_2|}{2} \qquad y_b = \frac{y_1 + y_2}{2}$$

$$\Rightarrow \quad x_p = \frac{2p_T^{avg}\cosh(y^*)e^{+y_b}}{\sqrt{s}} \qquad x_{Pb} = \frac{2p_T^{avg}\cosh(y^*)e^{-y_b}}{\sqrt{s}}$$

$$R_{CP}^{\frac{0-10\%}{60-90\%}}(p_T^{avg}, y_b, y^*) = \frac{\frac{1}{< T_{AB}^{0-10\%} >}\frac{1}{N_{evt}^{0-10\%}}\frac{dN_{dijet}^{0-10\%}}{dp_T^{avg}dy_b dy^*}}{\frac{1}{< T_{AB}^{60-90\%} >}\frac{1}{N_{evt}^{60-90\%}}\frac{dN_{dijet}^{60-90\%}}{dp_T^{avg}dy_b dy^*}}$$

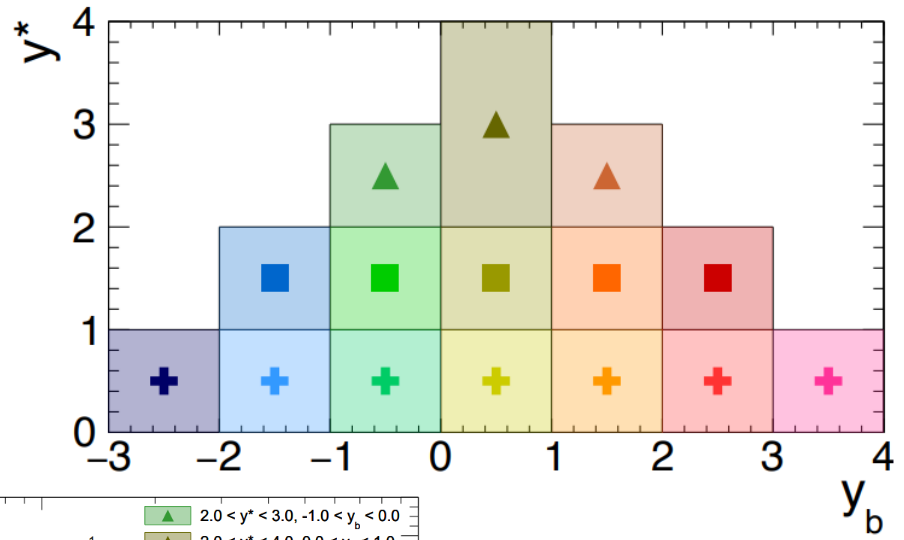

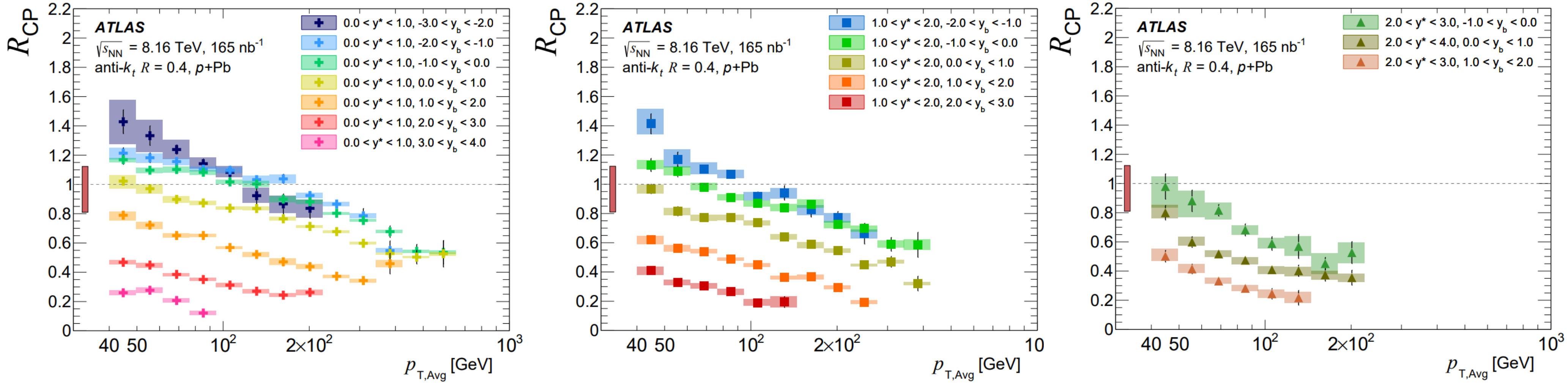

Different panels represent different y^* ranges.

General trend is more suppression with higher p_T^{avg} and y_b.

P+Pb Dijet Results in p_T^{avg}, y_b, y^*

$$p_{T,avg} = \frac{p_T^1 + p_T^2}{2} \qquad y^* = \frac{|y_1 - y_2|}{2} \qquad y_b = \frac{y_1 + y_2}{2}$$

$$x_p = \frac{2p_T^{avg}\cosh(y^*)e^{+y_b}}{\sqrt{s}} \qquad x_{Pb} = \frac{2p_T^{avg}\cosh(y^*)e^{-y_b}}{\sqrt{s}}$$

$$R_{CP}^{\frac{0-10\%}{60-90\%}}(p_T^{avg}, y_b, y^*) = \frac{\frac{1}{< T_{AB}^{0-10\%} >}\frac{1}{N_{evt}^{0-10\%}}\frac{dN_{dijet}^{0-10\%}}{dp_T^{avg}dy_b dy^*}}{\frac{1}{< T_{AB}^{60-90\%} >}\frac{1}{N_{evt}^{60-90\%}}\frac{dN_{dijet}^{60-90\%}}{dp_T^{avg}dy_b dy^*}}$$

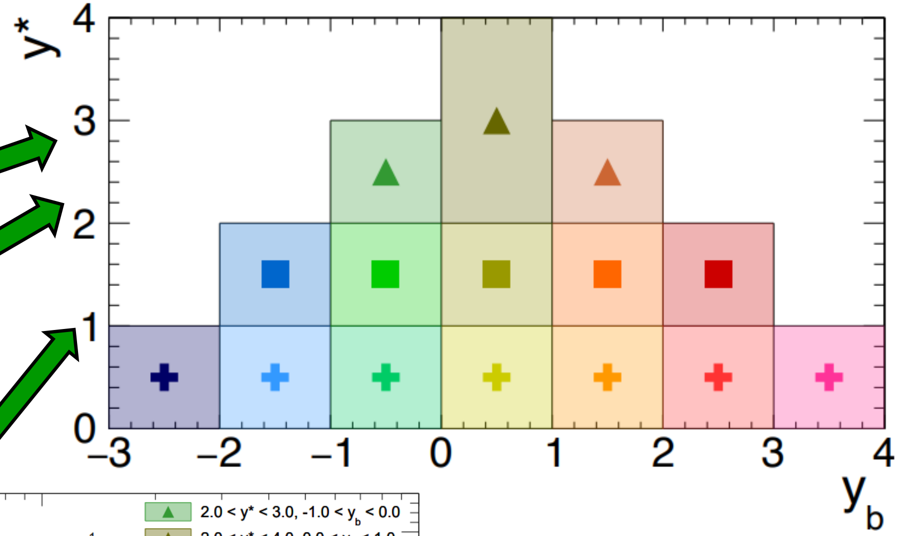

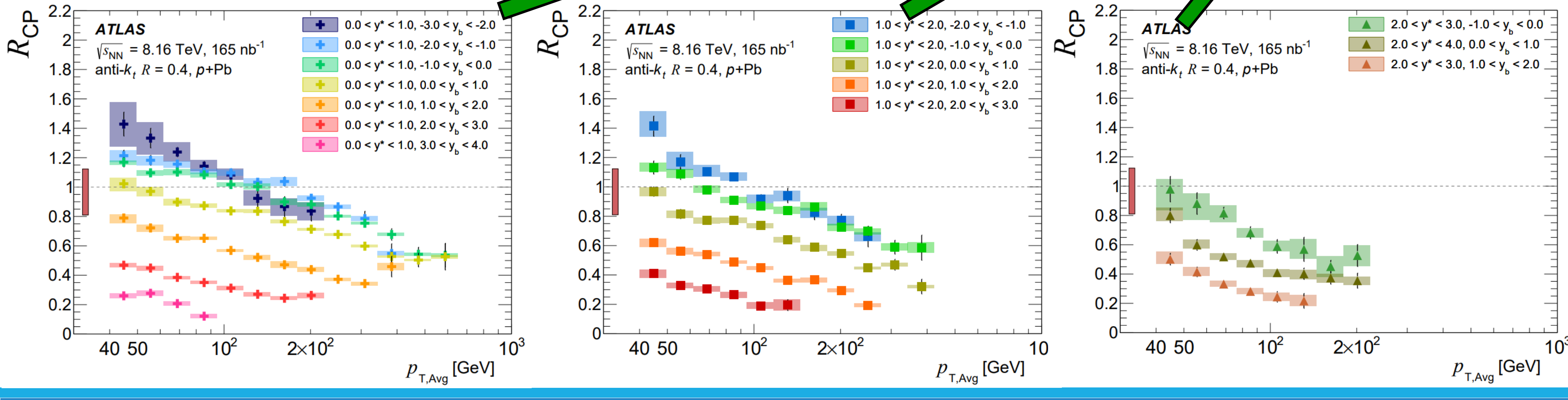

Different panels represent different y^* ranges.

General trend is more suppression with higher p_T^{avg} and y_b.

UPC Jets: Predicted Modifications

- After selecting which bins to report, we can demonstrate the sensitivity to nPDF effects by comparing modified to un-modified cross-sections for two different models (markers).
- Experimental uncertainties are shown on the plots, to show how the measurement sensitivity compares to effect sizes.

$$H_T = \sum_i p_T^i$$

$$x_A = \frac{M_{jets} e^{-y_{jets}}}{\sqrt{s_{NN}}}$$

$$z_\gamma = \frac{M_{jets} e^{+y_{jets}}}{\sqrt{s_{NN}}}$$

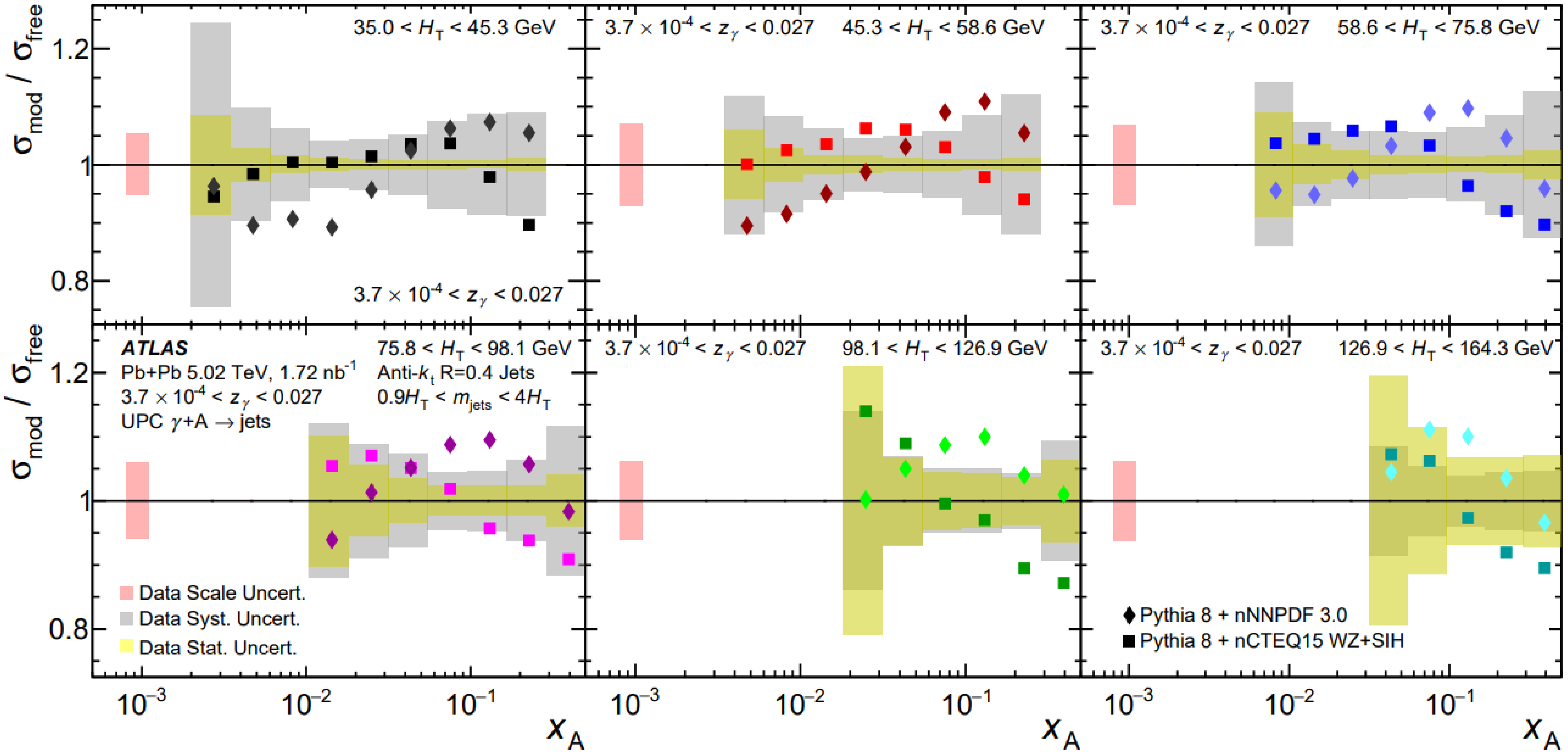

Importance of Forward Neutrons: *0n0n* Events

For the first time, ATLAS has observed dijet production in UPCs without nuclear breakup (0n0n).

Gaps are required on both sides of the detector: $\sum \Delta\eta > 2.0$

A factor of 10 more events are observed in data than are predicted from $\gamma\gamma \to$ jets, estimated by Pythia or comparison to $\gamma\gamma \to \mu^+\mu^-$ studies.

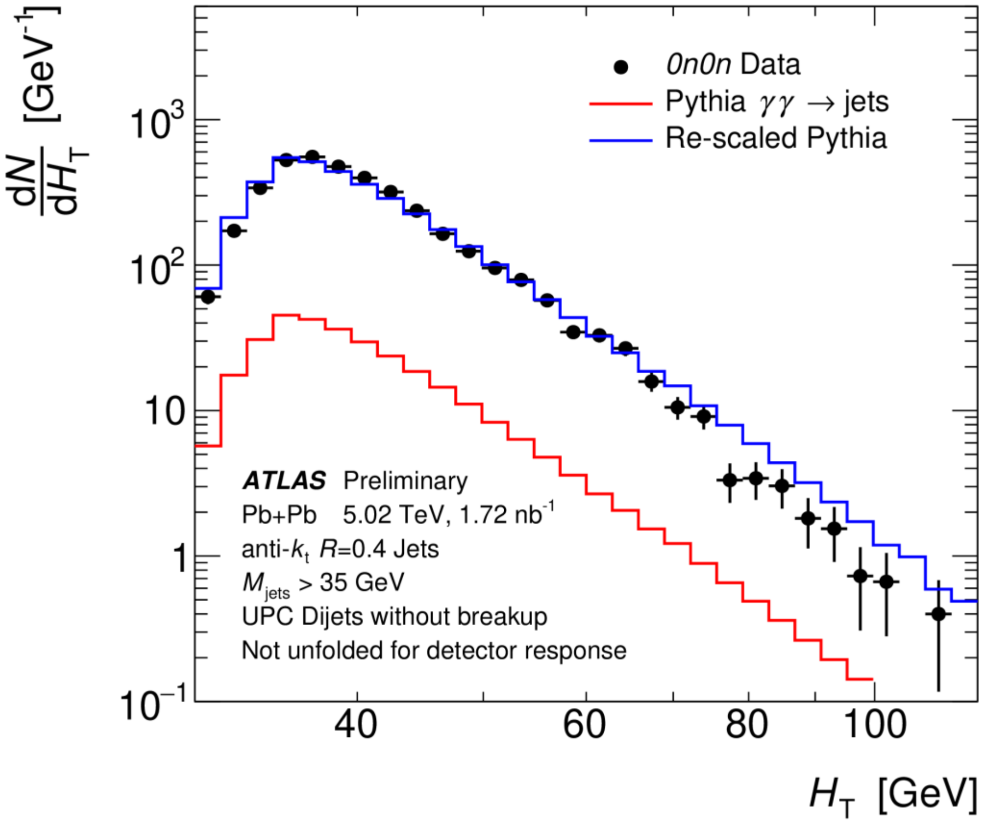

Importance of Forward Neutrons: *0n0n* Events

For the first time, ATLAS has observed dijet production in UPCs without nuclear breakup (0n0n).

Gaps are required on both sides of the detector: $\sum \Delta\eta > 2.0$

A factor of 10 more events are observed in data than are predicted from $\gamma\gamma \rightarrow$ jets, estimated by Pythia or comparison to $\gamma\gamma \rightarrow \mu^+\mu^-$ studies.

The distribution shapes are clearly different from pure $\gamma\gamma \rightarrow$ jets.

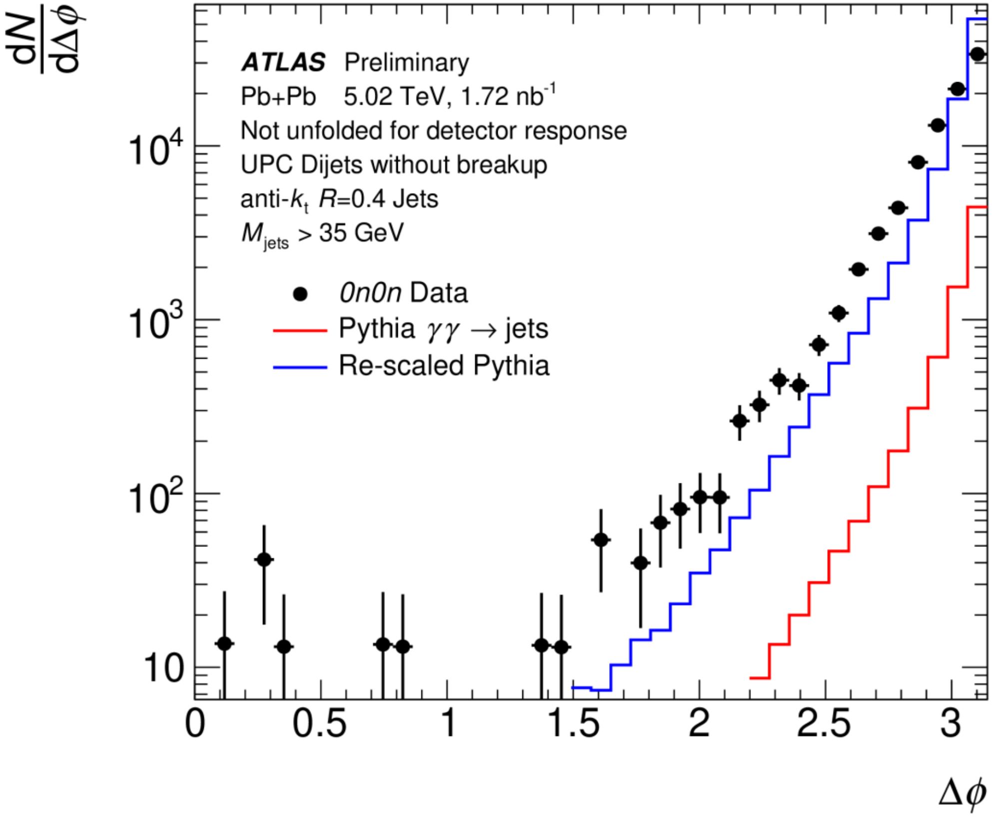

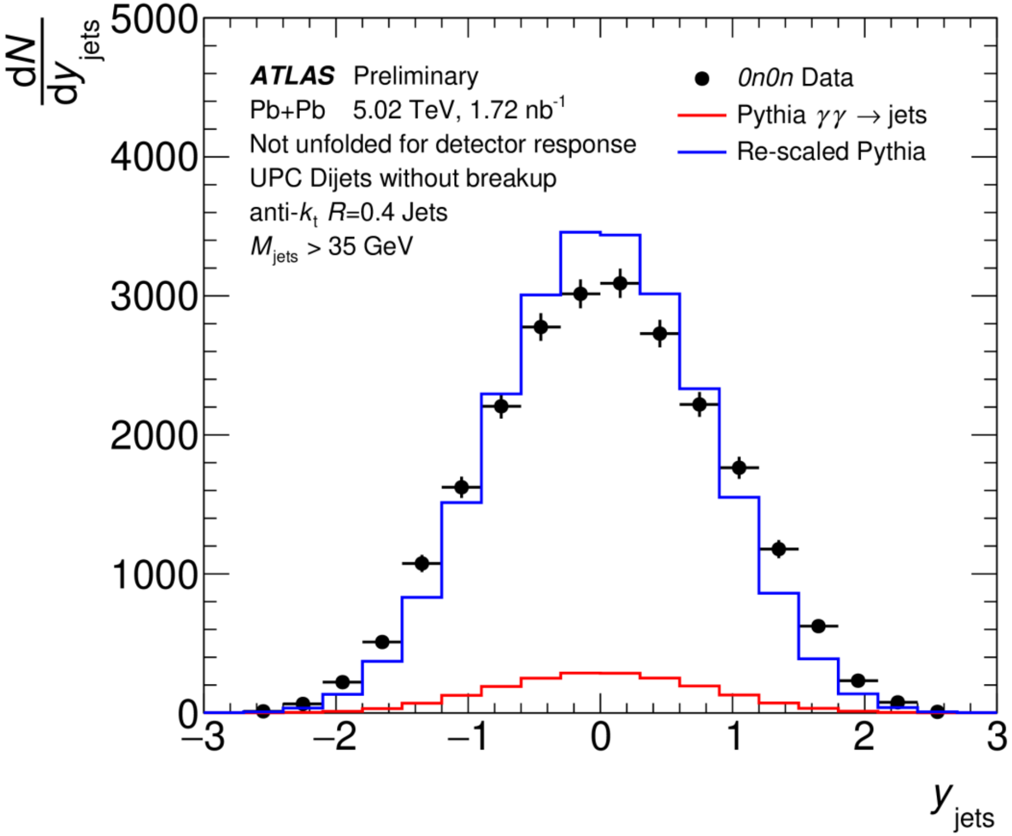

Importance of Forward Neutrons: *0n0n* Events

For the first time, ATLAS has observed dijet production in UPCs without nuclear breakup (0n0n).

Gaps are required on both sides of the detector: $\sum \Delta\eta > 2.0$

A factor of 10 more events are observed in data than are predicted from $\gamma\gamma \rightarrow$ jets, estimated by Pythia or comparison to $\gamma\gamma \rightarrow \mu^{+}\mu^{-}$ studies.

The distribution shapes are clearly different from pure $\gamma\gamma \rightarrow$ jets.

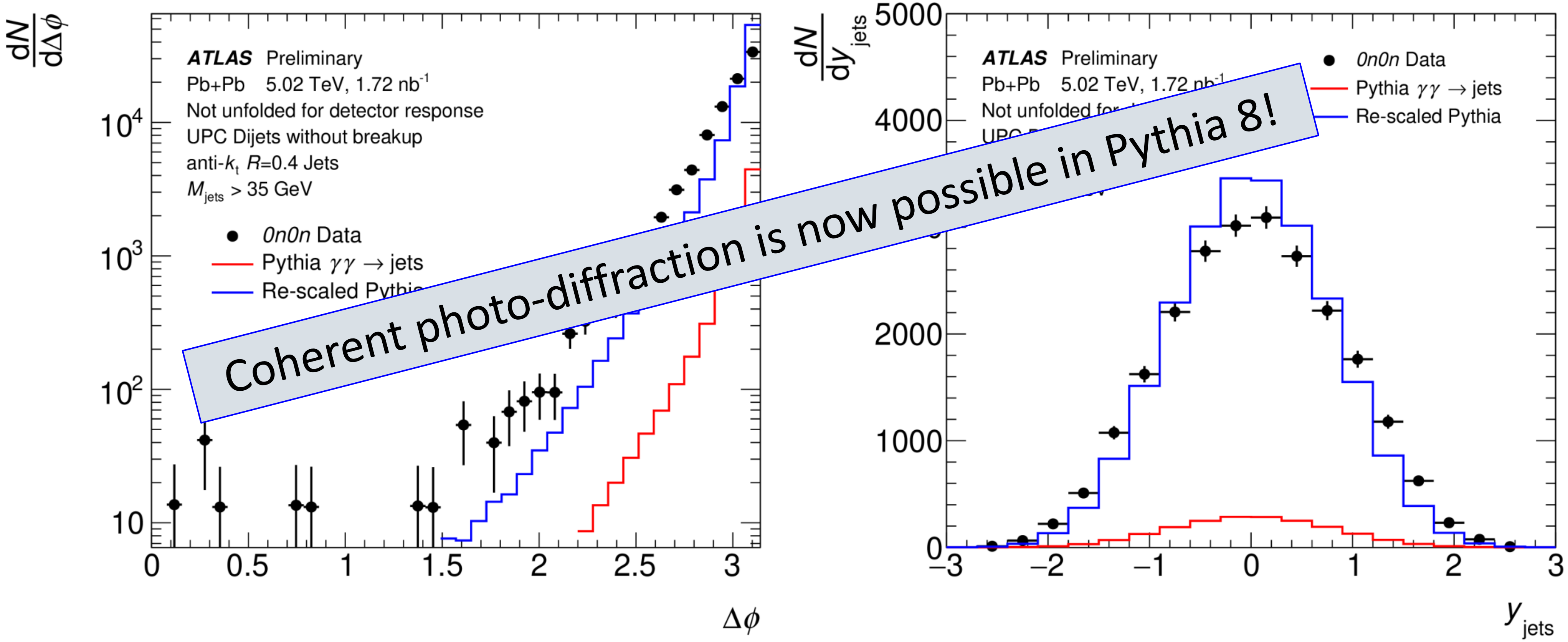

Theoretical Modeling of Nuclear Breakup

- The photon flux available through Pythia makes certain overly-simplified assumptions which we correct via modeling with STARlight.

We integrate over A-A impact parameter (b) and the impact parameter relative to the photon-emitting nucleus (s_A).

Correction for the probability of breakup due to additional EM interactions

Nuclear thickness function

$$F^{\mathrm{eff}}_{\gamma/A}(E_\gamma) \equiv \int \mathrm{d}^2 b\,\mathrm{d}^2 s_A\, P_{\text{no had}}(b)\, P_{\text{no EM}}(b)\, f_{\gamma/A}(E_\gamma, s)\, T_B(\vec{s}_A - \vec{b})$$

Correction for the probability of breakup due to hadronic interactions (overlap veto)

The photon flux from Pythia uses a point source, so this term corrects for coherent nuclear emission.